# The unique synaptic circuitry of specialized olfactory glomeruli in *Drosophila melanogaster*

Lydia Gruber[1], Rafael Cantera[2], Markus William Pleijzier[3], Michael Steinert[4], Thomas Pertsch[4], Bill S. Hansson[1#], Jürgen Rybak [1#]

1 Max Planck Institute for Chemical Ecology, Department of Evolutionary Neuroethology, 07745 Jena, Germany
2 Instituto de Investigaciones Biológicas Clemente Estable, Departamento de Biología del Neurodesarrollo, 11600 Montevideo, Uruguay
3 Neurobiology Division, MRC Laboratory of Molecular Biology, Cambridge, CB2 0QH, England, United Kingdom
4 Institute of Applied Physics, Abbe Center of Photonics, Friedrich Schiller University Jena, Albert Einstein Strasse 15, 07745 Jena, Germany

# contributed equally
*Correspondence: Jürgen Rybak (jrybak@ice.mpg.de)

**Keywords**: olfactory circuitry, connectome, *Drosophila melanogaster*, FIB-SEM, antennal lobe, glomerulus

## ABSTRACT

In the *Drosophila* olfactory system most odorants are encoded in the antennal lobe in a combinatory way, activating several glomerular circuits. However, odorants of particular ecological role for the fly are encoded through activation of a single specialized olfactory pathway. Comparative analyses of densely reconstructed connectomes of one broadly tuned glomerulus (DL5) and one narrowly tuned glomerulus (DA2) gained detailed insight into the variations of synaptic circuitries of glomeruli with different computational tasks. Our approach combined laser-branding of glomeruli of interest with volume based focused ion beam-scanning electron microscopy (FIB-SEM) to enable precise targeting and analysis of the two glomeruli. We discovered differences in their neuronal innervation, synaptic composition and specific circuit diagrams of their major cell types: olfactory sensory neurons (OSNs), uniglomerular projection neurons (uPNs) and multiglomerular neurons (MGNs). By comparing our data with a previously mapped narrowly tuned glomerulus (VA1v), we identified putative generic features of narrowly tuned glomerular circuits, including higher density of neuronal fibers and synapses, lower degree of OSN lateralization, stronger axo-axonic connections between OSNs, dendro-dendritic connections between many uPNs, and lower degree of presynaptic input on OSN axons. In addition, this work revealed that the dendrites of the single uPN in DL5 contain a substantial amount of autapses interconnecting distant regions of the dendritic tree**.** The comparative analysis of glomeruli allows to formulate synaptic motifs implemented in olfactory circuits with different computational demands.

## INTRODUCTION

Olfaction is an anatomically shallow sensory system. In mammals and invertebrates just one synapse separates the sensory periphery from the central brain (Su et al., 2009; Liang & Luo, 2010; Shepherd, 2011; Owald & Waddell, 2015; Dolan et al., 2018). In the olfactory system of *Drosophila melanogaster*, the first relay station of synaptic transmission is the antennal lobe (AL), which has a circuit architecture homologous to that of the vertebrate olfactory bulb (Boeckh et al., 1990; Sachse & Manzini, 2021; Shepherd et al., 2021). The fly AL consists of approximately 58 spherical compartments, called glomeruli, which can be distinguished by size, shape and location (Laissue et al., 1999; Gao et al., 2000; Vosshall et al., 2000; Grabe et al., 2015; Bates et al., 2020). Each glomerulus receives stereotypic input from axon terminals of olfactory sensory neurons (OSNs), which have their cell bodies and dendrites located in the antennae or maxillary palps (de Bruyne et al., 1999; Shanbhag et al., 1999; de Bruyne et al., 2001; Hallem et al., 2004; Benton et al., 2006). All the OSNs innervating a given glomerulus express a typical repertoire of ligand-gated chemoreceptors (Couto et al., 2005; Fishilevich & Vosshall, 2005; Benton et al., 2006), which represent a wide range of specifications, binding either a single, few, or many distinct chemicals (Hallem et al., 2004; Hallem & Carlson, 2006; Knaden et al., 2012; Münch & Galizia, 2016; Seki et al., 2017; Wicher & Miazzi, 2021).

Most OSNs project bilaterally to the corresponding glomeruli in the left and right AL (Gaudry et al., 2013; Tobin et al., 2017). In the AL, OSNs convey odor signals to excitatory uniglomerular projection neurons (uPNs), which branch only within a single glomerulus, or to inhibitory multiglomerular PNs (mPNs) and inhibitory or excitatory local interneurons (LNs) (Ng et al., 2002; Cuntz et al., 2007; Kazama & Wilson, 2008; Kreher et al., 2008; Kazama & Wilson, 2009; Masse et al., 2009; Tanaka et al., 2012; Ai & Hagio, 2013; Wilson, 2013; Bates et al., 2020). LNs innervate each several glomeruli and are the key modulatory neurons in the AL (Chou et al., 2010; Seki et al., 2010). The highly converging OSNs-to-PN signal transmission (Chen & Shepherd, 2005; Masse et al., 2009; Jeanne & Wilson, 2015) is lateralized, activating ipsilateral uPNs more strongly than contralateral ones (Agarwal & Isacoff, 2011; Gaudry et al., 2013; Tobin et al., 2017). From the AL, uPNs and mPNs relay processed signal information to higher brain centers (Norgate et al., 2006; Fiala, 2007; Jefferis et al., 2007; Keene & Waddell, 2007; Galizia, 2014; Guven-Ozkan & Davis, 2014; Strutz et al., 2014; Bates et al., 2020).

The stereotypic activity pattern elicited by distinct odorants encodes the odor space, represented in a so-called odotopic map of the AL according to the glomerular activation by distinct chemical classes. (Couto et al., 2005; Laissue & Vosshall, 2008; Knaden & Hansson, 2014; Grabe et al., 2015; Grabe & Sachse, 2018). Some odorants induce a fixed innate behavior (aversion or attraction), activating characteristically specific glomeruli (Semmelhack & Wang, 2009; Knaden et al., 2012; Knaden & Hansson, 2014; Gao et al., 2015; Grabe & Sachse, 2018). The encoding of hedonic valence already at the level of the AL is important for a fast odor coding. Most odorants

are encoded in a combinatorial manner in the fly AL by activating multiple OSNs types expressing broadly tuned receptors and their glomerular circuits, including broadly tuned uPNs (de Bruyne et al., 2001; Silbering & Galizia, 2007; Silbering et al., 2008; Masse et al., 2009; Galizia, 2014; Szyszka & Galizia, 2015; Sachse & Hansson, 2016; Seki et al., 2017). Certain chemoreceptors and their downstream glomerular circuits, however, have evolved a very high specificity and sensitivity to single or very few chemicals (Andersson et al., 2015; Haverkamp et al., 2018; Keesey & Hansson, 2021). These narrowly tuned glomerular circuits often belong to dedicated olfactory pathways, called "labeled lines", which process information regarding single odorants of particular importance for reproduction and survival (Kurtovic et al., 2007; Datta et al., 2008; Stensmyr et al., 2012; Dweck et al., 2015; Gao et al., 2015). An extreme example is the DA2 glomerulus, which responds exclusively to geosmin, an ecologically relevant chemical that alerts flies to the presence of harmful microbes, causing the fly to avoid laying eggs at these locations (Stensmyr et al., 2012). This dedicated olfactory pathway and its receptor sequence is conserved throughout evolution (Keesey et al., 2019; Keesey & Hansson, 2021). Another example is glomerulus VA1v, which responds to methyl laurate, a pheromone that induces a strongly attractive response in female flies leading to aggregation behavior (Dweck et al., 2015). DL5, on the other hand, is an example of a broadly tuned glomerulus, innervated by OSNs activated by several odorants, like E2-hexenal and benzaldehyde (Knaden et al., 2012; Münch & Galizia, 2016; Seki et al., 2017; Mohamed, Retzke, et al., 2019). This functional diversity suggests differences in neuronal composition and synaptic connectivity between broadly and narrowly tuned glomeruli.

A survey of neuronal composition across glomeruli revealed great variation in the numbers of the different types of neurons innervating narrowly and broadly tuned glomeruli (Grabe et al., 2016). In general, narrowly tuned glomeruli are innervated by more uPNs and fewer LNs compared with more broadly tuned glomeruli (Chou et al., 2010; Grabe et al., 2016). In addition, narrowly tuned OSNs receive less global LN inhibition than broadly tuned ones (Hong & Wilson, 2015; Grabe et al., 2020; Schlegel et al., 2021). For example, in female flies, the narrowly tuned glomerulus DA2 contains dendrites of 6-8 uPNs, whereas the broadly tuned glomerulus DL5 houses only 1 or 2 uPNs and has a higher number of innervating LNs. Interestingly, both glomeruli are innervated by the same number of OSNs (Grabe et al., 2016).

Little is known, however, about the microarchitecture of the synaptic circuitry in distinct glomeruli and, in particular, about ultrastructural differences between narrowly vs. broadly tuned glomerular circuits. Electron microscopy (EM) allows volume imaging with dense reconstruction of fine neurite branches and synapses in brain tissue at nanometer resolution, necessary to map synapses (Briggman & Denk, 2006; Cardona et al., 2009; Helmstaedter, 2013; Rybak, 2013; Meinertzhagen, 2018). The first ultrastructural insights into the synaptic connectivity of *Drosophila* olfactory glomeruli were obtained by studies based on serial section transmission EM (ssTEM) (Rybak, 2016; Tobin et al., 2017). Rybak *et al*. (2016) showed that all three basic classes of AL neurons make synapses with each other, while Tobin *et al*. (2017) revealed that the differences in

113 number of innervating uPNs between the left and right DM6 glomeruli are compensated by
114 differences in synaptic strength. With focused ion beam-scanning electron microscopy (FIB-SEM;
115 (Knott et al., 2008)) a complete reconstruction of all neurons in the narrowly tuned, pheromone
116 processing glomerulus VA1v was obtained (Horne et al., 2018). Recent technological innovations
117 in ssTEM, FIB-SEM and automated neuron reconstruction have made connectome datasets of the
118 adult *Drosophila* central nervous system available (Saalfeld et al., 2009; Zheng et al., 2018; P. H. Li
119 et al., 2020; Scheffer et al., 2020) and provided complete circuit descriptions of several brain
120 centres (Felsenberg et al., 2018; Dolan et al., 2019; Auer et al., 2020; Bates et al., 2020; Coates et
121 al., 2020; Huoviala et al., 2020; F. Li et al., 2020; Marin et al., 2020; Otto et al., 2020; Hulse et al.,
122 2021; Schlegel et al., 2021).
123 To understand how highly specialized glomerular circuits in dedicated olfactory pathways
124 differ in signal integration from broadly tuned circuits, we compared the microarchitecture and
125 synaptic connectivity of a narrowly tuned glomerulus (DA2) and a broadly tuned glomerulus (DL5).
126 By using a correlative workflow that combines transgenic markers with FIB-SEM, to identify these
127 glomeruli, we reconstructed OSNs, uPNs and multiglomerular neurons (MGNs), comprising both
128 local interneurons (LNs) and multiglomerular neurons (mPNs) of the AL combined. We mapped all
129 associated synapses and compared the circuit organization of both glomeruli.
130
131
132

133 **RESULTS**

134 **Volume-based electron microscopy of two different olfactory glomeruli**

135 To compare the synaptic circuitries of two olfactory glomeruli known to belong to either
136 narrowly or broadly tuned glomerular types in *Drosophila melanogaster*, we mapped all synapses
137 of glomeruli DA2 (right AL) and DL5 (left AL) in a single female fly (**Figure 1A-B**) with the aid of FIB-
138 SEM. A partial reconstruction of a second DA2 in another fly was used to measure neuronal volume
139 (see Methods). The reconstructions were based on high resolution (4x4x20 nm) datasets (**Figure 1**;
140 **Figure 1 – video 1),** thus allowing reconstruction of the finest neuronal branches (~20 nm diameter;
141 **Figure 1C-D**) as well as mapping chemical synapses (example in **Figure 1E**) in the two volumes of
142 interest (VOI). To restrict the imaging volume to the target VOIs, we employed a correlative
143 approach for the first time for a *Drosophila* EM volume reconstruction. Glomeruli DA2 and DL5
144 were identified by their size, shape and location in brains of transgenic flies (*Orco-GAL4; UAS-*
145 *GCaMP6s*) using the glomerular map of (Grabe et al., 2015). The flies expressed the green
146 fluorescent protein GCaMP6 coupled with calmodulin and M13 (a peptide sequence from myosin
147 light-chain kinase; **Figure 1A-B**). Subsequently, the identified glomeruli were marked by laser
148 branding using a two-photon laser (Bishop et al., 2011). These fiducial marks were apparent under
149 both light (Figure 1A-B) and electron microscopy **(Figure 1C-D)** and facilitated the delimitation of
150 the VOIs during FIB-SEM scanning. We produced two complete FIB-SEM datasets: one for
151 glomerulus DA2 and one for DL5 (pure imaging time for both glomeruli: ~60 h) and a partial dataset
152 for DA2 in a second fly, which was used for volumetric analysis (see data availability).
153

154 **Skeleton based neuron reconstruction and synapse identification**

155 We reconstructed all neurons within the two volumes of interest (VOIs) (example neuron:
156 **Figure 1F**) and mapped all their synaptic connections using an iterative skeleton-based
157 reconstruction approach, similar to previously reported procedures (Berck et al., 2016; Schneider-
158 Mizell et al., 2016; Zheng et al., 2018) with the aid of the web-based neuron reconstruction
159 software CATMAID (http://www.catmaid.org; RRID:SCR_006278; (Cardona et al., 2009; Schneider-
160 Mizell et al., 2016); **Figure 1 – video 1**). Synapses were identified by their presynaptic transmitter
161 release site, which in *Drosophila* is composed of a presynaptic density called a T-bar, surrounded
162 by synaptic vesicles and apposed postsynaptic elements (**Figure 1E**), as previously described
163 (Trujillo-Cenoz, 1969; Fröhlich, 1985; Rybak et al., 2016; Huang et al., 2018; P. H. Li et al., 2020). All
164 synapses observed in our FIB-SEM data sets were polyadic, i.e., each presynaptic site connected to
165 multiple postsynaptic sites (See example in **Figure 1E**), a feature of insect brain synapses
166 (Meinertzhagen & O'Neil, 1991; Malun et al., 1993; Prokop & Meinertzhagen, 2006; Hartenstein,
167 2016; Rybak et al., 2016). Some synapses had up to 16 postsynaptic sites (**Figure 2 – figure**
168 **supplement 1B**), i.e., one T-bar and 16 single synaptic profiles (i.e., sixteen 1:1 single output-input

169 connections). Short neuronal fragments (<10 µm), which could not be connected to any neuronal
170 fiber were designated as "orphans". These fragments represented 4% of the total length of all
171 traced neuronal fibers in DA2 and 6% in DL5 and contained about ~12% of all synaptic contacts in
172 both glomeruli.
173

174 **Glomerular neurons: classification, description and inventory**

175 Previous descriptions of the ultrastructural characteristics of the AL in *Drosophila* helped to
176 classify AL neurons into 3 main classes (**Figure 2A**) Olfactory sensory neurons (OSNs),
177 uniglomerular projection neurons (uPNs) and multiglomerular neurons (MGNs; cells that
178 interconnect multiple glomeruli). MGNs are further subdivided into multiglomerular projection
179 neurons (mPNs) and local interneurons (LNs) (Berck et al., 2016; Rybak et al., 2016; Gruber et al.,
180 2018; Horne et al., 2018; Zheng et al., 2018; Schlegel et al., 2021). Most of the neuronal profiles
181 within the MGN neuron class belong probably to inhibitory local neurons, as this cell type is the
182 most numerous and broadly arborizing of the multiglomerular cell types in the antennal lobe (AL)
183 (Chou et al., 2010; Lin et al., 2012). In addition, we observed a few neuronal fibers with an electron-
184 dense and vesicle-rich cytosol, which we interpreted to be either peptidergic neurons (Nässel &
185 Homberg, 2006; Eckstein et al., 2024) or the contralaterally projecting, serotonin-immunoreactive
186 deutocerebral (CSD) neuron, (Dacks et al., 2006; Goyal & Chaudhury, 2013; Zheng et al., 2018;
187 Coates et al., 2020; Eckstein et al., 2024). Except for these neuronal fibers containing abundant
188 electron-dense vesicles, all other neuronal fibers were assigned to either OSNs, uPNs or MGNs
189 based on their morphology (**Figure 2A, B;** see Methods).
190 OSNs formed large, elongated synaptic boutons (**Figure 2A**), had the largest volume/length
191 ratio of all three neuron classes (**Figure 2 – figure supplement 1A**) and displayed the lowest degree
192 of branching intensity of all neurons in both glomeruli (**Figure 2B**). In agreement with what had
193 been observed in other glomeruli (Rybak et al., 2016), the majority of output synapses formed by
194 OSN terminals were triads (1:3) and tetrads (1:4). However, the T-bars of OSN synapses showed
195 considerable size variation, with some of them large enough to accommodate up to 16
196 postsynaptic contacts (**Figure 2 – figure supplement 1B**)**.** The frequency of large T-bars was much
197 higher in OSNs than in other neuron classes with an average polyadicity (average number of
198 postsynaptic sites at each T-bar) of 6 (1:6; (**Table 1,** row 14). As OSNs had the greatest T-bar and
199 output density along their axons (**Table 1**, row 10-11) they also displayed the largest synaptic ratios
200 (both for the T-bars/input sites and output sites/input sites) of all neuron classes (**Table 1,** row 12-
201 13), which was in line with previous observations (Rybak et al., 2016).
202 The uPNs exhibited the highest degree of branching intensity of the three neuron classes in
203 both glomeruli (**Figure 2A-B**). They showed numerous very fine apical branches that frequently
204 connected multiple times via spines to the same presynaptic site, leading to an entangled 3D shape
205 typical for this neuron class (**Figure 2A**) (Rybak et al., 2016; Tobin et al., 2017; Schlegel et al., 2021).

uPNs had the smallest volume/length ratio of all neuron classes (for the DA2: **Figure 2 - supplement 1A**). In addition to having many fine branches, uPN dendrites also had enlarged regions with almost no cytosol that were packed with large mitochondrial profiles extending over considerable distances. These enlarged profiles showed a larger degree of mitochondria fission (dividing and segregating mitochondrion organelles; personal observation) than the other neuron classes with rather round and compact mitochondria (**Figure 2A**; FIB-SEM image; see data availability). Seven uPNs were found in DA2, confirming light microscopy findings (Grabe et al., 2016). Two of them (PN#1, PN#2; see data availability) branched broadly and innervated the full glomerulus, and received more synaptic input than the other 5 uPNs (PN#3-#7; **see Table S3**), which branched exclusively in sub-regions of the glomerulus, with partial overlap. In addition to abundant clear small vesicles (~20 nm in diameter) (Yasuyama et al., 2003; Strutz et al., 2014; Bates et al., 2020), uPN dendrites also displayed small electron-dense vesicles, as previously reported for PN axon terminals in the mushroom body calyx (Butcher et al., 2012; Yang et al., 2022). These electron-dense vesicles are packed with different types of neuropeptides that act as neuromodulators or co-transmitters (Gondré-Lewis et al., 2012; V. Croset et al., 2018; Eckstein et al., 2024). In both glomeruli, uPNs had the highest neuronal synaptic input density and the lowest T-bar and output density of the three neuron classes (**Table 1**, row 9-11; DA2 and DL5 differences: see next section). The synaptic ratios (T-bars/input sites and output sites/input sites) were much lower for uPNs than for the other neuron classes (**Table 1**, row 12-13). The majority of uPN dendritic output synapses (feedback synapses) were tetrads in both glomeruli, with an average polyadicity of around 5 (lower than in OSNs; (**Figure 2 – supplement 1**; **Table 1**, row 14).

The majority of the neuronal fibers in both glomeruli belonged to MGNs (**Figure 2A**). MGNs exhibited variable morphology and ultrastructure, as expected, but shared also some ultrastructural features. Their synaptic boutons were formed by thin fibers, thus the volume/length ratio of MGNs was lower than that of OSNs but greater than that of uPNs (**Figure 2 – figure supplement 1A**). A similar relationship was found for the number of output sites and the T-bar density along MGN fibers, which were smaller than in OSNs but larger than in uPNs (**Table 1**, row 10-11). In contrast, branching intensity in MGNs was larger than in OSNs but smaller than in uPNs (**Figure 2B**). The synaptic ratio of output-to-input sites was around one (**Table 1**, row 12-13). MGNs had the lowest polyadicity (~3) of the three neuron classes (**Table 1**, row 14) and their synapses were mainly triads (**Figure 2 – supplement 1D**). Interestingly, besides the abundant clear small vesicles (~20 nm in diameter), some MGNs had small electron-dense vesicles, most likely housing neuropeptides (Carlsson et al., 2010; Vincent Croset et al., 2018; Nässel, 2018).

## DA2 is more densely innervated and has a higher synapse density than DL5

In our FIB-SEM datasets the volume of glomerulus DA2 was 45% smaller than that of glomerulus DL5 (1500 $\mu m^3$ vs. 2640 $\mu m^3$), which is in agreement with measurements based on light

243 microscopy (DA2 = 1600 µm$^3$, DL5 = 2900 µm$^3$ (Grabe et al., 2016). We also confirmed that a similar
244 number of OSNs (44-46 OSNs) innervated both glomeruli (**Figure 2C**), and that each glomerulus
245 received input from OSNs originating in both the ipsilateral and contralateral antennae (Vosshall
246 et al., 2000; Grabe et al., 2016). Consistent with previous findings (Grabe et al., 2016), the DA2
247 glomerulus was innervated by 7 uPNs, whereas DL5 had a single uPN (**Figure 2C**). MGN cell
248 numbers could not be determined in our study due to their multiglomerular morphology, which
249 also prevented us from tracing MGN fibers to their soma due to our partial volume acquisition (see
250 Methods).
251 To investigate differences between DA2 and DL5 we turned our attention to their glomerular
252 innervation and synaptic composition. We measured the total length (sum in µm) of all neuronal
253 fibers of each neuron class within the DA2 and DL5 (**Figure 2C**; **Table 1**, row 1). In addition, we
254 counted all T-bars and their output sites (1:1 synaptic contacts) as well as all postsynaptic sites
255 (input sites) for all neuron fibers together and for each neuron class individually (**Table 1**, **row 2-**
256 **4**). We counted in total ~ 14 000 synaptic contacts and 2648 T-bars in DA2 and ~ 17 000 contacts
257 and 3387 T-bars in DL5 (**Figure 2C, Table 1, row 4**). Most of these synapses were triads and tetrads
258 (**Figure 2 – figure supplement 1B-D**). In order to compare DA2 and DL5 we normalized neuronal
259 length and synaptic numbers to glomerular volume. We then analyzed (**1**) the innervation density,
260 i.e., the length of neuronal fibers per glomerular volume (µm/µm$^3$) and (**2**) the glomerular synaptic
261 density (T-bar #, output site or input site #/µm$^3$). Data are reported in total for all neuronal fibers
262 of each neuron class (**Table 1, row 5-8**) and as an average for neuronal fibers of the respective
263 neuron class **(Figure 3)**. In addition, we compared (**3**) the average polyadicity for each neuron class
264 **(Figure 3)** and **(4)** the average neuronal synaptic density (T-bar, output and input site density along
265 each neuronal fiber) (#/µm) (**Figure 3 – figure supplement 1B**).
266 We observed that the average neuron innervation density of OSNs was 20% higher in DA2
267 than in DL5 (**Figure 3A**)**, Table S1**). Also, the glomerular synaptic density of input sites, output sites
268 and T-bars along OSNs was significantly higher in DA2 than in DL5 (**Figure 3A**). OSNs in DA2 formed
269 therefore more input sites, and much more T-bars and output sites per glomerular volume than in
270 DL5 (**Table 1**, row 7-8; relative differences: **Table S1**). In contrast, the density of input sites
271 distributed along the length of OSN fibers was similar in DA2 and DL5, whereas T-bar and output
272 site density along the OSN axons was significantly higher in DA2 (**Figure 3 – figure supplement 1A**).
273
274 We then asked if the DA2 glomerulus, due to its higher number of uPNs, also had a higher
275 uPN innervation density and synaptic density of its postsynaptic sites and/or presynaptic sites
276 compared to the DL5 glomerulus, which contains a single uPN. In the DA2, the fibers of the 7 uPNs
277 had almost the same total length as the fibers of the single uPN in the more voluminous DL5 (4652
278 µm in DA2 vs. 5015 µm in DL5; **Table 1**, row 1). The DA2 uPNs had in addition a total number of
279 input sites comparable to that of the single uPN in DL5 (3887 vs. 3955; **Table 1**, row 2).
280 Consequently, the total innervation density of the 7 DA2-uPNs was higher than that of the single

uPN in DL5 (**Table 1**, row 5), even though the average innervation density per DA2-uPN was lower compared with that of the DL5 (**Figure 3B**). The total glomerular synaptic input density of all uPNs was higher in DA2 as compared with DL5 (**Table 1**, row 6). On the other hand, the total glomerular synaptic density of the T-bars and output sites was similar in DA2 and DL5 (**Table 1**, rows 7-8). In line with these results, the neuronal density of T-bars and output sites was less in the DA2 uPNs compared with the DL5 single uPN, whereas the neuronal density of input sites was similar (**Figure 3 – figure supplement 1B; Table 1**, row 9-10). This resulted in synaptic ratios (T-bars-to-inputs and outputs-to-inputs) in the DL5 uPN that were nearly twice as high as those in the DA2 uPNs (**Table 1**; row 12-13).

We then hypothesized that DA2 would exhibit a lower innervation density of MGNs (mainly LNs) compared to DL5, as previous studies have reported that DA2 is innervated by fewer LNs (Chou et al., 2010; Grabe et al., 2016). However, we observed the opposite: the innervation density of MGNs was significantly higher in DA2 than in DL5 (**Figure 3C**), with slightly higher total innervation density (**Table 1,** row 5)**.** Interestingly, only the glomerular input density was significantly higher for DA2 MGNs compared to that found in DL5, not the glomerular synaptic density of output sites or of the T-bars (**Figure 3C**). However, the total glomerular synaptic density of input sites, output sites and T-bars were still higher in DA2 than in DL5 **(Table 1,** rows 6-8**). The** synaptic densities along the MGN fibers were similar in DA2 and DL5 (**Figure 3 – supplement 1**).

In summary, the DA2 glomerulus is more densely innervated than DL5 and has a more densely packed neuropil with more synaptic contacts relative to the DL5. The DA2 has a significantly higher innervation density and higher density of T-bars, output and input sites per volume (**Figure 3D**, **Table 1,** row 5-8**).** The degree of synapse polyadicity is also significantly higher in DA2 than in DL5 (**Figure 3D, Table 1,** row 14) due to a shift to higher polyadicity among OSN (**Figure 3A**) and MGN synapses (**Figure 3C**). OSNs show the strongest shift in polyadicity, with tetrads being the most abundant synapse type in DA2 whereas triads are the most abundant in DL5 OSNs (**Figure 2 – figure supplement 1B**)**.**

## Lateralization of OSN glomerular connectivity

In *Drosophila melanogaster*, the majority of olfactory glomeruli receive bilateral OSN input (Stocker et al., 1983; Stocker et al., 1990; Vosshall et al., 2000; Silbering et al., 2011) (see scheme in **Figure 4A**). Recent studies have shown that ipsi- and contralateral OSNs are asymmetric in their synaptic connectivity to other neurons in the majority of the glomeruli (Tobin et al., 2017; Schlegel et al., 2021) and that ipsi- and contralateral OSNs activate uPNs in an asymmetric way (Gaudry et al., 2013; Tobin et al., 2017). However, not all glomeruli appear to have the same degree of lateralized OSN connectivity (Schlegel et al., 2021). At least for one narrowly tuned pheromonal glomerulus (DA1), there is functional evidence that in female flies (but not in males) its uPNs are evenly activated by either ipsi- or contralateral antennal stimulation (Agarwal & Isacoff, 2011). We

318 hypothesized that this lack of lateralization could be a feature of other narrowly tuned glomeruli
319 in female flies.
320 Ipsi- and contralateral OSNs in DA2 and DL5 were identified based on the location and
321 trajectory of their axons (**Figure 4B**). In both glomeruli, ipsilateral OSN terminals were longer than
322 their contralateral counterparts within the VOI, while polyadicity was stronger in contralateral
323 axons. Synaptic density was not consistently higher or lower in ipsilateral OSNs compared to
324 contralateral ones in DA2 and DL5 (**Figure 4 – figure supplement 1**).
325 We observed that the synaptic output of ipsi- vs. contralateral OSNs was asymmetric, with
326 significant differences in the ipsi- and contralateral OSN output to either uPNs, OSNs or MGNs
327 (**Figure 4C**, DA2 and DL5). In agreement with previous observations in other glomeruli (Schlegel et
328 al., 2021), the output fraction to uPNs and OSNs was greater in ipsilateral OSNs than in
329 contralateral ones (**Figure 4C**, DA2 and DL5). Vice versa, the OSN output to MGNs was greater in
330 the contralateral glomerulus than in the ipsilateral side (**Figure 4C**, DA2 and DL5). However, the
331 differences between the medians and means were smaller in DA2 than in DL5 (**Figure 4C**;
332 differences between means: see data availability).
333 Our finding of less lateralized connections in the DA2 (**Figure 4C**, DA2 and DL5) was also
334 observed in another narrowly tuned glomerulus (VA1v; (Dweck et al., 2015)) for which connectome
335 data is available (Horne et al., 2018). In VA1v, the OSN output to uPNs and MGNs was significantly
336 asymmetric in the same manner as in DA2, i.e., with greater ipsilateral OSN output fractions to
337 uPNs and greater contralateral OSN output fraction to MGNs (**Figure 4C**). However, asymmetry in
338 the VA1v OSN output fractions was even less distinct than in DA2 (regarding both the difference
339 between the median and the mean; **Figure 4C** and data availability). In addition, in VA1v, the OSN
340 output fraction to other OSNs was symmetric (**Figure 4C**).
341 The OSN input, from either sister OSNs or MGNs, was asymmetric in DL5 but not in the narrowly
342 tuned glomeruli (**Figure 4D**). The inputs from uPNs to ipsi- or contralateral OSNs were not
343 compared due to their low numbers.
344 In summary, our data add to the knowledge of lateralized connectivity within olfactory
345 glomeruli and supports the hypothesis that narrowly tuned glomeruli have a lower degree of
346 lateralization of OSN connectivity compared with broadly tuned glomeruli.
347

348 **Glomeruli DA2 and DL5 differ in several features of their circuitry**

349 Next, we asked whether the synaptic circuitries of DA2 and DL5 differ from each other. We
350 counted each synaptic contact (**Table S3 and S4**) and categorized the distinct connection motifs
351 according to the neuron class to which the output and input neuron belonged (**Figure 5A; Table**
352 **S2).** Each connection motif (for example OSN>uPN, i.e., the OSN-to-uPN feedforward connection)
353 was then assessed for its relative synaptic strength, i.e., how many synaptic contacts of this

354 particular connection motif were found compared to the total number of synaptic contacts within
355 the respective circuitry (**Figure 5A-D**; see Methods).
356 We found that neurons from each class made synaptic contacts with each other in DA2 and
357 DL5, as previously reported for other glomeruli (Berck et al., 2016; Rybak et al., 2016; Tobin et al.,
358 2017; Horne et al., 2018; Schlegel et al., 2021). In both DA2 and DL5, OSNs provided the strongest
359 relative synaptic output, i.e., 49% of all synaptic connections in DA2 and 43% in DL5 were formed
360 by OSNs (**Figure 5B-C**). Thus, even though DA2 and DL5 had similar numbers of OSNs (44 and 46,
361 respectively), those in DA2 provided a stronger circuit output (14% stronger; **Table S2**) than those
362 in DL5 (**Figure 5B-C)**. In both glomeruli the main output partners of OSNs were MGNs and uPNs,
363 i.e., 27% of all circuitry connections in DA2 and 24% in DL5 were OSN>MGN connections, while
364 20% in DA2 and 18% in DL5 were OSN>uPN connections (**Figure 5B-C**). In DA2, interestingly, each
365 of the 7 uPNs received input from almost all OSNs and so could maintain a high degree of
366 convergent signal transmission (**Table S3**). In contrast, OSNs received the lowest relative input of
367 all neuron classes in DA2 and DL5 (7% and 8% respectively; **Figure 5B-C**). In line with previous
368 observations in other glomeruli (Horne et al., 2018; Schlegel et al., 2021), OSNs also made
369 abundant axo-axonic synapses with sister OSNs (2.6% in DA2 and 1.5% in DL5; **Figure 5B-C**). Thus,
370 the relative synaptic strength of the OSN>OSN connection was 70% stronger in DA2 than in DL5
371 (**Figure 5B-C; Table S2**).
372 The uPNs in both glomeruli had the weakest relative output of all neuron classes within their
373 circuitry, and this was even weaker (38%) in DA2 (**Figure 5B-C; Table S2**). In contrast, the relative
374 synaptic input onto uPNs was greater in DA2 than in DL5 (33% vs. 28%, respectively; **Figure 5B-C;**
375 16% stronger in DA2; **Table S2**), which is in line with our finding that in DA2, the uPNs provide more
376 input sites per unit of glomerular volume than in the DL5 (**Figure 3B-C**). In both glomeruli, the
377 feedback connections from uPNs (depicted in **Figure 5A**), were almost exclusively directed towards
378 MGNs, as previously reported for the broadly tuned DM6 and the narrowly tuned glomerulus VA1v
379 (Tobin et al., 2017; Horne et al., 2018). However, the relative synaptic strength of the uPN>MGN
380 connection was 40% weaker in DA2 than in DL5 (uPN>MGN: 10% in DA2 and 17% in DL5). Only a
381 few cases of uPN>OSN synaptic connections were observed (a total of 16 in DA2 and 26 in DL5)
382 representing a synaptic strength of 0.1% in DA2 and 0.2% in DL5 (**Table S2**). Finally, uPNs in DA2
383 also made 71 reciprocal synaptic connections (representing a synaptic strength of 0.6%; **Table S2**;
384 **Figure 5B**), consistent with electrophysiological evidence for reciprocal synaptic interactions
385 between sister uPNs (Kazama & Wilson, 2009). The single uPN of the DL5 had 54 dendro-dendritic
386 synapses (representing 0.4% of all DL5 synaptic contacts; **Figure 5C**), which were exclusively
387 autapses, i.e., synapses formed by a neuron onto itself. Dendritic uPN autapses exist also in DA2-
388 uPNs, but they were few: we observed only 14 autaptic uPN-uPN connections in DA2, which were
389 mainly located at the two longest uPN dendrites (for further analysis of autapses see next section).
390 MGNs received the strongest input in both glomeruli (60% of the total input in DA2 and 64%
391 in DL5; **Figure 5B-C**). This is in line with the observation that MGNs provided the majority of all

392 traced neuronal fibers in each glomerulus and had the highest innervation density of all neuron
393 classes; **Table 1**). The relative output strength of MGNs was similar in both glomerular circuits
394 (~40% of the total output in each glomerulus; **Figure 5B-C**). MGNs made many reciprocal synapses
395 to each other, accounting for 23% of all synapses in both glomeruli (**Figure 5B-C)**. The relative
396 synaptic strength between MGN>uPN was stronger in DA2 (12%) than DL5 (10%) (**Figure 5B-C**;
397 **Table S2**). The MGN>OSN feedback connection was relatively weak in both glomeruli (5% in DA2
398 vs. 6% in DL5; **Figure 5B-C**) but weaker (25%) in DA2 than in DL5 (**Table S2**).
399 We then looked at the fractional output and input of each neuron class (**Figure 5E', E''**). In
400 both glomeruli OSNs had a similar proportion of their synaptic output onto uPNs (40%-41%), onto
401 MGNs (55% in both) and onto sister OSNs (4%-5%) (**Figure 5E'**). From the uPNs perspective, over
402 93%-96% of their recurrent synaptic output was directed to MGNs in both DA2 and DL5, and few
403 synapses were directed onto OSNs (~1% of the uPN output; **Figure 5E'**). The uPN>uPN output
404 fraction of the 7 uPNs in DA2 (reciprocal synapses) was twice the uPN output fraction (autaptic) of
405 the single uPN dendrite in DL5 (6% vs. 3%; **Figure 5E'**). MGNs formed synaptic output mainly to
406 other MGNs (58%-59% of the total MGN output in DA2 and DL5). Among MGNs we found also rare
407 cases of autapses. The MGN>uPN output fraction was greater in DA2 (30%) than in DL5 (25%),
408 whereas the MGN>OSN output fraction was smaller in DA2 (12%) than in DL5 (16%; **Figure 5E'**).
409 Turning to the input fractions of each neuron class, we found that in both glomeruli, OSNs
410 received most of their input from MGNs (>50%). In DA2 the input fraction onto OSNs (MGN>OSN)
411 was smaller than in DL5 (63% vs. 78%; **Figure 5E''**). In contrast, the OSN input fraction from sister
412 OSNs was greater in DA2 (35% vs. 20%; **Figure 5E''**). In both glomeruli, the OSNs received only weak
413 uPN input (2%) (**Figure 5E''**). The input fractions onto the 7 uPNs, formed by uPNs, MGNs and OSNs,
414 in the DA2 and the single uPN in DL5 were similar (**Figure 5E''**). Most uPN input was delivered by
415 OSNs (~62% in both glomeruli) and less from MGNs (~36%). The uPN input fraction from other
416 uPNs in DA2 or the autaptic input from the single uPN in DL5 was small (2%; **Figure 5E''**). In DA2
417 the MGNs received a smaller fraction of uPN feedback input than in DL5 (17% vs. 26%; **Figure 5E''**)
418 but a greater OSN input fraction (45% vs. 38%; **Figure 5E''**). The fraction of MGN>MGN input was
419 similar in both glomeruli.
420 To further explore whether the differences found in the circuitry between DA2 and DL5
421 reported here might represent features characteristic of narrowly tuned glomeruli, we analyzed
422 connectome data from another narrowly tuned glomerulus (VA1v; (Horne et al., 2018). We
423 calculated the relative synaptic strength between OSNs (n=107), uPNs (n=5) and MGNs (n=74) in
424 the VA1v (**Figure 5D; Table S2**). We found that the two narrowly tuned glomeruli shared five circuit
425 features that differentiates them from the broadly tuned glomerulus DL5: First, OSNs in VA1v, as
426 reported above for DA2, displayed a stronger relative feedforward output to uPNs (22%) and to
427 MGNs (32%), which was even larger than in DA2 (**Figure 5D**). The uPNs and MGNs in VA1v, received
428 a larger fraction of OSN input than in DL5 (**Figure 5E''**). Second, the OSN>OSN synaptic output was
429 four times stronger (6%) than in DL5 (1.5%; **Figure 5B-D, Table S1**). This was also reflected in the

430 OSN output fraction to sister OSNs (10%), which in VA1v was more than twice that of DL5 (4%;
431 **Figure 5E'**) and in the much greater OSN input fraction (38%) to OSNs in the VA1v than in DL5 (20%;
432 **Figure 5E''**). This was in line with previous connectome analysis, showing much stronger OSN input
433 from sister OSNs in narrowly tuned glomeruli, such as DL4, DL3 or DA1 compared to the broadly
434 tuned ones, such as DM4 or DM1 (Schlegel et al., 2021). Third, in the VA1v the uPN>uPN relative
435 synaptic output was more than twice that of the DL5 uPN (mediated by autapses) (1% vs. 0.4% in
436 DL5; **Figure 5D**), which is in accordance with a much greater uPN output fraction to uPNs (14%) in
437 VA1v than in DL5 (3%) (**Figure 5E'**). Forth, VA1v uPNs had fewer feedback synapses onto MGNs
438 than in DL5 (relative synaptic strength of uPN>MGN connection: 6% vs. 17%; **Figure 5C-D**), also
439 reflected in a smaller output fraction from uPNs to MGNs in VA1v than in DL5 (81% vs. 96%; **Figure**
440 **5E'**). In agreement, the MGN input fraction from uPNs in VA1v was much smaller than in DL5 (10%
441 vs. 26%; **Figure 5E''**). Fifth, OSNs in VA1v received a smaller MGN input fraction than DL5 OSNs
442 (60% vs. 78%; **Figure 5E''**).
443 In addition to the shared connectivity differences (either stronger or weaker) between DA2
444 and VA1v that distinguish them from DL5, two connection motifs were found to be stronger in DA2
445 and DL5 than in VA1v: The MGN>uPN connection showed a synaptic strength of 12% and 10% in
446 DA2 and DL5 vs. 8% in VA1v (**Figure 5B-D, Table S2**). In agreement with this, the MGN output
447 fraction to uPNs (**Figure 5E'**, MGN output) and the MGN input fraction in uPNs was greater in DA2
448 and DL5 than in VA1v (**Figure 5E''**, uPN input). The relative synaptic strength in MGN>MGN motifs
449 was similar between DA2 and DL5 (23%; **Figure 5B-C**), but weaker in VA1v (17%; **Figure 5D, Table**
450 **S2**). This was also reflected in a smaller MGN output and input fraction from or to MGNs (**Figure**
451 **5E' and E''**).
452 In summary, the two narrowly tuned glomerular circuits studied here shared five circuit
453 features when compared with the broadly tuned glomerular circuit (all glomerular circuit features
454 in DA2, DL5 and VA1v are shown in **Figure 6A**). These features were (1) a stronger OSN>uPN and
455 OSN>MGN connection, (2) a much stronger axo-axonic communication between sister OSNs, (3) a
456 stronger dendro-dendritic connection between uPN dendrites, (4) lateralization of OSN
457 connectivity is weaker in narrowly tuned circuits of DA2/Va1v, (5) less feedback from uPNs to
458 MGNs and (6) less feedback from MGNs to OSNs (**Figure 6B**). These findings, which may have
459 important computational implications for glomerular circuits processing a single odorant identity,
460 distinguish them from broadly tuned circuits and are summarized in the graphical representation
461 in **Figure 8**.
462

463 **Autapses in the large DL5 uPN connect distant regions of its dendritic tree**

464 Autapses (synapses made by a neuron upon itself) have seldomly been reported in the
465 *Drosophila* central nervous system (Takemura et al., 2015; Horne et al., 2018). In the DA2
466 glomerulus, we found few autapses in uPNs and MGNs (**Figure 5C; Figure 7A**). In contrast, within

467 the dendritic tree of the single DL5 uPN, three observers independently identified 54 autaptic
468 connections (see Methods). This represents 3% of the output connections of this neuron and 0.4%
469 of all synaptic contacts in the whole glomerulus (**Figure 7A**; **Figure 5C; E'**). We found that these
470 autapses were not distributed evenly along the dendritic tree of the DL5 uPN. Some dendritic
471 branches received several autaptic inputs, whereas other had no autaptic input (**Figure 7A**) and we
472 hypothesized that these autapses could connect distant parts of this very large dendritic tree. We
473 thus analyzed the exact location and distribution of their presynaptic and postsynaptic sites (**Figure**
474 **7A**) We discovered a difference in the distribution of the pre- and postsynaptic elements of DL5
475 autapses. While their presynaptic T-bars were evenly distributed at basal (strahler order: 5) and at
476 distal regions (strahler order: 1-4), 95% of their postsynaptic sites were located in the most distal
477 region (strahler order 2-1; **Figure 7B-C**). We also calculated the geodesic distance (i.e., along-the-
478 arbor distance) from pre- and post-synaptic sites to the basal root node, which is the node point
479 where the DL5 uPN enters the glomerulus and is equivalent to the closest point to the soma in our
480 reconstruction. The geodesic distance to the basal root node from the presynaptic site was
481 significantly shorter than for postsynaptic sites (**Figure 7 – figure supplement 1B**). The pre- and
482 postsynaptic sites of each autapses were either close to each other along the dendritic tree, or
483 distant from each other (see examples in the dendrogram depicted in **Figure 7D**). Thus, the
484 geodesic distance between pre- and postsynaptic sites, (see scheme in **Figure 7E**), as well as the
485 number of branching points between pre- and postsynaptic partners, were bimodally distributed
486 (**Figure 7F-G**). Autapses that connected distant dendritic branches were more frequent than those
487 that connected close dendritic branches (**Figure 7E-G**). In summary, we found abundant autapses
488 within the uPN dendrite of DL5 and they were unevenly distributed, with many output sites located
489 in a few sub-branches connecting distal dendritic regions.

490 **DISCUSSION**

491 We hypothesized that specialized, narrowly tuned olfactory glomeruli differ in their
492 ultrastructure and microcircuitry from broadly tuned glomeruli. By comparing data from dense
493 reconstructions of two narrowly tuned olfactory glomeruli with that of a broadly tuned glomerulus
494 in *Drosophila melanogaster,* we identified prominent features of narrowly tuned glomeruli related
495 to synaptic composition, lateralization of sensory input and synaptic circuitry.
496

497 ## Glomerular circuit analysis: a correlative approach

498 The small size of olfactory glomeruli in *Drosophila* gave us the opportunity to reconstruct
499 and analyze the dense connectome of entire glomeruli with volume-based electron microscopy in
500 a reasonable time period. Here we developed a correlative workflow that combines transgenic
501 neuron labeling with near-infra-red-laser-branding for precise volume targeting. We then used FIB-
502 SEM (Bishop et al., 2011) to resolve glomerular networks at the synaptic level. A similar procedure
503 was used recently to investigate single cellular organelles (Ronchi et al., 2021). An advantage of
504 this approach is that it facilitates localization of the volume of interest with high precision and
505 consequently limits to a minimum the volume to be scanned and reconstructed. At the same time,
506 the limitation in volume is a drawback of our workflow, as it was impossible to reconstruct neurons
507 back to their soma. This fact prevented the identification of individual neurons as in other
508 connectome studies (Berck et al., 2016; Eichler et al., 2017; Horne et al., 2018; Zheng et al., 2018;
509 Bates et al., 2020; Scheffer et al., 2020; Xu et al., 2020; Schlegel et al., 2021).
510 We provide data on innervation and synapse density of olfactory sensory neurons (OSNs),
511 uniglomerular projection neurons (uPNs) and multiglomerular neurons (MGNs) in the *Drosophila*
512 AL. We observed a higher innervation density of all neuron types – primarily uPNs and MGNs – as
513 well as higher density of synaptic contacts along OSN terminals in the narrowly tuned DA2
514 compared with DL5. These results suggest that narrowly tuned glomeruli have a more densely
515 packed neuropil, with more numerous synaptic connections in the feedforward motifs OSN>uPN
516 and OSN>MGN. Overall, our observations on synapse density were comparable with previous
517 reports (Mosca & Luo, 2014; Rybak et al., 2016; Horne et al., 2018).
518

519 ## Specific features of narrowly tuned glomerular circuits

520 Our analysis ultimately revealed six circuit features shared by the narrowly tuned glomeruli
521 DA2 and VA1v (with VA1v data analyzed from Horne et al., 2018) that distinguish them from the
522 circuitry of the broadly tuned DL5 and may represent adaptations specific to such dedicated
523 glomerular circuits (see summary in **Figure 8**). However, future studies, analyzing the precise
524 number of synaptic connections across a larger number of individuals are needed to assess intra-
525 and inter-animal variability (Schlegel et al., 2024). In addition, combining these anatomical

526 observations with physiological studies and computational modeling are essential to evaluate the
527 functional relevance of the observed connectivity differences and to test our hypothesis regarding
528 generic circuit-level distinctions between narrowly and broadly tuned olfactory glomeruli (**Figure**
529 **8**).

530 **The OSN>uPN feedforward connection is stronger in narrowly tuned glomeruli**

531 Presynaptic OSN terminals provide the major input to uPNs in insect olfactory glomeruli
532 (Hansson & Anton, 2000; Chen & Shepherd, 2005; Kazama & Wilson, 2008; Lei et al., 2010; Tobin
533 et al., 2017; Horne et al., 2018; Rybak & Hansson, 2018; Schlegel et al., 2021). Here we showed
534 that this connection is stronger in DA2 and VA1v than in DL5 (**Figure 5 and 6**). A strong OSNs>uPN
535 synaptic connection will drive non-linear signal amplification, which improves signal detection at
536 low odor concentrations (Ng et al., 2002; Bhandawat et al., 2007; Kazama & Wilson, 2008; Masse
537 et al., 2009). A larger number of synapses of this type could be an adaptation to improve this
538 amplification effect, as shown by artificial increase of synaptic sites in the AL (Acebes & Ferrus,
539 2001) and in lateral horn dendrites (Liu et al., 2022).
540 Each of the 7 uPNs in DA2 received convergent synaptic input from almost all DA2-OSNs.
541 This is in agreement with reports on the narrowly tuned glomeruli DA1 and VA1v (Agarwal &
542 Isacoff, 2011; Jeanne & Wilson, 2015; Horne et al., 2018) and for broadly tuned glomeruli (Vosshall
543 et al., 2000; Chen & Shepherd, 2005; Kazama & Wilson, 2009; Masse et al., 2009; Tobin et al.,
544 2017). High OSN>uPN convergence is the main driver of highly correlated activity among uPNs in
545 pheromone coding glomeruli in flies as well as moths (Kazama & Wilson, 2009; Rospars et al.,
546 2014). High convergence in the lateral horn improves signal transmission from uPNs to lateral horn
547 neurons without sacrificing speed (Jeanne & Wilson, 2015; Huoviala et al., 2020). In the mushroom
548 body calyces, however, the high degree of convergence is only pursued for DA2 uPNs, which
549 converge onto few Kenyon cells, whereas VA1v uPNs synapse randomly onto many dispersed
550 Kenyon cells (Caron et al., 2013; F. Li et al., 2020), indicating diverse signal integration in the
551 mushroom body.
552 From our study, we hypothesize that in narrowly tuned glomerular circuits, which have
553 more uPNs, the maintained strong OSN>uPN convergence, improve signal transmission accuracy.
554 Secondly, a stronger OSN>uPN connection might compensate for the lack of OSN>uPN signal
555 transmission sites in the case of odorants activating OSNs in a single glomerulus.

556 **Reciprocal connections between sister OSNs and sister uPNs are stronger in narrowly tuned**
557 **glomeruli**

558 The reciprocal OSN-OSN synapse is generally stronger in narrowly tuned glomeruli DA1, DL3
559 and DL4, compared with broadly tuned glomeruli DL5, DM1, DM4 and DM6 (Suh et al., 2004;
560 Knaden et al., 2012; Dweck et al., 2015; Ebrahim et al., 2015; Grabe et al., 2016; Seki et al., 2017;

561 Tobin et al., 2017; Schlegel et al., 2021). A high degree of axo-axonic synapses between sister OSNs
562 was also found in VA1v (Horne et al., 2018; Schlegel et al., 2021) and DA2 but not in the DL5 (this
563 study). Hence, we suggest that a strong OSN-OSN connection is a characteristic feature of the
564 synaptic circuitry of narrowly tuned olfactory glomeruli. Axo-axonic connections have also been
565 reported between gustatory and mechanosensory neurons in *Drosophila* larvae (Miroschnikow et
566 al., 2018) and in the olfactory epithelium and the olfactory bulb of vertebrates (Hirata, 1964;
567 Shepherd et al., 2021). In vertebrates, axo-axonic synapses between excitatory sensory neurons
568 are involved in correlated transmitter release (Cover & Mathur, 2021), reminiscent of correlated
569 uPN activity due to reciprocal synaptic and electric coupling in the *Drosophila* AL and LH (Kazama
570 & Wilson, 2009; Huoviala et al., 2020). A strong OSN-OSN connection also has the potential to
571 increase the correlation of OSN spiking events and therefore facilitate a robust OSN signal (de la
572 Rocha et al., 2007).
573 Reciprocal dendro-dendritic synapses between sister uPNs are reported here for the DA2
574 have been reported previously also for glomeruli DM6, DM4, VA7 and VA1v (Kazama & Wilson,
575 2009; Rybak et al., 2016; Tobin et al., 2017; Horne et al., 2018). These types of synapses enhance
576 uPN signal correlation (Kazama & Wilson, 2009), as reported for mitral and tufted cells of the
577 vertebrate olfactory bulb, the circuit equivalent to PNs of insect ALs (Christie et al., 2005; McTavish
578 et al., 2012; Shepherd et al., 2021). In *Drosophila* multiple uPNs could induce correlated PN
579 depolarization events, which improve the signal-to-noise-ratio of PN signal transmission (Chen &
580 Shepherd, 2005; Kazama & Wilson, 2009; Jeanne & Wilson, 2015).
581 In summary, our data give evidence that reciprocal OSN-OSN and uPN-uPN connections are
582 a prominent feature of the synaptic circuit of narrowly tuned glomeruli. We suggest that those
583 reciprocal OSN-OSN and uPN-uPN connections support correlation of neuronal activity and
584 therefore boosts signal induced depolarization events. This will in turn enhance the signal-to-noise
585 ratio (accuracy) and transmission probability of weak and/or irregular odorant input, increasing
586 processing speed.

587 **Less lateralization in the OSN bilateral connectivity in narrowly tuned glomeruli**

588 In *Drosophila*, most OSN axons project bilaterally and form synapses in their corresponding
589 glomerulus on both the left and right brain hemispheres (Stocker et al., 1990; Vosshall et al., 2000;
590 Couto et al., 2005; Kazama & Wilson, 2009; Silbering et al., 2011; Tobin et al., 2017; Schlegel et al.,
591 2021). This is rarely observed in other insects and absent in vertebrates (Stocker et al., 1983;
592 Masson & Mustaparta, 1990; Galizia et al., 1998; Hansson & Anton, 2000; Anton et al., 2003;
593 Parthasarathy & Bhalla, 2013; Dalal et al., 2020). In the mammalian olfactory system, bilateral
594 comparison of olfactory input only occurs in higher brain centers (Dalal et al., 2020). In flies,
595 bilateral sensory input enables them to discriminate odor sources of different spatial origin
596 through bilateral comparison of olfactory stimulation (Borst & Heisenberg, 1982; Duistermars et
597 al., 2009; Gaudry et al., 2013; Mohamed, Hansson, et al., 2019; Taisz et al., 2023). Asymmetric OSN

connectivity, shown for many olfactory OSNs (Tobin et al., 2017; Schlegel et al., 2021) seems to be the origin of a bilateral contrast in the uPN response (Agarwal & Isacoff, 2011; Gaudry et al., 2013; Tobin et al., 2017; Taisz et al., 2023), and is most likely the key to precise odor source localization (Taisz et al., 2023). Bilateral comparison is also used in the lateral horn (a higher olfactory brain center in *Drosophila*) for odorant position coding (Mohamed, Hansson, et al., 2019). However, not all glomeruli are similar in the magnitude of bilateral asymmetry with respect to their OSN connectivity (Schlegel et al., 2021) or their uPN responses (Agarwal & Isacoff, 2011).

In agreement with observations in most of the olfactory glomeruli (Schlegel et al., 2021; Taisz et al., 2023), we found that glomeruli DL5, DA2 and VA1v have ipsilaterally asymmetric OSN synaptic output to excitatory uPNs and sister OSNs and contralaterally an enhanced OSN>MGN output (**Figure 4**). We believe that, in agreement with a recent study, these asymmetric connections determine a strong left-right-contrast in the uPN response, akin to a "winner-takes-all" principle (Taisz et al., 2023).

We also observed that the degree of bilateral OSN asymmetry in DA2 and VA1v was much weaker than in DL5 (**Figure 4**). Weakly lateralized OSN connectivity is perhaps insufficient to induce an adequate bilateral contrast necessary for odor source localization. Recent work supports this idea by showing the importance of the interplay of asymmetric OSN signaling and LN inhibition to enhance the bilateral contrast of uPN activity and to facilitate navigation (Taisz et al., 2023).

Why do these narrowly tuned glomeruli have weaker bilateral contrast than broadly tuned glomeruli? The answer could lie in the ecological significance of the individual odorants. Geosmin, encoded by glomerulus DA2 (Stensmyr et al., 2012), and the pheromone methyl laurate, encoded by glomerulus VA1v (Dweck et al., 2015), act at short distances, mainly when the fly is walking and not flying. Perhaps, the behavioral response to geosmin or methyl laurate does not need a precise odor source location. On the other hand, food odor detection at a distance, which happens mainly at flying conditions, needs continuous processing of odor position and body alignment to navigate towards the odor source (Thoma et al., 2015; Demir et al., 2020). The bilateral OSN projection onto uPNs in DA2 and VA1v potentially has a distinct function other than odor position coding and could, via the enhancement of the effect of convergence of OSN>uPN signal transmission, enhance odor signal amplification (Bhandawat et al., 2007; Kazama & Wilson, 2009; Masse et al., 2009; Jeanne & Wilson, 2015).

### Distinct synaptic integration of local modulatory neurons in narrowly tuned glomeruli

MGNs are composed of multiglomerular projection neurons (mPNs) that project directly to the LH (Jefferis et al., 2007; Strutz et al., 2014; Bates et al., 2020) and inhibitory and excitatory local interneurons (LNs) that interconnect the AL glomeruli (Masse et al., 2009; Okada et al., 2009; Chou et al., 2010; Seki et al., 2010; Liu & Wilson, 2013). Since LNs are the most numerous and broadly arborizing of the multiglomerular cell types in the AL (Chou et al., 2010; Lin et al., 2012), we focus our discussion on these neurons. A quantitative analysis of MGN connectivity in the VA1v

635 glomerulus - where LNs and multiglomerular projection neurons (mPNs) were classified separately
636 - supports this focus. It shows that 84% of the MGN output originates from LNs, and 57% of MGN
637 input is received by LNs. When excluding the major OSN>mPN and OSN>LN input, the majority of
638 remaining MGN input is from LNs (73%) (data source: (Horne et al., 2018). Multiglomerular LNs
639 play a crucial role in modulating OSN-to-uPN signal transmission within the olfactory glomeruli
640 (Masse et al., 2009; Chou et al., 2010; Seki et al., 2010; Galizia, 2014; Szyszka & Galizia, 2015).
641 Previous observations have shown that glomeruli DA2 and VA1v have a lower number of
642 innervating LNs (Chou et al., 2010; Grabe et al., 2016) and receive less global interglomerular LN
643 inhibition than broadly tuned glomeruli (Hong & Wilson, 2015). We therefore assumed that DA2
644 or VA1v would have a lower LN innervation density and less LN synaptic integration in their
645 circuitry. However, we did not observe a general lower synaptic integration in DA2 **(Figure 5**) and
646 found a greater MGN innervation density, and a higher density of input sites than in DL5. VA1v
647 MGNs on the other hand received less synaptic input and provided less output in its glomerular
648 circuit than MGNs in DL5.
649 Taking a closer look at particular synaptic connection motifs of MGNs we saw that narrowly
650 tuned glomeruli had a relatively weak uPN>MGN feedback (**Figure 6, see also Figure 8**). uPN
651 feedback onto LNs and their reciprocal connection (LN>uPN) were reported in *Drosophila* and
652 other insects, such as honey bees, cockroaches and moths, but their function is still poorly
653 understood (Boeckh & Tolbert, 1993; Sun et al., 1997; Sachse & Galizia, 2002). In the honey bee
654 reciprocal dendro-dendritic synapses between excitatory and inhibitory neurons enhance signal
655 contrast and the reliability of true signal representations throughout the AL (Yokoi et al., 1995;
656 Sachse & Galizia, 2002). Here we could not differentiate the LN types involved in the uPN>MGN
657 synaptic motif. However, the prevailing uPN>LN synapses involve mainly widespread pan-
658 glomerular LNs in the adult (Horne et al., 2018) and larval AL (Berck et al., 2016) which are
659 important for combinatorial coding (Galizia, 2014; Sachse & Hansson, 2016). Thus, weaker
660 uPN>MGN feedback in the narrowly tuned DA2 and VA1v circuits might be a compensatory
661 mechanism to lower the computational demand of interglomerular communication for odor
662 identity coding.
663 We also observed that OSNs received less MGN feedback in the narrowly tuned DA2 and
664 VA1v than in the DL5, suggesting that the OSNs in DA2 and VA1v receive relatively weak
665 presynaptic input. Pan-glomerular GABAergic LNs constitute the main input to OSN presynaptic
666 sites (Berck et al., 2016; Schlegel et al., 2021). These inhibitory LNs are prime candidates for
667 mediating presynaptic inhibition onto OSNs (Wilson & Laurent, 2005; Olsen & Wilson, 2008; Chou
668 et al., 2010; Olsen et al., 2010) and thought to drive balanced glomerular gain control. They play a
669 key role in odor identity coding by modulating both the balance and dynamics of incoming and
670 varying odor intensities (Olsen & Wilson, 2008; Root et al., 2008; Silbering et al., 2008; Asahina et
671 al., 2009; Wang, 2012; Galizia, 2014; Hong & Wilson, 2015; Szyszka & Galizia, 2015; Sachse &
672 Hansson, 2016). Our data support these observations and provide an argument for why narrowly

673 tuned OSNs receive much lower inhibition during AL stimulation with odorants activating other
674 OSN populations (Hong & Wilson, 2015). Even though DA2 and VA1v might receive less
675 interglomerular inhibition, their OSN>MGN output is still strong, in agreement with studies
676 showing that throughout the AL, global lateral inhibition mediated by LNs scales with general OSN
677 activation (Olsen & Wilson, 2008; Hong & Wilson, 2015).
678 In summary, narrowly tuned circuits are probably influenced more strongly by
679 intraglomerular than by interglomerular modulation. Narrowly tuned circuits perhaps have greater
680 computational capacities in intraglomerular modulation of signal transmission, which could be
681 important for example for PN fine-tuning and response adjustment (Ng et al., 2002; Assisi et al.,
682 2012).
683 Above we discussed putative generic features of narrowly tuned glomerular circuits.
684 Besides these circuit features, we found a strong MGN>MGN connection in the aversive glomerular
685 circuits DA2 and DL5 in contrast to a much weaker MGN>MGN connection in the attractive
686 glomerulus VA1v (Knaden et al., 2012; Stensmyr et al., 2012; Knaden & Hansson, 2014; Dweck et
687 al., 2015; Mohamed, Retzke, et al., 2019). Why do aversive olfactory circuits have a stronger
688 MGN>MGN connection than attractive circuits? In the larval *Drosophila* AL, reciprocal LN>LN
689 synapses induce disinhibition induced by a strong connection between the pan-glomerular LNs and
690 a bilateral projecting LN, the Keystone LN, which synapses strongly onto pan-glomerular LNs and
691 selectively onto OSNs, which are activated by attractive food odors. This is thought to be a key
692 feature to switch from homogenous to heterogeneous presynaptic inhibition and therefore to a
693 selective gain control enhancing contrast between attractive and aversive odor activation (Berck
694 et al., 2016). Such balanced inhibitory systems could also be present in the adult *Drosophila* AL,
695 reflected in the strong LN>LN connection in DA2 and DL5. Disinhibition of interglomerular
696 presynaptic inhibition in aversive glomeruli circuits might be important for the fly to stay vigilant
697 to aversive odors, while perceiving attractive cues, for example during feeding conditions so that
698 a fast switch in behavior can be initiated if necessary.
699

700 **Autaptic connection within the dendritic tree of a single uPN**

701 We observed autapses along the large dendritic tree of the single DL5-uPN. To our
702 knowledge, this is the first report of bulk dendro-dendritic autapses in the *Drosophila* olfactory
703 system, indicating a cell-type specific occurrence of autapses in the DL5-uPN as reported for other
704 cell types in the optic lobe (Takemura et al., 2015). Autapses are also reported to be present at
705 different frequencies in different types of neurons in the mammalian brain (Van der Loos & Glaser,
706 1972; Tamás et al., 1997; Bekkers, 1998; Bacci & Huguenard, 2006; Ikeda & Bekkers, 2006; Bekkers,
707 2009; Saada et al., 2009). In *Drosophila,* most uPNs are cholinergic (Yasuyama & Salvaterra, 1999;
708 Yasuyama et al., 2003; Kazama & Wilson, 2008; Tanaka et al., 2012; V. Croset et al., 2018) and the
709 DL5-uPN autapses reported here might activate either nicotinic or muscarinic acetylcholine

postsynaptic receptors**.** Muscarinic acetylcholine receptors have an inhibitory effect in the Kenyon cells of the mushroom body (Bielopolski et al., 2019), but mediate excitation in the AL (Rozenfeld et al., 2019)**.**

What could be the function of these autaptic feedback loops within the DL5-uPN dendritic tree? Recent studies in vertebrates show that excitatory autapses enhance neuron bursting and excitability (Guo et al., 2016; Wiles et al., 2017; Yin et al., 2018). Autaptic inhibitory connections have been implicated in circuit synchronization, spike-timing precision, self-stabilization of neuronal circuits and feedback inhibition (Ikeda & Bekkers; Van der Loos & Glaser, 1972; Tamás et al., 1997; Bekkers, 1998; Bacci & Huguenard, 2006; Saada et al., 2009).

Autapses in the DL5 uPN form mainly long-distance feedback loops, connecting distinct dendritic subtrees and the basal dendrite region (closer to the soma) with distal branches. This spatial segregation is similar to the distribution of non-autaptic pre- and postsynaptic sites in *Drosophila* uPNs, where presynaptic sites are located more frequently at basal dendrites than postsynapses (Rybak et al., 2016) and in other insects, such as *Periplaneta americana* and moths (Malun, 1991; Sun et al., 1997; Lei et al., 2010). Dendro-dendritic autaptic feedback loops connecting basal to distal branches and distinct dendritic subtrees of a large dendritic tree might facilitate activity correlation between distant dendritic subunits, as described for non-autaptic, reciprocal uPN>uPN connections (Kazama & Wilson, 2009). This could be important in a large compartmentalized dendrite that receives inhomogeneous excitation by several OSNs at distinct dendritic sites, in order to enhance synchronized depolarization events along the dendrite, supporting signal integration (Graubard et al., 1980; Tran-Van-Minh et al., 2015). Clustered autapses could mediate local signal input amplification for distinct dendritic subunits (Kumar et al., 2018; Liu et al., 2022). Autaptic contacts, finally, could be able to shift the uPN membrane depolarization towards the spiking threshold, and enhance the firing probability during activation.

In conclusion, we provide a comprehensive comparative analysis of the ultrastructure and synaptic circuitry of two functionally diverse olfactory glomeruli with distinct computational demands, processing either single odorant information in a dedicated olfactory pathway (DA2) or input regarding several odorants and taking part in combinatory coding across distributed glomeruli (DL5). Our work provides an opportunity to gain insight into variations in network architecture and provides fundamental knowledge for future understanding of glomerular processing. By comparing our data with those from another narrowly tuned glomerulus (VA1v), we distilled prominent circuit features that suggest that narrowly tuned glomerular circuits encode odor signals with a weaker left-right-contrast, improved accuracy, stronger signal amplification and stronger intraglomerular signal modulation relative to broadly tuned glomeruli. Our findings reveal the existence of autapses in olfactory glomeruli and indicate that dendro-dendritic autapses play an important role in dendritic signal integration.

746 **MATERIAL AND METHODS:**

747 **Fly line and fly rearing**

748 Flies of the genotype *Orco-GAL4; UAS-GCaMP6s* (Vosshall et al., 2000) were obtained from the
749 Bloomington *Drosophila* Stock Center (https://bdsc.indiana.edu) and reared on standard
750 *Drosophila* food at 25°C and 70% humidity on a 12 h:12 h day: night cycle. Seven-days old female
751 flies were used. In these flies, Orco-positive olfactory sensory cells emit green fluorescence, making
752 possible to identify individual glomeruli.
753

754 **Brain dissection and fixation for Focus Ion Beam Microscopy-Scanning electron microscopy (FIB-**
755 **SEM)**

756 Two 7-day old female flies were anesthetized with nitric oxide (with Sleeper TAS; INJECT+MATIC,
757 Switzerland) and decapitated with forceps. Heads were dipped for one minute in 0.05% Triton X-
758 100 in 0.1M Sorensen's phosphate buffer, pH 7.3 and transferred to a droplet of freshly prepared
759 ice-cooled fixative (2.5% glutaraldehyde and 2.0% paraformaldehyde in 0.1M Sørensen's
760 phosphate buffer, pH 7.3; as in (Karnovsky, 1965). The proboscis was removed and the back of the
761 head was opened to improve fixative penetration. After 5-10 minutes, the brain was dissected out
762 of the head capsule and post-fixed for two hours on ice. Fixation was stopped by rinsing the brain
763 several times in ice-cooled 0.1M Sørensen's phosphate buffer, pH 7.3 (after (Rybak et al., 2016)).
764

765 **Laser branding of glomeruli for identification during FIB-SEM microscopy**

766 To identify the glomeruli of interest at the ultrastructural level and to limit to a minimum the
767 volume of tissue to be scanned with FIB-SEM, near-infrared laser branding (NIRB,(Bishop et al.,
768 2011). Glomeruli of interest were first located with light microscopy in brains of *Orco-GAL4; UAS-*
769 *GCaMP6s* flies using a confocal microscope (ZEISS LSM 710 NLO, Carl Zeiss, Jena, Germany), a 40x
770 water immersion objective (W Plan-Apochromat 40x/1.0 DIC VIS-IR, Carl Zeiss, Jena, Germany), a
771 laser wavelength of 925 nm at 30% laser power and ZEN software (Carl Zeiss, Jena, Germany). Once
772 glomeruli DA2 or DL5 were identified by means of location, shape and size the volume of interest
773 (VOI) was tagged with fiducial marks ("laser-branded") close to the borders of the glomerulus
774 (**Figure 1A-B**), using an infrared Chameleon Ultra diode-pumped laser (Coherent, Santa Clara, USA)
775 at wavelength 800 nm and at 75-90% of laser power). Two laser scan rounds were performed for
776 each induced fiducial brand. DA2 (right AL) and DL5 (left AL) were laser-branded in the same fly. A
777 second glomerulus DA2 was marked in the right AL of another fly.
778

779 **Transmission Electron Microscopy**

780 Brains were rinsed with 2.5% sodium-cacodylate buffer and post-fixed in 1% osmium tetroxide and
781 1% potassium ferrocyanide in cacodylate buffer for 2 hours. After rinsing with cacodylate buffer
782 the brains were dehydrated with a graded acetone series (30%-100% acetone), including an

783 additional *en bloc* staining step in-between, in which the brains were incubated in 1% uranyl
784 acetate in 50% acetone for 30 minutes in the dark, and gradually infiltrated with Araldite (glycerol-
785 based aromatic epoxy resins; Serva, Germany). In the final step, the tissue was embedded in pure
786 resin and left in a 60°C incubator to polymerize for 48h. Resin blocks were trimmed with a Reichert
787 UltraTrim microtome (Leica, Deer Park, USA) and the fiducial laser marks were then located in
788 semi-thin sections. To check tissue quality before performing high-resolution volume-based
789 electron microscopy, serial sections 50 nm in thickness were cut with a diamond knife (Ultra 45°,
790 Diatome, Switzerland) on a Reichert Ultracut S ultramicrotome (Leica, Deer Park, Germany),
791 collected on single slot grids (2 x 1 mm), and imaged with a JEM 1400 electron microscope (Jeol,
792 Freising, Germany) operated at 80 kV. Digital micrographs were obtained with a Gatan Orius SC
793 1000 CCD camera (Gatan Orius SC 1000; Gatan, Pleasanton, USA) controlled with the Gatan
794 Microscopy Suite software Vers. 2.31.734.0.
795 .

796 **Focused Ion Beam-Scanning Electron Microscopy (FIB-SEM)**

797 Before serial Focused Ion Beam milling and Scanning Electron Microscopy imaging (FIB-SEM; (Knott
798 et al., 2008; Xu et al., 2017), the surface of the trimmed block was coated with a conductive carbon
799 layer to prevent charging artifacts. A FEI Helios NanoLab G3 UC (FEI, Hillsboro, USA) was used for
800 FIB-SEM process. The laser marks used to landmark the Volume-of-Interest (VOI) were visible
801 across the surface of the block. The VOI surface was protected via a local deposition of platinum
802 using a gas injection system for subsequent ion and electron beam deposition. The material
803 surrounding the VOI at the front and the side was removed to reduce re-deposition of material
804 during FIB-SEM. Serial images across the entire VOI were generated by repeated cycles of milling
805 slices orthogonal to the block surface via FIB and imaging via SEM the newly exposed surface. The
806 tissue was milled with a focused beam of gallium ions using FEI's Tomahawk ion column
807 (accelerating voltage: 30 kV, beam current: 790 pA, milling steps: 20 nm). FEI's Elstar electron
808 column was used to create the backscattered electron contrast images using an In-Column
809 Detector (accelerating voltage. 3kV; 1.6 nA; dwell time: 10 µs). The DA2 and DL5 volumes in the
810 first fly were imaged with a resolution of 4.9 x 4.9 x 20 $nm^3$/vox (DA2: 769 images with 4096 x 3536
811 pix; DL5: 976 images with 5218 x 3303 pix). The volume of a second DA2 in a second fly was imaged
812 with a resolution of 4.4 x 4.4 x 20 $nm^3$/vox (571 images with 4096 x 3536 pix). The milling/imaging
813 cycles were controlled with the Auto Slice and View 4.0 software (FEI, Hilsboro, USA).
814

815 **Image alignment, 3D reconstruction and segmentation**

816 FIB-SEM image stacks were aligned by maximizing the Pearson correlation coefficient of the central
817 part of two consecutive images using template matching from the openCV library
818 (https://opencv.org). Dense reconstructions of the glomeruli were produced by manually tracing
819 all neuronal fibers and by annotating all synapses within the two glomeruli, using a skeleton-based
820 reconstruction procedure similar to previous approaches (Berck et al., 2016; Schneider-Mizell et

821 al., 2016; Zheng et al., 2018). Up to five independent tracers and two reviewers participated in an
822 iterative reconstruction process using the web-based reconstruction software CATMAID
823 (http://www.catmaid.org; RRID:SCR_006278; (Saalfeld et al., 2009; Schneider-Mizell et al., 2016);
824 **Figure 1D, Figure 1 – video 1**), performing a dense reconstruction of synaptic neuropil. In a second
825 fly, neurons of a DA2 glomerulus were manually reconstructed with the volume-based
826 reconstruction method TrakEM2 (Cardona et al., 2012), an ImageJ (Fiji) plugin
827 (https://imagej.net/TrakEM2).
828
829 **Neuron visualization**
830 Reconstructed neurons were visualized using CATMAID 3D visualization (http://www.catmaid.org
831 and using Blender 3D, an open-source 3D software (https://www.blender.org/; **Figure 7 – figure**
832 **supplement 1**). Neuron data from CATMAID were imported and shaded by Strahler order using an
833 existing CATMAID plugin for Blender (https://github.com/schlegelp/CATMAID-to-Blender; Schlegel
834 et al., 2016). Volume-based reconstructions were visualized as surface shapes in CATMAID
835 imported from TrakEM2 (https://imagej.net/TrakEM2).
836
837 **Glomerular border definition**
838 The definition of the boundary between olfactory glomeruli was based on the combination of
839 several structural features: the spatial position of pre- and postsynaptic elements along OSN axons,
840 the position of the majority of uPN postsynaptic sites, the faint glial leaflets scattered at the
841 periphery of the glomerulus, and the fiducial laser marks (**Figure 1B, D**).
842
843 **Neuron identification**
844 Neuronal fibers were assigned to one of three pre-defined neuron classes: OSNs, uPNs, and MGNs.
845 The classification was based on their 3D shape (**Figure 2A**), their branching intensity (**Figure 2B**),
846 the average diameter of their fibers (neuronal profiles: **Figure 2A -** FIB-SEM image; exemplary
847 volume-based reconstruction), the ratio of T-bars-to-input sites and the size of their T-bars, which
848 were either "small" (few postsynaptic connections) or "large" (many postsynaptic connections
849 **Figure 2 – supplement 1B-D)**. In addition, several intracellular features helped to classify neuron
850 classes: the shape and appearance of mitochondria, the size and electron density of vesicles and
851 the amount of synaptic spinules (small filopodia-like invaginations of neighboring cells (**Figure 2A**
852 **-** FIB-SEM image; (Gruber et al., 2018). OSNs and uPNs could be counted, due to their uniglomerular
853 character, by means of the identification of the axons (OSNs) or main dendrites (uPNs) entering
854 the glomerulus. The number of MGNs could not be counted because of their pan-glomerular
855 projection patterns in the AL. Ipsi- and contralateral OSNs in DA2 and DL5 were identified based
856 on the trajectory of axonal fibers and their entry location in each glomerulus, (example neurons:
857 **Figure 4B).** Ipsilateral OSNs reach the glomerulus from the ipsilateral antennal nerve and leave the

858 glomerulus towards the antennal lobe commissure (ALC: (Tanaka et al., 2012). Contralateral OSNs
859 reach the glomerulus projecting from the ALC.
860
861 **Data analysis**
862 With the aid of the web-based software CATMAID (http://www.catmaid.org) the following
863 properties were quantified: glomerular volume, neuronal fiber length (in µm), number of fiber
864 branching points, number of synaptic input and output sites and T-bars (see data availability). In a
865 second fly, the volume of neurons in DA2 was measured (**Figure 2 – supplement 1A**) with the aid
866 of TrakEM2 (Cardona et al., 2012), an ImageJ (Fiji) plugin (https://imagej.net/TrakEM2). The
867 following calculations were performed:

868 1. $Innervation\ density = \frac{total\ neuron\ length\ (\mu m)}{glomerular\ volume\ (\mu m^3)}$,
869 a. calculated as a ratio: (1) the sum of all neuronal fibers of each neuron class or (2) all
870 together (**Table 1**) or (3) for each neuron individually (**Figure 3**)
871 2. $Glomerular\ synaptic\ density = \frac{\#\ of\ synaptic\ inputs,-\ outputs\ or\ T-bars}{glomerular\ volume\ (\mu m^3)}$,
872 a. calculated as a ratio: (1) the sum of all neuronal fibers of each neuron class or (2) all
873 together (**Table 1**) or (3) for each neuron individually (**Figure 3**)
874 3. $Neuronal\ synaptic\ density = \frac{\#\ of\ synaptic\ inputs-,outputs\ or\ T-bars}{neuronal\ fiber\ length\ (\mu m)}$ (**Table 1; Figure 3 –**
875 **figure supplement 1**)
876 4. $Synaptic\ ratios = \frac{\#\ of\ T-bars\ or\ outputs}{inputs}$ (represents the average for each neuron class;
877 **Table 1**)
878 5. $Polyadicity = \frac{\#\ of\ outputs}{T-bars}$ (represents the average number of postsynaptic sites at a T-bar
879 of each neuron class; **Table 1 and Figure 1E**)
880 6. $\text{Relative differences} = \frac{respective\ value\ target\ glomerulus-value\ \ source\ \ glomerulus}{source\ glomerulus} \times 100$
881 (**Table S1; Table S2**)
882 7. $\text{Relative synaptic strength} = \frac{\#\ of\ synaptic\ contacts\ from\ neuron\ class\ A\ to\ B}{\#\ all\ synaptic\ contacts\ in\ corresponding\ glomerulus}$ (**Table S1;**
883 **Table S2**)
884 8. $\text{Fraction of output} = \frac{\#\ of\ outputs\ of\ neuron\ class\ A\ directed\ to\ neuron\ class\ B}{total\ \#\ of outputs\ of\ neuron\ class\ A} \times 100$
885 9. $\text{Fraction of input} = \frac{\#\ of\ \ inputs\ from\ neuron\ class\ A\ from\ class\ B}{total\ \#\ of\ inputs\ of\ neuron\ class\ A} \times 100$

886 Graphs were made with the programming language R and RStudio (R Core Team, 2018) using the
887 packages 'ggplot2' and 'reshape' (see data availability) or with Python (see data availability). EM
888 and fluorescence images were visualized with ImageJ (Fiji) (http://fiji.sc/; (Schindelin et al., 2012)
889 (and All figures were compiled with Adobe Illustrator CS5 software (Adobe Inc.).

890 Statistical analysis was performed with R Studio (R Studio Team, 2016) using the packages
891 'ggsignif'. Differences between samples DA2 and DL5 or between ipsilateral and contralateral OSNs
892 were tested for significance with a two-sided student's t-test if sample size was normally
893 distributed, or with Wilcoxon two sample test if the data was not normally distributed (noted in
894 figure legend). Data is in all cases represented as mean + standard deviation.
895

896 **Analysis of autapses**

897 The location of autapses, the measurement of their geodesic distance (distance along the neuronal
898 dendrite) and the number of branching points from point A (presynaptic site) to B (postsynaptic
899 profile) was analyzed with Python using the package 'neuroboom'
900 https://github.com/markuspleijzier/neuroboom (see also data availability).
901

902 **Data availability**

903 Full datasets for DA2 and DL5 (X_DA2 -rAL, X_DL5-lAL) and the partial dataset of DA2 (VII_DA2-rAL)
904 will be available through the public CATMAID instance:
905 https://catmaid.ice.mpg.de/catmaid_2020.02.15/. The partial dataset of DA2 are shown Neurons
906 are named according to their neuron classification. The neuroboom Python package was used for
907 dendrogram analysis, available at https://github.com/markuspleijzier/neuroboom and
908 https://pypi.org/project/neuroboom/. Further newly generated source codes can be made
909 available upon request.
910

911 **Acknowledgments**

912 The authors are most grateful to Katrin Buder (Leibnitz Institute on Aging, Jena) for the support
913 with electron microscopy sample preparation, and Veit Grabe (MPI for Chemical Ecology, Jena) for
914 advice on two-photon imaging. Great thanks also to Albert Cardona for discussion on synaptic
915 networks, him, and Tom Kazimiers (Kazmos GmbH, Dresden) and Martin Niebergall (MPI for
916 Chemical Ecology, Jena) for instruction in the use of CATMAID. The neuronal reconstructions were
917 conducted with the outstanding support of Damilola E. Akinyemi**,** Eckard E. Schumann, and
918 Michael Adewoye (MPI for Chemical Ecology, Jena). We thank Martin Nawrot and Magdalena
919 Springer (University of Cologne) for constructive comments and discussions about autapses. The
920 work was supported by Roland Kilper and Ute Müller (aura optik GmbH, Jena), the European
921 Regional Development Fund, by funds from the DFG (grant no. 430592330), in the Priority Program
922 'Evolutionary Optimization of Neuronal Processing' (DFG-SPP 2205) and by the Max Planck Society.

## REFERENCES


Acebes, A., & Ferrus, A. (2001). Increasing the Number of Synapses Modifies Olfactory Perception in Drosophila. *Journal of Neuroscience*, *21*(16), 6264–6273.

Agarwal, G., & Isacoff, E. (2011). Specializations of a pheromonal glomerulus in the Drosophila olfactory system. *Journal of Neurophysiology*, *105*(4), 1711-1721. https://doi.org/10.1152/jn.00591.2010

Ai, H., & Hagio, H. (2013). Morphological analysis of the primary center receiving spatial information transferred by the waggle dance of honeybees. *Journal of Comparative Neurology*, *521*(11), 2570-2584. https://doi.org/10.1002/cne.23299

Andersson, M. N., Löfstedt, C., & Newcomb, R. D. (2015). Insect olfaction and the evolution of receptor tuning [Review]. *Frontiers in Ecology and Evolution*, *3*. https://doi.org/10.3389/fevo.2015.00053

Anton, S., van Loon, J. J., Meijerink, J., Smid, H. M., Takken, W., & Rospars, J. P. (2003). Central projections of olfactory receptor neurons from single antennal and palpal sensilla in mosquitoes. *Arthropod Struct Dev*, *32*(4), 319-327. https://doi.org/10.1016/j.asd.2003.09.002

Asahina, K., Louis, M., Piccinotti, S., & Vosshall, L. B. (2009). A circuit supporting concentration-invariant odor perception in Drosophila. *J Biol*, *8*(1), 9. https://doi.org/10.1186/jbiol108

Assisi, C., Stopfer, M., & Bazhenov, M. (2012). Excitatory Local Interneurons Enhance Tuning of Sensory Information. *PLOS Computational Biology*, *8*(7), e1002563. https://doi.org/10.1371/journal.pcbi.1002563

Auer, T. O., Khallaf, M. A., Silbering, A. F., Zappia, G., Ellis, K., Álvarez-Ocaña, R., Arguello, J. R., Hansson, B. S., Jefferis, G. S. X. E., Caron, S. J. C., Knaden, M., & Benton, R. (2020). Olfactory receptor and circuit evolution promote host specialization. *Nature*. https://doi.org/10.1038/s41586-020-2073-7

Bacci, A., & Huguenard, J. R. (2006). Enhancement of spike-timing precision by autaptic transmission in neocortical inhibitory interneurons. *Neuron*, *49*(1), 119-130. https://doi.org/10.1016/j.neuron.2005.12.014

Bates, A. S., Schlegel, P., Roberts, R. J. V., Drummond, N., Tamimi, I. F. M., Turnbull, R., Zhao, X., Marin, E. C., Popovici, P. D., Dhawan, S., Jamasb, A., Javier, A., Serratosa Capdevila, L., Li, F., Rubin, G. M., Waddell, S., Bock, D. D., Costa, M., & Jefferis, G. (2020). Complete Connectomic Reconstruction of Olfactory Projection Neurons in the Fly Brain. *Curr Biol*, *30*(16), 3183-3199 e3186. https://doi.org/10.1016/j.cub.2020.06.042

Bekkers, J. M. (1998). Neurophysiology: are autapses prodigal synapses? *Curr Biol*, *8*(2), R52-55. https://doi.org/10.1016/s0960-9822(98)70033-8

Bekkers, J. M. (2009). Synaptic Transmission: Excitatory Autapses Find a Function? *Current biology*, *19*(7), R296-R298. https://doi.org/http://dx.doi.org/10.1016/j.cub.2009.02.010

Benton, R., Sachse, S., Michnick, S. W., & Vosshall, L. B. (2006). Atypical Membrane Topology and Heteromeric Function of *Drosophila* Odorant Receptors In Vivo. *PLoS Biol*, *4*(2), 240-257. https://doi.org/10.1371/journal.pbio.0040020

Berck, M. E., Khandelwal, A., Claus, L., Hernandez-Nunez, L., Si, G., Tabone, C. J., Li, F., Truman, J. W., Fetter, R. D., Louis, M., Samuel, A. D. T., & Cardona, A. (2016). The wiring diagram of a glomerular olfactory system [JOUR]. *eLife*, *5*, e14859. https://doi.org/10.7554/eLife.14859

Bhandawat, V., Olsen, S. R., Gouwens, N. W., Schlief, M. L., & Wilson, R. I. (2007). Sensory processing in the *Drosophila* antennal lobe increases reliability and separability of ensemble odor representations [Research Support, N.I.H., Extramural
Research Support, Non-U.S. Gov't
Research Support, U.S. Gov't, Non-P.H.S.]. *Nat Neurosci*, *10*(11), 1474-1482. https://doi.org/10.1038/nn1976

Bielopolski, N., Amin, H., Apostolopoulou, A. A., Rozenfeld, E., Lerner, H., Huetteroth, W., Lin, A. C., & Parnas, M. (2019). Inhibitory muscarinic acetylcholine receptors enhance aversive olfactory learning in adult Drosophila. *eLife*, *8*. https://doi.org/10.7554/eLife.48264

Bishop, D., Nikic, I., Brinkoetter, M., Knecht, S., Potz, S., Kerschensteiner, M., & Misgeld, T. (2011). Near-infrared branding efficiently correlates light and electron microscopy [10.1038/nmeth.1622]. *Nat Meth*, *8*(7), 568-570. https://doi.org/10.1038/nmeth.1622

Boeckh, J., Distler, P., Ernst, K. D., Hösl, M., & Malun, D. (1990). Olfactory bulb and antennal lobe. In D. Schild (Ed.), *NATO ASI Series, Vol. H39: Chemosensory Information Processing* (pp. 201-227). Springer Verl.

Boeckh, J., & Tolbert, L. P. (1993). Synaptic organization and development of the antennal lobe in insects [Review]. *Microscopy research and technique*, *24*(3), 260-280. https://doi.org/10.1002/jemt.1070240305

Borst, A., & Heisenberg, M. (1982). Osmotropotaxis inDrosophila melanogaster. *Journal of comparative physiology*, *147*(4), 479-484. https://doi.org/10.1007/BF00612013

Briggman, K. L., & Denk, W. (2006). Towards neural circuit reconstruction with volume electron microscopy techniques [Review]. *Curr Opin Neurobiol*, *16*(5), 562-570. https://doi.org/10.1016/j.conb.2006.08.010

Butcher, N. J., Friedrich, A. B., Lu, Z., Tanimoto, H., & Meinertzhagen, I. A. (2012). Different classes of input and output neurons reveal new features in microglomeruli of the adult *Drosophila* mushroom body calyx. *J Comp Neurol*, *520*(10), 2185-2201. https://doi.org/10.1002/cne.23037

Cardona, A., Saalfeld, S., Schindelin, J., Arganda-Carreras, I., Preibisch, S., Longair, M., Tomancak, P., Hartenstein, V., & Douglas, R. J. (2012). TrakEM2 Software for Neural Circuit Reconstruction. *PLoS ONE*, *7*(6), e38011. https://doi.org/10.1371/journal.pone.0038011

Cardona, A., Saalfeld, S., Tomancak, P., & Hartenstein, V. (2009). *Drosophila* brain development: closing the gap between a macroarchitectural and microarchitectural approach. *Cold Spring Harb Symp Quant Biol*, *74*, 235-248. https://doi.org/10.1101/sqb.2009.74.037

Carlsson, M. A., Diesner, M., Schachtner, J., & Nässel, D. R. (2010). Multiple neuropeptides in the Drosophila antennal lobe suggest complex modulatory circuits. *Journal of Comparative Neurology*, *518*(16), 3359-3380.

Caron, S. J. C., Ruta, V., Abbott, L. F., & Axel, R. (2013). Random convergence of olfactory inputs in the Drosophila mushroom body. *Nature*, *497*(7447), 113-117. https://doi.org/10.1038/nature12063

Chen, W. R., & Shepherd, G. M. (2005). The olfactory glomerulus: A cortical module with specific functions. *Journal of Neurocytology*, *34*, 353–360.

Chou, Y. H., Spletter, M. L., Yaksi, E., Leong, J. C., Wilson, R. I., & Luo, L. (2010). Diversity and wiring variability of olfactory local interneurons in the *Drosophila* antennal lobe [Comparative Study

Research Support, N.I.H., Extramural
Research Support, Non-U.S. Gov't]. *Nat Neurosci*, *13*(4), 439-449. https://doi.org/10.1038/nn.2489

Christie, J. M., Bark, C., Hormuzdi, S. G., Helbig, I., Monyer, H., & Westbrook, G. L. (2005). Connexin36 mediates spike synchrony in olfactory bulb glomeruli. *Neuron*, *46*(5), 761-772. https://doi.org/10.1016/j.neuron.2005.04.030

Coates, K. E., Calle-Schuler, S. A., Helmick, L. M., Knotts, V. L., Martik, B. N., Salman, F., Warner, L. T., Valla, S. V., Bock, D. D., & Dacks, A. M. (2020). The Wiring Logic of an Identified Serotonergic Neuron That Spans Sensory Networks. *The Journal of Neuroscience*, *40*(33), 6309-6327. https://doi.org/10.1523/jneurosci.0552-20.2020

Couto, A., Alenius, M., & Dickson, B. J. (2005). Molecular, anatomical, and functional organization of the *Drosophila* olfactory system [Comparative Study
Research Support, Non-U.S. Gov't]. *Current biology*, *15*(17), 1535-1547. https://doi.org/10.1016/j.cub.2005.07.034

Cover, K. K., & Mathur, B. N. (2021). Axo-axonic synapses: Diversity in neural circuit function. *J Comp Neurol*, *529*(9), 2391-2401. https://doi.org/10.1002/cne.25087

Croset, V., Treiber, C. D., & Waddell, S. (2018). Cellular diversity in the Drosophila midbrain revealed by single-cell transcriptomics. *eLife*, *7*. https://doi.org/10.7554/eLife.34550

Croset, V., Treiber, C. D., & Waddell, S. (2018). Cellular diversity in the Drosophila midbrain revealed by single-cell transcriptomics. *eLife*, *7*, e34550. https://doi.org/10.7554/eLife.34550

Cuntz, H., Borst, A., & Segev, I. (2007). Optimization principles of dendritic structure [Research Support, Non-U.S. Gov't]. *Theor Biol Med Model*, *4*, 21. https://doi.org/10.1186/1742-4682-4-21

Dacks, A. M., Christensen, T. A., & Hildebrand, J. G. (2006). Phylogeny of a serotonin-immunoreactive neuron in the primary olfactory center of the insect brain [Comparative Study
Research Support, N.I.H., Extramural
Research Support, Non-U.S. Gov't]. *J Comp Neurol*, *498*(6), 727-746. https://doi.org/10.1002/cne.21076

Dalal, T., Gupta, N., & Haddad, R. (2020). Bilateral and unilateral odor processing and odor perception. *Commun Biol*, *3*(1), 150. https://doi.org/10.1038/s42003-020-0876-6

Datta, S. R., Vasconcelos, M. L., Ruta, V., Luo, S., Wong, A., Demir, E., Flores, J., Balonze, K., Dickson, B. J., & Axel, R. (2008). The *Drosophila* pheromone cVA activates a sexually dimorphic neural circuit [Research Support, Non-U.S. Gov't]. *Nature*, *452*(7186), 473-477. https://doi.org/10.1038/nature06808

de Bruyne, M., Clyne, P. J., & Carlson, J. R. (1999). Odor coding in a model olfactory organ: the *Drosophila* maxillary palp. *Journal of Neuroscience*, *19*(11), 4520-4532. http://www.jneurosci.org/content/19/11/4520.full.pdf

de Bruyne, M., Foster, K., & Carlson, J. R. (2001). Odor Coding in the *Drosophila* Antenna. *Neuron*, *30*(2), 537-552. https://doi.org/10.1016/S0896-6273(01)00289-6

de la Rocha, J., Doiron, B., Shea-Brown, E., Josić, K., & Reyes, A. (2007). Correlation between neural spike trains increases with firing rate. *Nature*, *448*(7155), 802-806. https://doi.org/10.1038/nature06028

Demir, M., Kadakia, N., Anderson, H. D., Clark, D. A., & Emonet, T. (2020). Walking Drosophila navigate complex plumes using stochastic decisions biased by the timing of odor encounters. *eLife*, *9*. https://doi.org/10.7554/eLife.57524

Dolan, M.-J., Frechter, S., Bates, A. S., Dan, C., Huoviala, P., Roberts, R. J. V., Schlegel, P., Dhawan, S., Tabano, R., Dionne, H., Christoforou, C., Close, K., Sutcliffe, B., Giuliani, B., Li, F., Costa, M., Ihrke, G., Meissner, G. W., Bock, D. D., . . . Jefferis, G. S. X. E. (2019). Neurogenetic dissection of the Drosophila lateral horn reveals major outputs, diverse behavioural functions, and interactions with the mushroom body. *eLife*, *8*, e43079. https://doi.org/10.7554/eLife.43079

Dolan, M. J., Belliart-Guérin, G., Bates, A. S., Frechter, S., Lampin-Saint-Amaux, A., Aso, Y., Roberts, R. J. V., Schlegel, P., Wong, A., Hammad, A., Bock, D., Rubin, G. M., Preat, T., Plaçais, P. Y., & Jefferis, G. (2018). Communication from Learned to Innate Olfactory Processing Centers Is Required for Memory Retrieval in Drosophila. *Neuron*, *100*(3), 651-668.e658. https://doi.org/10.1016/j.neuron.2018.08.037

Duistermars, B. J., Chow, D. M., & Frye, M. A. (2009). Flies require bilateral sensory input to track odor gradients in flight. *Current biology*, *19*(15), 1301-1307.

Dweck, H. K. M., Ebrahim, S. A. M., Thoma, M., Mohamed, A. A. M., Keesey, I. W., Trona, F., Lavista-Llanos, S., Svatoš, A., Sachse, S., Knaden, M., & Hansson, B. S. (2015). Pheromones mediating copulation and attraction in *Drosophila*. *Proceedings of the National Academy of Sciences*, *112*(21), E2829-E2835. https://doi.org/10.1073/pnas.1504527112

Ebrahim, S. A. M., Dweck, H. K. M., Stökl, J., Hofferberth, J. E., Trona, F., Weniger, K., Rybak, J., Seki, Y., Stensmyr, M. C., Sachse, S., Hansson, B. S., & Knaden, M. (2015). *Drosophila* Avoids Parasitoids by Sensing Their Semiochemicals via a Dedicated Olfactory Circuit. *PLoS Biol*, *13*(12), e1002318. https://doi.org/10.1371/journal.pbio.1002318

Eckstein, N., Bates, A. S., Champion, A., Du, M., Yin, Y., Schlegel, P., Lu, A. K.-Y., Rymer, T., Finley-May, S., Paterson, T., Parekh, R., Dorkenwald, S., Matsliah, A., Yu, S.-C., McKellar, C., Sterling, A., Eichler, K., Costa, M., Seung, S., . . . Funke, J. (2024). Neurotransmitter classification from electron microscopy images at synaptic sites in Drosophila melanogaster. *Cell*, *187*(10), 2574-2594.e2523. https://doi.org/10.1016/j.cell.2024.03.016

Eichler, K., Li, F., Litwin-Kumar, A., Park, Y., Andrade, I., Schneider-Mizell, C. M., Saumweber, T., Huser, A., Eschbach, C., Gerber, B., Fetter, R. D., Truman, J. W., Priebe, C. E., Abbott, L. F., Thum, A. S., Zlatic, M., & Cardona, A. (2017). The complete connectome of a learning and memory centre in an insect brain. *Nature*, *548*(7666), 175-182. https://doi.org/10.1038/nature23455

Felsenberg, J., Jacob, P. F., Walker, T., Barnstedt, O., Edmondson-Stait, A. J., Pleijzier, M. W., Otto, N., Schlegel, P., Sharifi, N., Perisse, E., Smith, C. S., Lauritzen, J. S., Costa, M., Jefferis, G. S. X. E., Bock, D. D., & Waddell, S. (2018). Integration of Parallel Opposing Memories Underlies Memory Extinction. *Cell*, *175*(3), 709-722.e715. https://doi.org/https://doi.org/10.1016/j.cell.2018.08.021

Fiala, A. (2007). Olfaction and olfactory learning in Drosophila: recent progress. *Curr Opin Neurobiol*, *17*(6), 720-726. https://doi.org/10.1016/j.conb.2007.11.009

Fishilevich, E., & Vosshall, L. B. (2005). Genetic and functional subdivision of the *Drosophila* antennal lobe. *Current biology*, *15*(17), 1548-1553. https://doi.org/10.1016/j.cub.2005.07.066

Fröhlich, A. (1985). Freeze-Fracture Study of an Invertebrate Multiple-Contact Synapse: The Fly Photoreceptor Tetrad. *Journal of Comparative Neurology*, *241*(3), 311-326. https://doi.org/10.1002/cne.902410306

Galizia, C. G. (2014). Olfactory coding in the insect brain: data and conjectures. *European Journal of Neuroscience*, *39*(11), n/a-n/a. https://doi.org/10.1111/ejn.12558

Galizia, C. G., Nagler, K., Holldobler, B., & Menzel, R. (1998). Odour coding is bilaterally symmetrical in the antennal lobes of honeybees (Apis mellifera). *European Journal of Neuroscience*, *10*(9), 2964-2974.

Gao, Q., Yuan, B., & Chess, A. (2000). Convergent projections of Drosophila olfactory neurons to specific glomeruli in the antennal lobe. *Nature*.

Gao, X. J., Clandinin, T. R., & Luo, L. (2015). Extremely Sparse Olfactory Inputs Are Sufficient to Mediate Innate Aversion in *Drosophila PLoS ONE*, *10*(4), e0125986. https://doi.org/10.1371/journal.pone.0125986

Gaudry, Q., Hong, E. J., Kain, J., de Bivort, B. L., & Wilson, R. I. (2013). Asymmetric neurotransmitter release enables rapid odour lateralization in *Drosophila*. *Nature*, *493*(7432), 424-428. https://doi.org/10.1038/nature11747

Gondré-Lewis, M. C., Park, J. J., & Loh, Y. P. (2012). Chapter Two - Cellular Mechanisms for the Biogenesis and Transport of Synaptic and Dense-Core Vesicles. In K. W. Jeon (Ed.), *International Review of Cell and Molecular Biology* (Vol. 299, pp. 27-115). Academic Press. https://doi.org/https://doi.org/10.1016/B978-0-12-394310-1.00002-3

Goyal, R. K., & Chaudhury, A. (2013). Structure activity relationship of synaptic and junctional neurotransmission. *Autonomic Neuroscience: Basic and Clinical*, *176*(1), 11-31. https://doi.org/10.1016/j.autneu.2013.02.012

Grabe, V., Baschwitz, A., Dweck, Hany K. M., Lavista-Llanos, S., Hansson, Bill S., & Sachse, S. (2016). Elucidating the Neuronal Architecture of Olfactory Glomeruli in the *Drosophila* Antennal Lobe. *Cell Reports*, *16*(12), 3401-3413. https://doi.org/10.1016/j.celrep.2016.08.063

Grabe, V., & Sachse, S. (2018). Fundamental principles of the olfactory code. *Biosystems*, *164*, 94-101. https://doi.org/10.1016/j.biosystems.2017.10.010

Grabe, V., Schubert, M., Strube-Bloss, M., Reinert, A., Trautheim, S., Lavista-Llanos, S., Fiala, A., Hansson, B. S., & Sachse, S. (2020). Odor-Induced Multi-Level Inhibitory Maps in Drosophila. *eNeuro*, *7*(1). https://doi.org/10.1523/eneuro.0213-19.2019

Grabe, V., Strutz, A., Baschwitz, A., Hansson, B. S., & Sachse, S. (2015). Digital in vivo 3D atlas of the antennal lobe of *Drosophila melanogaster*. *Journal of Comparative Neurology*, *523*(3), 530-544. https://doi.org/10.1002/cne.23697

Graubard, K., Raper, J. A., & Hartline, D. K. (1980). Graded synaptic transmission between spiking neurons. *Proc Natl Acad Sci U S A*, *77*(6), 3733-3735. https://doi.org/10.1073/pnas.77.6.3733

Gruber, L., Rybak, J., Hansson, B. S., & Cantera, R. (2018). Synaptic Spinules in the Olfactory Circuit of Drosophila melanogaster [Perspective]. *Front Cell Neurosci*, *12*(86), 86. https://doi.org/10.3389/fncel.2018.00086

Guo, D., Wu, S., Chen, M., Perc, M., Zhang, Y., Ma, J., Cui, Y., Xu, P., Xia, Y., & Yao, D. (2016). Regulation of Irregular Neuronal Firing by Autaptic Transmission. *Sci Rep*, *6*, 26096. https://doi.org/10.1038/srep26096

Guven-Ozkan, T., & Davis, R. L. (2014). Functional neuroanatomy of *Drosophila* olfactory memory formation. *Learning & Memory*, *21*(10), 519-526. https://doi.org/10.1101/lm.034363.114

Hallem, E. A., & Carlson, J. R. (2006). Coding of odors by a receptor repertoire. *Cell*, *125*(1), 143-160. https://doi.org/10.1016/j.cell.2006.01.050

Hallem, E. A., Ho, M. G., & Carlson, J. R. (2004). The molecular basis of odor coding in the Drosophila antenna. *Cell*, *117*(7), 965-979. https://doi.org/10.1016/j.cell.2004.05.012

Hansson, B. S., & Anton, S. (2000). Function and morphology of the antennal lobe: new developments. *Annu Rev Entomol*, *45*, 203-231. https://doi.org/10.1146/annurev.ento.45.1.203

Hartenstein, V. (2016). The Central Nervous System of Invertebrates. In S. V. Shepherd (Ed.), *The Wiley Handbook of Evolutionary Neuroscience* (pp. 173-235). https://doi.org/https://doi.org/10.1002/9781118316757.ch8

Haverkamp, A., Hansson, B. S., & Knaden, M. (2018). Combinatorial Codes and Labeled Lines: How Insects Use Olfactory Cues to Find and Judge Food, Mates, and Oviposition Sites in Complex Environments. *Front Physiol*, *9*, 49. https://doi.org/10.3389/fphys.2018.00049

Helmstaedter, M. (2013). Cellular-resolution connectomics: challenges of dense neural circuit reconstruction [Perspective]. *Nature Methods*, *10*(6), 501-507. https://doi.org/10.1038/nmeth.2476

Hirata, Y. (1964). Some observations on the fine structure of the synapses in the olfactory bulb of the mouse, with particular reference to the atypical synaptic configurations. *Archivum histologicum japonicum*, *24*(3), 293-302.

Hong, E. J., & Wilson, R. I. (2015). Simultaneous encoding of odors by channels with diverse sensitivity to inhibition. *Neuron*, *85*(3), 573-589. https://doi.org/10.1016/j.neuron.2014.12.040

Horne, J. A., Langille, C., McLin, S., Wiederman, M., Lu, Z., Xu, C. S., Plaza, S. M., Scheffer, L. K., Hess, H. F., & Meinertzhagen, I. A. (2018). A resource for the *Drosophila* antennal lobe provided by the connectome of glomerulus VA1v. *eLife*, *7*, e37550. https://doi.org/10.7554/eLife.37550

Huang, G. B., Scheffer, L. K., & Plaza, S. M. (2018). Fully-Automatic Synapse Prediction and Validation on a Large Data Set [Original Research]. *Frontiers in Neural Circuits*, *12*(87). https://doi.org/10.3389/fncir.2018.00087

Hulse, B. K., Haberkern, H., Franconville, R., Turner-Evans, D. B., Takemura, S.-y., Wolff, T., Noorman, M., Dreher, M., Dan, C., Parekh, R., Hermundstad, A. M., Rubin, G. M., & Jayaraman, V. (2021). A connectome of the Drosophila central complex reveals network motifs suitable for flexible navigation and context-dependent action selection. *eLife*, *10*, e66039. https://doi.org/10.7554/eLife.66039

Huoviala, P., Dolan, M.-J., Love, F. M., Myers, P., Frechter, S., Namiki, S., Pettersson, L., Roberts, R. J. V., Turnbull, R., Mitrevica, Z., Breads, P., Schlegel, P., Bates, A. S., Rodrigues, T., Aso, Y., Bock, D., Rubin, G. M., Stensmyr, M., Card, G., . . . Jefferis, G. S. X. E. (2020). Neural circuit basis of aversive odour processing in *Drosophila* from sensory input to descending output. 394403. https://doi.org/10.1101/394403

Ikeda, K., & Bekkers, J. M. Autapses. *Current biology*, *16*(9), R308. https://doi.org/10.1016/j.cub.2006.03.085

1185 Ikeda, K., & Bekkers, J. M. (2006). Autapses. *Curr Biol*, *16*(9), R308.
1186 https://doi.org/10.1016/j.cub.2006.03.085
1187 Jeanne, James M., & Wilson, Rachel I. (2015). Convergence, Divergence, and Reconvergence in a
1188 Feedforward Network Improves Neural Speed and Accuracy. *Neuron*, *88*(5), 1014-1026.
1189 https://doi.org/10.1016/j.neuron.2015.10.018
1190 Jefferis, G. S., Potter, C. J., Chan, A. M., Marin, E. C., Rohlfing, T., Maurer, C. R., Jr., & Luo, L.
1191 (2007). Comprehensive maps of *Drosophila* higher olfactory centers: spatially segregated
1192 fruit and pheromone representation [Research Support, N.I.H., Extramural
1193 Research Support, Non-U.S. Gov't]. *Cell*, *128*(6), 1187-1203.
1194 https://doi.org/10.1016/j.cell.2007.01.040
1195 Karnovsky, M. J. (1965). A formaldehyde-glutaraldehyde fixative of high osmolarity for use in
1196 electron microscopy. *Journal of Cellular Biology*, *27*, 137.
1197 Kazama, H., & Wilson, R. I. (2008). Homeostatic Matching and Nonlinear Amplification at
1198 Identified Central Synapses. *Neuron*, *58*(3), 401-413.
1199 https://doi.org/http://dx.doi.org/10.1016/j.neuron.2008.02.030
1200 Kazama, H., & Wilson, R. I. (2009). Origins of correlated activity in an olfactory circuit [Research
1201 Support, N.I.H., Extramural
1202 Research Support, Non-U.S. Gov't]. *Nat Neurosci*, *12*(9), 1136-1144.
1203 https://doi.org/10.1038/nn.2376
1204 Keene, A. C., & Waddell, S. (2007). Drosophila olfactory memory: single genes to complex neural
1205 circuits [10.1038/nrn2098]. *Nat Rev Neurosci*, *8*(5), 341-354.
1206 http://dx.doi.org/10.1038/nrn2098
1207 Keesey, I. W., & Hansson, B. S. (2021). 10 - The neuroethology of labeled lines in insect olfactory
1208 systems. In G. J. Blomquist & R. G. Vogt (Eds.), *Insect Pheromone Biochemistry and*
1209 *Molecular Biology (Second Edition)* (pp. 285-327). Academic Press.
1210 https://doi.org/https://doi.org/10.1016/B978-0-12-819628-1.00010-9
1211 Keesey, I. W., Zhang, J., Depetris-Chauvin, A., Obiero, G. F., Knaden, M., & Hansson, B. S. (2019).
1212 Evolution of a pest: towards the complete neuroethology of Drosophila suzukii and the
1213 subgenus Sophophora. *bioRxiv*, 717322. https://doi.org/10.1101/717322
1214 Knaden, M., & Hansson, B. S. (2014). Mapping odor valence in the brain of flies and mice. *Curr*
1215 *Opin Neurobiol*, *24*(1), 34-38. https://doi.org/10.1016/j.conb.2013.08.010
1216 Knaden, M., Strutz, A., Ahsan, J., Sachse, S., & Hansson, B. S. (2012). Spatial representation of
1217 odorant valence in an insect brain. *Cell Reports*, *1*, 392-399.
1218 https://doi.org/10.1016/j.celrep.2012.03.002
1219 Knott, G., Marchman, H., & Lich, B. (2008). Serial Section Scanning Electron Microscopy of Adult
1220 Brain Tissue Using Focused Ion Beam Milling. *Journal of Neuroscience*, *28*(12), 2964-2959.
1221 https://doi.org/10.1523/JNEUROSCI.3189-07.2008
1222 Kreher, S. A., Mathew, D., Kim, J., & Carlson, J. R. (2008). Translation of sensory input into
1223 behavioral output via an olfactory system. *Neuron*, *59*(1), 110-124.
1224 https://doi.org/10.1016/j.neuron.2008.06.010
1225 Kumar, A., Schiff, O., Barkai, E., Mel, B. W., Poleg-Polsky, A., & Schiller, J. (2018). NMDA spikes
1226 mediate amplification of inputs in the rat piriform cortex. *eLife*, *7*, e38446.
1227 https://doi.org/10.7554/eLife.38446

Kurtovic, A., Widmer, A., & Dickson, B. J. (2007). A single class of olfactory neurons mediates behavioural responses to a Drosophila sex pheromone. *Nature*, *446*(7135), 542-546. https://doi.org/10.1038/nature05672

Laissue, P. P., Reiter, C., Hiesinger, P. R., Halter, S., Fischbach, K. F., & Stocker, R. F. (1999). Three-dimensional reconstruction of the antennal lobe in *Drosophila melanogaster*. *The Journal of Comparative Neurology*, *405*(4), 543-552. https://doi.org/10.1002/(sici)1096-9861(19990322)405:4<543::aid-cne7>3.0.co;2-a

Laissue, P. P., & Vosshall, L. B. (2008). The Olfactory Sensory Map in *Drosophila*. In G. M. Technau (Ed.), *Brain Development in Drosophila melanogaster* (pp. 102-114 ). Springer.

Lei, H., Oland, L. A., Riffell, J. A., Beyerlein, A., & Hildebrand, J. G. (2010). Microcircuits for Olfactory Information Processing in the Antennal Lobe of *Manduca sexta*. In G. M. Shepherd & S. Grillner (Eds.), *Handbook of Brain Microcircuits* (pp. 417-426). Oxford University Press.

Li, F., Lindsey, J. W., Marin, E. C., Otto, N., Dreher, M., Dempsey, G., Stark, I., Bates, A. S., Pleijzier, M. W., Schlegel, P., Nern, A., Takemura, S. Y., Eckstein, N., Yang, T., Francis, A., Braun, A., Parekh, R., Costa, M., Scheffer, L. K., . . . Rubin, G. M. (2020). The connectome of the adult Drosophila mushroom body provides insights into function. *eLife*, *9*. https://doi.org/10.7554/eLife.62576

Li, P. H., Lindsey, L. F., Januszewski, M., Zheng, Z., Bates, A. S., Taisz, I., Tyka, M., Nichols, M., Li, F., Perlman, E., Maitin-Shepard, J., Blakely, T., Leavitt, L., Jefferis, G. S. X. E., Bock, D., & Jain, V. (2020). Automated Reconstruction of a Serial-Section EM *Drosophila* Brain with Flood-Filling Networks and Local Realignment. *bioRxiv*, 605634. https://doi.org/10.1101/605634

Liang, L., & Luo, L. (2010). The olfactory circuit of the fruit fly *Drosophila melanogaster*. *Sci China Life Sci*, *53*(4), 472-484. https://doi.org/10.1007/s11427-010-0099-z

Lin, S., Kao, C.-F., Yu, H.-H., Huang, Y., & Lee, T. (2012). Lineage analysis of Drosophila lateral antennal lobe neurons reveals notch-dependent binary temporal fate decisions. *PLoS biology*, *10*(11), e1001425-e1001425. https://doi.org/10.1371/journal.pbio.1001425

Liu, T. X., Davoudian, P. A., Lizbinski, K. M., & Jeanne, J. M. (2022). Connectomic features underlying diverse synaptic connection strengths and subcellular computation. *Current biology*, *32*(3), 559-569.e555. https://doi.org/https://doi.org/10.1016/j.cub.2021.11.056

Liu, W. W., & Wilson, R. I. (2013). Glutamate is an inhibitory neurotransmitter in the *Drosophila* olfactory system. *Proceedings of the National Academy of Sciences*, *110*(25), 10294–10299. https://doi.org/10.1073/pnas.1220560110

Malun, D. (1991). Inventory and distribution of synapses of identified uniglomerular projection neurons in the antennal lobe of Periplaneta americana [Research Support, Non-U.S. Gov't]. *Journal of Comparative Neurology*, *305*(2), 348-360. https://doi.org/10.1002/cne.903050215

Malun, D., Waldow, U., Kraus, D., & Boeckh, J. (1993). Connections between the Deutocerebrum and the Protocerebrum, and Neuroanatomy of Several Classes of Deutocerebral Projection Neurons in the Brain of Male Periplaneta-Americana. *Journal of Comparative Neurology*, *329*(2), 143-162. <Go to ISI>://A1993KM85800001 http://onlinelibrary.wiley.com/doi/10.1002/cne.903290202/abstract

Marin, E. C., Büld, L., Theiss, M., Sarkissian, T., Roberts, R. J. V., Turnbull, R., Tamimi, I. F. M., Pleijzier, M. W., Laursen, W. J., Drummond, N., Schlegel, P., Bates, A. S., Li, F., Landgraf,

M., Costa, M., Bock, D. D., Garrity, P. A., & Jefferis, G. (2020). Connectomics Analysis Reveals First-, Second-, and Third-Order Thermosensory and Hygrosensory Neurons in the Adult Drosophila Brain. *Curr Biol*, *30*(16), 3167-3182.e3164. https://doi.org/10.1016/j.cub.2020.06.028

Masse, N. Y., Turner, G. C., & Jefferis, G. S. (2009). Olfactory information processing in Drosophila [Research Support, Non-U.S. Gov't Review]. *Curr Biol*, *19*(16), R700-713. https://doi.org/10.1016/j.cub.2009.06.026

Masson, C., & Mustaparta, H. (1990). Chemical information processing in the olfactory system of insects. *Physiological Review*, *70(1)*, 199-245.

McTavish, T., Migliore, M., Shepherd, G., & Hines, M. (2012). Mitral cell spike synchrony modulated by dendrodendritic synapse location [Original Research]. *Frontiers in Computational Neuroscience*, *6*. https://doi.org/10.3389/fncom.2012.00003

Meinertzhagen, I. A. (2018). Of what use is connectomics? A personal perspective on the *Drosophila* connectome [comment review]. *Journal of Experimental Biology*, *221*(10), jeb164954. https://doi.org/10.1242/jeb.164954 %J The Journal of Experimental Biology

Meinertzhagen, I. A., & O'Neil, S. D. (1991). Synaptic organization of columnar elements in the lamina of the wild type in Drosophila melanogaster. *Journal of Comparative Neurology*, *305*, 232-263. http://onlinelibrary.wiley.com/store/10.1002/cne.903050206/asset/903050206_ftp.pdf?v=1&t=im4yu4xk&s=2429254fe941f5e871b7f48dd61813e66d9397a6

Miroschnikow, A., Schlegel, P., Schoofs, A., Hueckesfeld, S., Li, F., Schneider-Mizell, C. M., Fetter, R. D., Truman, J. W., Cardona, A., & Pankratz, M. J. (2018). Convergence of monosynaptic and polysynaptic sensory paths onto common motor outputs in a Drosophila feeding connectome. *eLife*, *7*, e40247. https://doi.org/10.7554/eLife.40247

Mohamed, A. A. M., Hansson, B. S., & Sachse, S. (2019). Third-Order Neurons in the Lateral Horn Enhance Bilateral Contrast of Odor Inputs Through Contralateral Inhibition in Drosophila. *Front Physiol*, *10*, 851. https://doi.org/10.3389/fphys.2019.00851

Mohamed, A. A. M., Retzke, T., Das Chakraborty, S., Fabian, B., Hansson, B. S., Knaden, M., & Sachse, S. (2019). Odor mixtures of opposing valence unveil inter-glomerular crosstalk in the Drosophila antennal lobe. *Nat Commun*, *10*(1), 1201. https://doi.org/10.1038/s41467-019-09069-1

Mosca, T. J., & Luo, L. (2014). Synaptic organization of the *Drosophila* antennal lobe and its regulation by the Teneurins [Journal Article]. *eLife*, *3*(3), e03726. https://doi.org/10.7554/eLife.03726

Münch, D., & Galizia, C. G. (2016). DoOR 2.0 - Comprehensive Mapping of Drosophila melanogaster Odorant Responses [Article]. *Scientific Reports*, *6*, 21841. https://doi.org/10.1038/srep21841
http://www.nature.com/articles/srep21841#supplementary-information

Nässel, D. R. (2018). Substrates for Neuronal Cotransmission With Neuropeptides and Small Molecule Neurotransmitters in Drosophila. *Front Cell Neurosci*, *12*, 83. https://doi.org/10.3389/fncel.2018.00083

Nässel, D. R., & Homberg, U. (2006). Neuropeptides in interneurons of the insect brain [Research Support, Non-U.S. Gov't

Review]. *Cell Tissue Res*, *326*(1), 1-24. https://doi.org/10.1007/s00441-006-0210-8

Ng, M., Roorda, R. D., Lima, S. Q., Zemelman, B. V., Morcillo, P., & Miesenböck, G. (2002). Transmission of Olfactory Information between Three Populations of Neurons in the Antennal Lobe of the Fly. *Neuron*, *36*(3), 463-474. https://doi.org/10.1016/s0896-6273(02)00975-3

Norgate, M., Lee, E., Southon, A., Farlow, A., Batterham, P., Camakaris, J., & Burke, R. (2006). Essential Roles in Development and Pigmentation for the *Drosophila* Copper Transporter DmATP7. *Molecular Biology of the Cell*, *17*(1), 475-484. https://doi.org/10.1091/mbc.E05-06-0492

Okada, R., Awasaki, T., & Ito, K. (2009). Gamma-aminobutyric acid (GABA)-mediated neural connections in the *Drosophila* antennal lobe. *Journal of Comparative Neurology*, *514*(1), 74-91. https://doi.org/10.1002/cne.21971

Olsen, S. R., Bhandawat, V., & Wilson, R. I. (2010). Divisive normalization in olfactory population codes. *Neuron*, *66*(2), 287-299. https://doi.org/10.1016/j.neuron.2010.04.009

Olsen, S. R., & Wilson, R. I. (2008). Lateral presynaptic inhibition mediates gain control in an olfactory circuit. *Nature*, *452*(7190), 956-960. https://doi.org/10.1038/nature06864

Otto, N., Pleijzier, M. W., Morgan, I. C., Edmondson-Stait, A. J., Heinz, K. J., Stark, I., Dempsey, G., Ito, M., Kapoor, I., Hsu, J., Schlegel, P. M., Bates, A. S., Feng, L., Costa, M., Ito, K., Bock, D. D., Rubin, G. M., Jefferis, G. S. X. E., & Waddell, S. (2020). Input Connectivity Reveals Additional Heterogeneity of Dopaminergic Reinforcement in Drosophila. *Current biology*, *30*(16), 3200-3211.e3208. https://doi.org/https://doi.org/10.1016/j.cub.2020.05.077

Owald, D., & Waddell, S. (2015). Olfactory learning skews mushroom body output pathways to steer behavioral choice in Drosophila. *Current Opinion in Neurobiology*, *35*, 178-184. https://doi.org/10.1016/j.conb.2015.10.002

Parthasarathy, K., & Bhalla, U. S. (2013). Laterality and symmetry in rat olfactory behavior and in physiology of olfactory input. *J Neurosci*, *33*(13), 5750-5760. https://doi.org/10.1523/jneurosci.1781-12.2013

Prokop, A., & Meinertzhagen, I. A. (2006). Development and structure of synaptic contacts in Drosophila [Review]. *Semin Cell Dev Biol*, *17*(1), 20-30. https://doi.org/10.1016/j.semcdb.2005.11.010

Ronchi, P., Mizzon, G., Machado, P., D'Imprima, E., Best, B. T., Cassella, L., Schnorrenberg, S., Montero, M. G., Jechlinger, M., Ephrussi, A., Leptin, M., Mahamid, J., & Schwab, Y. (2021). High-precision targeting workflow for volume electron microscopy. *J Cell Biol*, *220*(9). https://doi.org/10.1083/jcb.202104069

Root, C. M., Masuyama, K., Green, D. S., Enell, L. E., Nassel, D. R., Lee, C. H., & Wang, J. W. (2008). A presynaptic gain control mechanism fine-tunes olfactory behavior [Comparative Study Research Support, N.I.H., Extramural
Research Support, Non-U.S. Gov't]. *Neuron*, *59*(2), 311-321. https://doi.org/10.1016/j.neuron.2008.07.003

Rospars, J.-P., Grémiaux, A., Jarriault, D., Chaffiol, A., Monsempes, C., Deisig, N., Anton, S., Lucas, P., & Martinez, D. (2014). Heterogeneity and Convergence of Olfactory First-Order Neurons Account for the High Speed and Sensitivity of Second-Order Neurons. *PLOS Computational Biology*, *10*(12), e1003975. https://doi.org/10.1371/journal.pcbi.1003975

Rozenfeld, E., Lerner, H., & Parnas, M. (2019). Muscarinic Modulation of Antennal Lobe GABAergic Local Neurons Shapes Odor Coding and Behavior. *Cell Rep*, *29*(10), 3253-3265.e3254. https://doi.org/10.1016/j.celrep.2019.10.125

Rybak, J. (2013). Exploring Brain Connectivity in Insect Model Systems of Learning and Memory. In R. Menzel & P. Benjamin (Eds.), *Invertebrate Learning and Memory* (pp. 26-40). Academic Press. https://doi.org/10.1016/b978-0-12-415823-8.00004-6

Rybak, J. (2016). Perspective-Brain atlases for studying neuronal circuitry in arthropods. In A. Schmidt-Rhaesa, S. Harzsch, & G. Purschke (Eds.), *Structure and Evolution of Invertebrate Nervous Systems* (Vol. 1). Oxford University Press. https://doi.org/10.1093/acprof:oso/9780199682201.001.0001

Rybak, J., & Hansson, B. S. (2018). Olfactory Microcircuits in *Drosophila Melanogaster*. In G. M. Shepherd & S. Grillner (Eds.), *Handbook of Brain Microcircuits* (2nd ed., pp. 361-367). Oxford University Press. https://doi.org/10.1093/med/9780190636111.003.0030

Rybak, J., Talarico, G., Ruiz, S., Arnold, C., Cantera, R., & Hansson, B. S. (2016). Synaptic circuitry of identified neurons in the antennal lobe of *Drosophila melanogaster*. *J Comp Neurol*, *524*(9), 1920-1956. https://doi.org/10.1002/cne.23966

Saada, R., Miller, N., Hurwitz, I., & Susswein, A. J. (2009). Autaptic excitation elicits persistent activity and a plateau potential in a neuron of known behavioral function. *Curr Biol*, *19*(6), 479-484. https://doi.org/10.1016/j.cub.2009.01.060

Saalfeld, S., Cardona, A., Hartenstein, V., & Tomančák, P. (2009). CATMAID: collaborative annotation toolkit for massive amounts of image data. *Bioinformatics*, *25*(15), 1984-1986. https://doi.org/10.1093/bioinformatics/btp266

Sachse, S., & Galizia, C. G. (2002). Role of inhibition for temporal and spatial odor representation in olfactory output neurons: a calcium imaging study [Research Support, Non-U.S. Gov't]. *Journal of Neurophysiology*, *87*(2), 1106-1117. http://www.ncbi.nlm.nih.gov/pubmed/11826074
http://jn.physiology.org/content/87/2/1106.full.pdf

Sachse, S., & Hansson, B. S. (2016). Research spotlight: Olfactory coding in *Drosophila melanogaster*. In A. Schmidt-Rhaesa, S. Harzsch, & G. Purschke (Eds.), *Structure and Evolution of Invertebrate Nervous Systems* (pp. 640-645). Oxford University Press.

Sachse, S., & Manzini, I. (2021). Editorial for the special issue "Olfactory Coding and Circuitries". *Cell Tissue Res*, *383*(1), 1-6. https://doi.org/10.1007/s00441-020-03389-1

Scheffer, L. K., Xu, C. S., Januszewski, M., Lu, Z., Takemura, S.-y., Hayworth, K. J., Huang, G. B., Shinomiya, K., Maitlin-Shepard, J., Berg, S., Clements, J., Hubbard, P. M., Katz, W. T., Umayam, L., Zhao, T., Ackerman, D., Blakely, T., Bogovic, J., Dolafi, T., . . . Plaza, S. M. (2020). A connectome and analysis of the adult Drosophila central brain. *eLife*, *9*, e57443. https://doi.org/10.7554/eLife.57443

Schindelin, J., Arganda-Carreras, I., Frise, E., Kaynig, V., Longair, M., Pietzsch, T., Preibisch, S., Rueden, C., Saalfeld, S., Schmid, B., Tinevez, J.-Y., White, D. J., Hartenstein, V., Eliceiri, K., Tomancak, P., & Cardona, A. (2012). Fiji: an open-source platform for biological-image analysis [10.1038/nmeth.2019]. *Nat Meth*, *9*(7), 676-682. https://doi.org/http://www.nature.com/nmeth/journal/v9/n7/abs/nmeth.2019.html#supplementary-information

Schlegel, P., Bates, A. S., Stürner, T., Jagannathan, S. R., Drummond, N., Hsu, J., Serratosa Capdevila, L., Javier, A., Marin, E. C., Barth-Maron, A., Tamimi, I. F. M., Li, F., Rubin, G. M., Plaza, S. M., Costa, M., & Jefferis, G. S. X. E. (2021). Information flow, cell types and stereotypy in a full olfactory connectome. *eLife*, *10*, e66018. https://doi.org/10.7554/eLife.66018

Schlegel, P., Yin, Y., Bates, A. S., Dorkenwald, S., Eichler, K., Brooks, P., Han, D. S., Gkantia, M., dos Santos, M., Munnelly, E. J., Badalamente, G., Serratosa Capdevila, L., Sane, V. A., Fragniere, A. M. C., Kiassat, L., Pleijzier, M. W., Stürner, T., Tamimi, I. F. M., Dunne, C. R., . . . FlyWire, C. (2024). Whole-brain annotation and multi-connectome cell typing of Drosophila. *Nature*, *634*(8032), 139-152. https://doi.org/10.1038/s41586-024-07686-5

Schneider-Mizell, C. M., Gerhard, S., Longair, M., Kazimiers, T., Li, F., Zwart, M. F., Champion, A., Midgley, F. M., Fetter, R. D., Saalfeld, S., & Cardona, A. (2016). Quantitative neuroanatomy for connectomics in *Drosophila* [JOUR]. *eLife*, *5*, e12059. https://doi.org/10.7554/eLife.12059

Seki, Y., Dweck, H. K. M., Rybak, J., Wicher, D., Sachse, S., & Hansson, B. S. (2017). Olfactory coding from the periphery to higher brain centers in the Drosophila brain. *BMC Biol*, *15*(1), 56. https://doi.org/10.1186/s12915-017-0389-z

Seki, Y., Rybak, J., Wicher, D., Sachse, S., & Hansson, B. S. (2010). Physiological and morphological characterization of local interneurons in the *Drosophila* antennal lobe. *Journal of Neurophysiology*, *104*(2), 1007-1019. https://doi.org/jn.00249.2010 [pii] 10.1152/jn.00249.2010

Semmelhack, J. L., & Wang, J. W. (2009). Select Drosophila glomeruli mediate innate olfactory attraction and aversion. *Nature*, *459*(7244), 218-223.

Shanbhag, S. R., Muller, B., & Steinbrecht, R. A. (1999). Atlas of olfactory organs of *Drosophila melanogaster* - 1. Types, external organization, innervation and distribution of olfactory sensilla. *International Journal of Insect Morphology & Embryology*, *28*(4), 377-397. https://doi.org/Doi 10.1016/S0020-7322(99)00039-2

Shepherd, G. M. (2011). The Olfactory Bulb: A Simple System in the Mammalian Brain. In *Comprehensive Physiology*. John Wiley & Sons, Inc. https://doi.org/10.1002/cphy.cp010125

Shepherd, G. M., Rowe, T. B., & Greer, C. A. (2021). An Evolutionary Microcircuit Approach to the Neural Basis of High Dimensional Sensory Processing in Olfaction [Hypothesis and Theory]. *Frontiers in Cellular Neuroscience*, *15*. https://doi.org/10.3389/fncel.2021.658480

Silbering, A. F., & Galizia, C. G. (2007). Processing of odor mixtures in the Drosophila antennal lobe reveals both global inhibition and glomerulus-specific interactions. *J Neurosci*, *27*(44), 11966-11977. https://doi.org/10.1523/jneurosci.3099-07.2007

Silbering, A. F., Okada, R., Ito, K., & Galizia, C. G. (2008). Olfactory information processing in the *Drosophila* antennal lobe: anything goes? [Research Support, Non-U.S. Gov't]. *Journal of Neuroscience*, *28*(49), 13075-13087. https://doi.org/10.1523/JNEUROSCI.2973-08.2008

Silbering, A. F., Rytz, R., Grosjean, Y., Abuin, L., Ramdya, P., Jefferis, G. S., & Benton, R. (2011). Complementary Function and Integrated Wiring of the Evolutionarily Distinct *Drosophila* Olfactory Subsystems. *Journal of Neuroscience*, *31*(38), 13357-13375. https://doi.org/10.1523/JNEUROSCI.2360-11.2011

Stensmyr, M. C., Dweck, H. K., Farhan, A., Ibba, I., Strutz, A., Mukunda, L., Linz, J., Grabe, V., Steck, K., Lavista-Llanos, S., Wicher, D., Sachse, S., Knaden, M., Becher, P. G., Seki, Y., & Hansson, B. S. (2012). A conserved dedicated olfactory circuit for detecting harmful microbes in *Drosophila* [Research Support, Non-U.S. Gov't]. *Cell*, *151*(6), 1345-1357. https://doi.org/10.1016/j.cell.2012.09.046

Stocker, R. F., Lienhard, M. C., Borst, A., & Fischbach, K. F. (1990). Neuronal architecture of the antennal lobe in Drosophila melanogaster [Research Support, Non-U.S. Gov't]. *Cell Tissue Res*, *262*(1), 9-34. http://www.ncbi.nlm.nih.gov/pubmed/2124174

Stocker, R. F., Singh, R. N., Schorderet, M., & Siddiqi, O. (1983). Projection patterns of different types of antennal sensilla in the antennal glomeruli of Drosophila melanogaster. *Cell Tissue Res*, *232*(2), 237-248. https://doi.org/10.1007/bf00213783

Strutz, A., Soelter, J., Baschwitz, A., Farhan, A., Grabe, V., Rybak, J., Knaden, M., Schmuker, M., Hansson, B. S., & Sachse, S. (2014). Decoding odor quality and intensity in the *Drosophila* brain [Journal Article]. *eLife*, *3*, e04147. https://doi.org/10.7554/eLife.04147

Su, C.-Y., Menuz, K., & Carlson, J. R. (2009). Olfactory Perception: Receptors, Cells, and Circuits. *Cell*, *139*(1), 45-59. https://doi.org/10.1016/j.cell.2009.09.015

Suh, G. S. B., Wong, A. M., Hergarden, A. C., Wang, J. W., Simon, A. F., Benzer, S., Axel, R., & Anderson, D. J. (2004). A single population of olfactory sensory neurons mediates an innate avoidance behaviour in *Drosophila* [10.1038/nature02980]. *Nature*, *431*(7010), 854-859. https://doi.org/http://www.nature.com/nature/journal/v431/n7010/suppinfo/nature02980_S1.html

Sun, X. J., Tolbert, L. P., & Hildebrand, J. G. (1997). Synaptic organization of the uniglomerular projection neurons of the antennal lobe of the moth *Manduca sexta*: a laser scanning confocal and electron microscopic study [Research Support, Non-U.S. Gov't Research Support, U.S. Gov't, P.H.S.]. *Journal of Comparative Neurology*, *379*(1), 2-20. http://www.ncbi.nlm.nih.gov/pubmed/9057110 http://onlinelibrary.wiley.com/store/10.1002/(SICI)1096-9861(19970303)379:1<2::AID-CNE2>3.0.CO;2-8/asset/2_ftp.pdf?v=1&t=grdo04po&s=b68ed1d52d77c02ebf63b625d79aa4a8ec21b1bd

Szyszka, P., & Galizia, C. G. (2015). Olfaction in Insects. In R. L. Doty (Ed.), *Handbook of Olfaction and Gustation* (3 ed., pp. 531-546). John Wiley & Sons, Inc. https://doi.org/10.1002/9781118971758.ch22

Taisz, I., Donà, E., Münch, D., Bailey, S. N., Morris, B. J., Meechan, K. I., Stevens, K. M., Varela-Martínez, I., Gkantia, M., Schlegel, P., Ribeiro, C., Jefferis, G., & Galili, D. S. (2023). Generating parallel representations of position and identity in the olfactory system. *Cell*, *186*(12), 2556-2573.e2522. https://doi.org/10.1016/j.cell.2023.04.038

Takemura, S.-y., Xu, C. S., Lu, Z., Rivlin, P. K., Parag, T., Olbris, D. J., Plaza, S., Zhao, T., Katz, W. T., Umayam, L., Weaver, C., Hess, H. F., Horne, J. A., Nunez-Iglesias, J., Aniceto, R., Chang, L.-A., Lauchie, S., Nasca, A., Ogundeyi, O., . . . Scheffer, L. K. (2015). Synaptic circuits and their variations within different columns in the visual system of Drosophila. *Proceedings of the National Academy of Sciences*, *112*(44), 13711-13716. https://doi.org/10.1073/pnas.1509820112

Tamás, G., Buhl, E. H., & Somogyi, P. (1997). Massive Autaptic Self-Innervation of GABAergic Neurons in Cat Visual Cortex. *The Journal of Neuroscience*, *17*(16), 6352-6364. https://doi.org/10.1523/jneurosci.17-16-06352.1997

Tanaka, N. K., Endo, K., & Ito, K. (2012). The organization of antennal lobe-associated neurons in the adult *Drosophila* melanogaster brain. *Journal of Comparative Neurology*, *520*(18), 4067-4130. https://doi.org/10.1002/cne.23142

Thoma, M., Hansson, B. S., & Knaden, M. (2015). High-resolution Quantification of Odor-guided Behavior in Drosophila melanogaster Using the Flywalk Paradigm. *J Vis Exp*(106), e53394. https://doi.org/10.3791/53394

Tobin, W. F., Wilson, R. I., & Lee, W.-C. A. (2017). Wiring variations that enable and constrain neural computation in a sensory microcircuit. *eLife*, *6*, e24838. https://doi.org/10.7554/eLife.24838

Tran-Van-Minh, A., Cazé, R. D., Abrahamsson, T., Cathala, L., Gutkin, B. S., & DiGregorio, D. A. (2015). Contribution of sublinear and supralinear dendritic integration to neuronal computations [Review]. *Frontiers in Cellular Neuroscience*, *9*. https://doi.org/10.3389/fncel.2015.00067

Trujillo-Cenoz, O. (1969). Some Aspects of the Structural Organization of the Medulla in Muscoid Flies I. *J Ultrastructural Research*, *27*, 533-553.

Van der Loos, H., & Glaser, E. M. (1972). Autapses in neocortex cerebri: synapses between a pyramidal cell's axon and its own dendrites. *Brain Res*, *48*, 355-360. https://doi.org/10.1016/0006-8993(72)90189-8

Vosshall, L. B., Wong, A. M., & Axel, R. (2000). An olfactory sensory map in the fly brain. *Cell*, *102*(2), 147-159. https://doi.org/10.1016/S0092-8674(00)00021-0

Wang, J. W. (2012). Presynaptic modulation of early olfactory processing in *Drosophila*. *Developmental neurobiology*, *72*(1), 87-99. https://doi.org/10.1002/dneu.20936

Wicher, D., & Miazzi, F. (2021). Functional properties of insect olfactory receptors: ionotropic receptors and odorant receptors. *Cell Tissue Res*, *383*(1), 7-19. https://doi.org/10.1007/s00441-020-03363-x

Wiles, L., Gu, S., Pasqualetti, F., Parvesse, B., Gabrieli, D., Bassett, D. S., & Meaney, D. F. (2017). Autaptic Connections Shift Network Excitability and Bursting. *Sci Rep*, *7*, 44006. https://doi.org/10.1038/srep44006

Wilson, R. I. (2013). Early Olfactory Processing in Drosophila: Mechanisms and Principles. *Annual review of neuroscience*, *36*, 217-241. https://doi.org/10.1146/annurev-neuro-062111-150533

Wilson, R. I., & Laurent, G. (2005). Role of GABAergic inhibition in shaping odor-evoked spatiotemporal patterns in the Drosophila antennal lobe. *J Neurosci*, *25*(40), 9069-9079. https://doi.org/10.1523/jneurosci.2070-05.2005

Xu, C. S., Hayworth, K. J., Lu, Z., Grob, P., Hassan, A. M., García-Cerdán, J. G., Niyogi, K. K., Nogales, E., Weinberg, R. J., & Hess, H. F. (2017). Enhanced FIB-SEM systems for large-volume 3D imaging. *eLife*, *6*, e25916. https://doi.org/10.7554/eLife.25916

Xu, C. S., Januszewski, M., Lu, Z., Takemura, S.-y., Hayworth, K. J., Huang, G., Shinomiya, K., Maitin-Shepard, J., Ackerman, D., Berg, S., Blakely, T., Bogovic, J., Clements, J., Dolafi, T., Hubbard, P., Kainmueller, D., Katz, W., Kawase, T., Khairy, K. A., . . . Plaza, S. M. (2020). A

Connectome of the Adult *Drosophila* Central Brain. *bioRxiv*, 2020.2001.2021.911859. https://doi.org/10.1101/2020.01.21.911859

Yang, K., Liu, T., Wang, Z., Liu, J., Shen, Y., Pan, X., Wen, R., Xie, H., Ruan, Z., Tan, Z., Chen, Y., Guo, A., Liu, H., Han, H., Di, Z., & Zhang, K. (2022). Classifying Drosophila olfactory projection neuron boutons by quantitative analysis of electron microscopic reconstruction. *iScience*, *25*(5), 104180. https://doi.org/https://doi.org/10.1016/j.isci.2022.104180

Yasuyama, K., Meinertzhagen, I. A., & Schurmann, F. W. (2003). Synaptic connections of cholinergic antennal lobe relay neurons innervating the lateral horn neuropile in the brain of *Drosophila melanogaster* [Research Support, Non-U.S. Gov't]. *J Comp Neurol*, *466*(3), 299-315. https://doi.org/10.1002/cne.10867

Yasuyama, K., & Salvaterra, P. M. (1999). Localization of choline acetyltransferase-expressing neurons in *Drosophila* nervous system. *Microscopy research and technique*, *45*(2), 65-79. http://onlinelibrary.wiley.com/doi/10.1002/(SICI)1097-0029(19990415)45:2<65::AID-JEMT2>3.0.CO;2-0/abstract

Yin, L., Zheng, R., Ke, W., He, Q., Zhang, Y., Li, J., Wang, B., Mi, Z., Long, Y.-s., Rasch, M. J., Li, T., Luan, G., & Shu, Y. (2018). Autapses enhance bursting and coincidence detection in neocortical pyramidal cells. *Nat Commun*, *9*(1), 4890. https://doi.org/10.1038/s41467-018-07317-4

Yokoi, M., Mori, K., & Nakanishi, S. (1995). Refinement of odor molecule tuning by dendrodendritic synaptic inhibition in the olfactory bulb. *Proceedings of the National Academy of Sciences*, *92*(8), 3371-3375. https://doi.org/doi:10.1073/pnas.92.8.3371

Zheng, Z., Lauritzen, J. S., Perlman, E., Robinson, C. G., Nichols, M., Milkie, D., Torrens, O., Price, J., Fisher, C. B., Sharifi, N., Calle-Schuler, S. A., Kmecova, L., Ali, I. J., Karsh, B., Trautman, E. T., Bogovic, J. A., Hanslovsky, P., Jefferis, G. S. X. E., Kazhdan, M., . . . Bock, D. D. (2018). A Complete Electron Microscopy Volume of the Brain of Adult Drosophila melanogaster. *Cell*, *174*(3), 730-743.e722. https://doi.org/https://doi.org/10.1016/j.cell.2018.06.019

**FIGURES**

**Figure 1: A correlative approach to analyze the ultrastructure of identified olfactory glomeruli**
**A-B:** Two-photon laser scans of the antennal lobe in *Orco-Gal4; UAS-GCaMP6s* flies where Orco-positive olfactory sensory neurons (OSNs) in the glomerular neuropil were labeled by GCaMP (green fluorescence). Glomeruli DA2 (A) and DL5 (B) are encircled. Schematics show their relative position in the antennal lobe. Once the glomerulus of interest was identified, its boundaries were delineated using fiducial marks (white triangles) via laser branding, which enabled their identification at the ultrastructural level. **C-D**: Representative images of the same glomeruli (DA2 in **C** and DL5 in **D**) obtained with focused-ion-beam electron microscopy (FIB-SEM), showing their ultrastructure. Asterisks indicate the main neurite of uniglomerular projection neurons entering the glomerulus. White triangle shows a 2-photon laser mark (see also **A** and **B**). **E**: FIB-SEM image of a polyadic synapse: the presynaptic site (red arrowhead) is composed of a T-bar shaped presynaptic density, surrounded by small vesicles, and is apposed to several postsynaptic profiles (cyan dots). Scheme of a tetrad synapse: a presynaptic site with its T-bar (red arrowhead) forms four output connections (arrows) with four postsynaptic input sites (cyan dots). **F:** A skeleton-based reconstruction of an OSN axon terminal (green line) with presynaptic (red dots) and postsynaptic sites (cyan dots). The dark grey shading surrounding the OSN trace represents the volume-based reconstruction of the same neuron. Tracing and reconstruction were performed within the FIB-SEM dataset (light grey area).

**Figure 2: Neuron classification and neuronal composition of the DA2 and DL5 glomeruli**
**A**: Representative examples of each neuron class in glomeruli DA2 and DL5. Shown are FIB-SEM images (left column), volumetric neuronal reconstructions (middle column), and skeleton-based neuron traces (right column) for olfactory sensory neurons (OSNs, green), uniglomerular projection neurons (uPNs, magenta), and multiglomerular neurons (MGNs, blue). Key ultrastructural features including T-bars (black triangle), mitochondria (asterisks) and spinules (white triangle) are indicated on the FIB-SEM images. Volumetric reconstructions (middle column) depict the general morphology of each neuron class. On the skeleton traces, presynaptic and postsynaptic sites are marked with red and cyan dots, respectively (right column). **B:** Average branching intensity (branching points per µm of neuronal-fiber length) for each neuron class OSNs, uPNs and MGNs in DA2 and DL5. Data represent mean+ standard deviation (error bars). Data points represent single values. Means were compared using Wilcoxon two-sample test. No significant differences of branching points/µm were observed for OSNs or MGNs between glomeruli (significance was not tested for uPNs due to the presence of a single uPN in DL5). **C**: Schematic summary, for each glomerulus, showing its volume (in $\mu m^3$), the number of neurons per class (excluding MGNs), the total fiber length of all neurons for each neuron class and the total number of individual synaptic contacts.

**Table 1. Glomerular innervation and synaptic composition**
Quantitative comparison of neuronal and synaptic parameters between glomeruli DA2 and DL5 for each neuron class- OSNs (green), uPNs (magenta) and MGNs (blue) – as well as the combined totals. **Row 1**: Total length of all neurons per neuron class and the overall total length for all neurons for each glomerulus. **Row 2-4**: Synapse counts: number of input sites (inputs), output

sites (outputs) and T-bars. **Row 5**: Innervation density: calculated as total neuron length (µm; row 1)/glomerular volume (µm$^3$); glomerular volumes: DA2=1500 µm$^3$ and DL5=2600 µm$^3$ (see Figure 1C). **Row 6-8**: Synaptic density per unit glomerular volume (µm$^3$): total number of all input sites (inputs), output sites (outputs) and T-bars for each neuron class and all neurons divided by glomerular volume. **Row 9-11**: Average synaptic density along neuronal fibers (see also Figure 3 – supplement 1): number of inputs, outputs or T-bars per µm of neuron length. **Row 12-13:** Average synaptic ratios: T-bars-to-inputs or outputs-to-inputs. **Row 14:** Polyadicity: the average number of postsynaptic sites at each T-bar in DA2 and DL5. The ratios in rows 12-14 were calculated based on synaptic counts normalized to neuron length (rows 9-11). The color shading highlights values with a relative difference greater than 20% between DA2 and DL5 (see relative differences Table S1). Dark shades highlight values greater in DA2 than DL5 (green = OSNs), magenta = uPNs), blue = MGNs); light shades indicate values lower in DA2 than in DL5.

**Figure 3: Innervation density and synaptic density in DA2 and DL5**

**A-E**: Quantification of average glomerular innervation density of OSNs (**A**), uPNs (**B**), MGNs (**C**) and all glomerular neurons combined (**D**); and synaptic density of input sites (inputs), output sites (outputs), T-bars and average polyadicity. Innervation density: total length (µm) of each neuronal fiber normalized to one µm$^3$ of glomerular (glom.) volume. Synaptic density: number of input sites, output sites, or T-bars for each neuronal fiber normalized to one µm$^3$ of glomerular volume. Polyadicity: average number of single output sites per T-bar for each neuronal fiber. Data for DA2 shown in dark colors and for DL5 in light colors. Number of neurons in DA2: OSNs (green) n= 44; uPNs (magenta) n= 7; MGNs (blue) n=180; all neurons n=231, in DL5: OSNs n=46; uPN n=1; MGNs n=221; all neurons n=268. Data are presented as mean with standard deviation (error bars). Data points represent single neuron values. Means were compared using either Student's t-test (OSNs) or Wilcoxon two-sample test (MGNs and all neurons). uPNs were not compared to the single uPN of th DL5 glomerulus. Significance value: $p>0.05$ (not significant, no star), $p\leq0.05$ (*), $p\leq0.01$ (**), $p\leq0.001$ (***). Values are provided at data availability; polyadicity values are listed in Table 1, row 14.

**Figure 4: Lateralization of OSN terminals in the antennal lobes**

**A**: Illustration of an ipsilateral (dark green) and a contralateral (light green) OSN with dendrites in the corresponding antennae and their axonal projections to the ipsilateral olfactory glomerulus in the antennal lobe (AL) (dashed rectangle). **B**: Exemplary skeleton traces of an ipsilateral (dark green) and a contralateral (light green) OSN terminal inside glomerulus DA2. The ipsilateral OSN axons reach the glomerulus via the ipsilateral antennal nerve (arrow down) and leave the glomerulus towards the AL commissure (arrow up) while OSN axons originating at the contralateral antenna reach the glomerulus via the AL commissure. Red dots: presynaptic sites; blue dots: postsynaptic sites. **C**: Boxplots showing the fraction of synaptic output to uPNs (in magenta), - to OSNs (in green) or - to MGNs (in blue), for the ipsilateral OSNs (dark green boxplot) and contralateral OSNs (light green), respectively, in the DA2, DL5 and VA1v glomeruli. **D**: Boxplots showing the fraction of synaptic input of the same ipsilateral and contralateral OSNs that they receive from OSNs and MGNs. Connection polarity is indicated by arrows in the schematic neuronal drawings on the left of each plot. Dots represent single values. Means were compared using Student's T-test. Significance value: $p>0.05$ (not significant, no star)), $p\leq0.05$ (*),

p≤0.01 (**), p≤0.001 (***). Mean and Median values are provided at data availability. The data for glomerulus VA1v was extracted from (Horne et al., 2018).

**Figure 5: Strength of synaptic connections between neuron classes in the circuitry of DA2, DL5 and VA1v.**

**A:** Schematic representation of the principal connection motifs among the neuron classes OSNs (green), uPNs (magenta) and MGNs (blue). Synaptic connections directed towards uPNs are defined as feedforward and those directed towards OSNs or from uPNs to MGNs are classified as feedback connections (indicated by arrows). **B-D**: Alluvial diagrams of the glomerular circuitry in DA2 (**B**), DL5 (**C**) and VA1v (**D**). Each diagram shows the relative synaptic strength calculated as the proportion of 1:1 single synaptic contact between each neuron class in relation to the total number of synaptic contacts in their respective glomerulus. The synaptic strength between each neuron class, given as percentage, is indicated by the thickness of the lines. The proportions (as percentage) of output (left side) or input (right side) are illustrated by colored rectangles to the left or right of each alluvial diagram. The total number of synaptic contacts is indicated below the diagrams. Percentages of the relative synaptic strength and synaptic counts are listed in the supplementary Table S1. **E:** Stacked bar charts depict output (E') and input (E'') fractions (given as percentages) of each neuron class: OSNs (green), uPNs (magenta), MGNs (blue), schematically illustrated next to the bar charts respectively, to each of the other neuron classes for glomeruli DA2, DL5 and VA1v. Fractions are color-coded according to the neuron class of the respective connecting partner.

**Figure 6: Differences in connectivity strength in glomeruli DA2, DL5 and VA1v**

**A**: Schematic representation of synaptic connection motifs (arrows) between OSNs (green), uPNs (magenta), and MGNs (blue) in glomeruli DA2, DL5 and VA1v. The number of neurons of each class - or truncated neuronal fibers (indicated in brackets) - is shown within the corresponding circle. **B**: Diagrams of connection motifs (left) that are consistently stronger or weaker in DA2 and VA1v compared to DL5. Relative differences (expressed as percentages) between DA2 and DL5, and between VA1v and DL5 are illustrated as upward (stronger) or downward (weaker) arrows, with arrow intensity indicating the magnitude of the difference (see legend at the bottom) from the perspective of the target glomerulus (as defined in the table header). All relative differences values are provided in Table S2.

**Figure 7: Distribution of pre- and postsynaptic partners of autapses in the uPN dendrite of the DL5**

**A**: Distribution of autaptic presynaptic (red dots) and postsynaptic (cyan dots) sites mapped onto a dendrogram of the single uPN dendrite in glomerulus DL5. The basal root node (black dot) marks the entry site of the uPN dendrite into the glomerulus (i.e., the point closest to its soma). Clusters of autaptic input sites along specific branches are encircled. **B**: Simplified dendrogram of the uPN illustrating distinct strahler orders, with distal branches (orders 1-4) and at basal branches (orders 5-8); see legend on the right. **C**: Distribution of autaptic presynaptic (left) and postsynaptic (right) input sites along the dendrite, shown as proportions at each corresponding strahler order (color coded). Note that autaptic postsynaptic sites are located almost exclusively at the most distal dendritic branches. **D**: Dendrogram of the DL5-uPN showing the locations of

presynaptic sites (triangles) and postsynaptic sites (circles) for selected autapses (color-matched pairs). Autapses with large geodesic distance between their components are labeled with numbers; those with short distances are encircled and labeled with letters. **E**: Schemes of the dendrogram illustrating the location of the presynaptic (red dot) and postsynaptic (cyan dot) sites of individual autapses, the geodesic distance between them (measured along the dendrite in µm), and the number of branching points (orange dots) separating the pre- and postsynaptic components. **F**: Histogram showing the number of autapses grouped by geodesic distance between their pre- and postsynaptic sites (as illustrated in E). **G**: the number of autapses categorized by the number of branch points between their pre- and postsynapses along the uPN dendrite (as illustrated in E).

**Figure 8. Graphic summary illustrating general differences between narrowly and broadly tuned olfactory circuits.**

Graphic summary of key circuit features that distinguish the two narrowly tuned olfactory glomeruli studied here (dark grey circle) from a broadly tuned on (light grey circle). Olfactory glomeruli are the first relay station where olfactory information is processed before being transmitted to higher brain centers, including the lateral horn (LH) and mushroom body calyces (MBc). The model is based on a comparative analysis of the narrowly tuned circuits of DA2 and VA1v, and the broadly tuned circuit of DL5. Circuit components include uniglomerular projection neurons (uPNs, magenta), local interneurons (LNs, blue), and olfactory sensory neurons (OSNs, green) from both ipsilateral and contralateral brain hemispheres. In the narrowly tuned circuits, multiple uPNs are present, whereas in the broadly tuned circuit LNs are more numerous, as indicated by the number of circles. Connectivity strength between neuronal types is inferred from synaptic counts (1:1 presynaptic-postsynaptic sites) and is represented by the size of the connecting triangles. Differences in neuron number are indicated by the number of circles. In narrowly tuned circuits, OSNs exhibit stronger synaptic output **(1)** and form stronger reciprocal connections with sister OSNs **(2)** and uPNs **(3).** The lateralization of OSN connectivity is reduced compared to broadly tuned circuits, where ipsilateral output to uPNs and contralateral output to the LNs dominates **(4).** Feedback synapses from uPNs to LNs **(5)** and from LNs to OSNs **(6)** are weaker in narrowly tuned circuits. In contrast, the broadly tuned circuit DL5 exhibits weaker OSN output and stronger lateralization of OSN inputs. Additionally, autapses are observed in the single uPN of DL5, whereas reciprocal uPN connections are a feature of narrowly tuned circuits. The model attributes to LNs the features quantified for a larger group of neurons (multiglomerular neurons, MGNs), of which the great majority are LNs, as discussed in the main text.

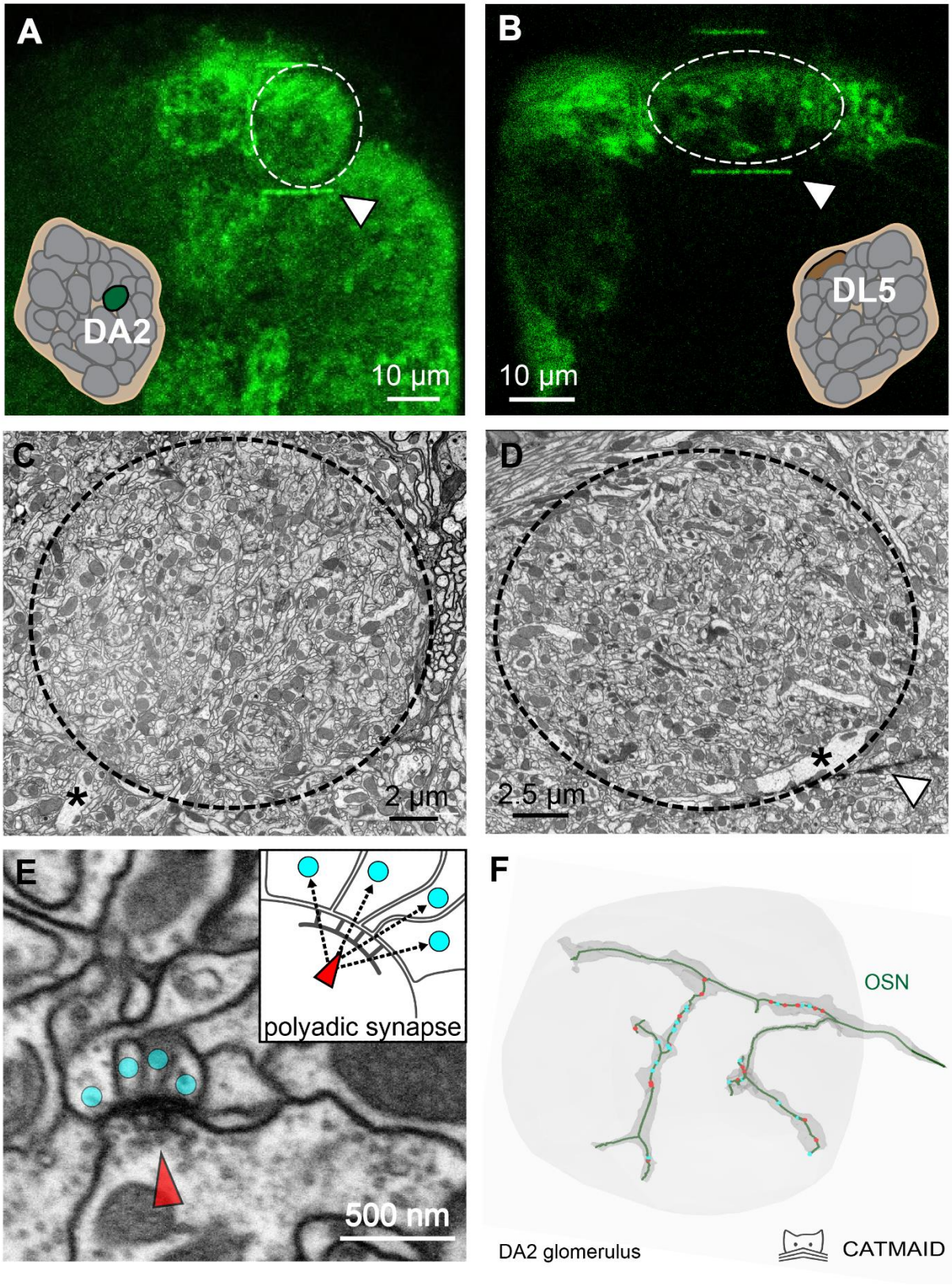
A
DA2
10 µm
B
DL5
10 µm
C
2 µm
D
2.5 µm
E
polyadic synapse
500 nm
F
OSN
DA2 glomerulus
CATMAID

**Figure 1**

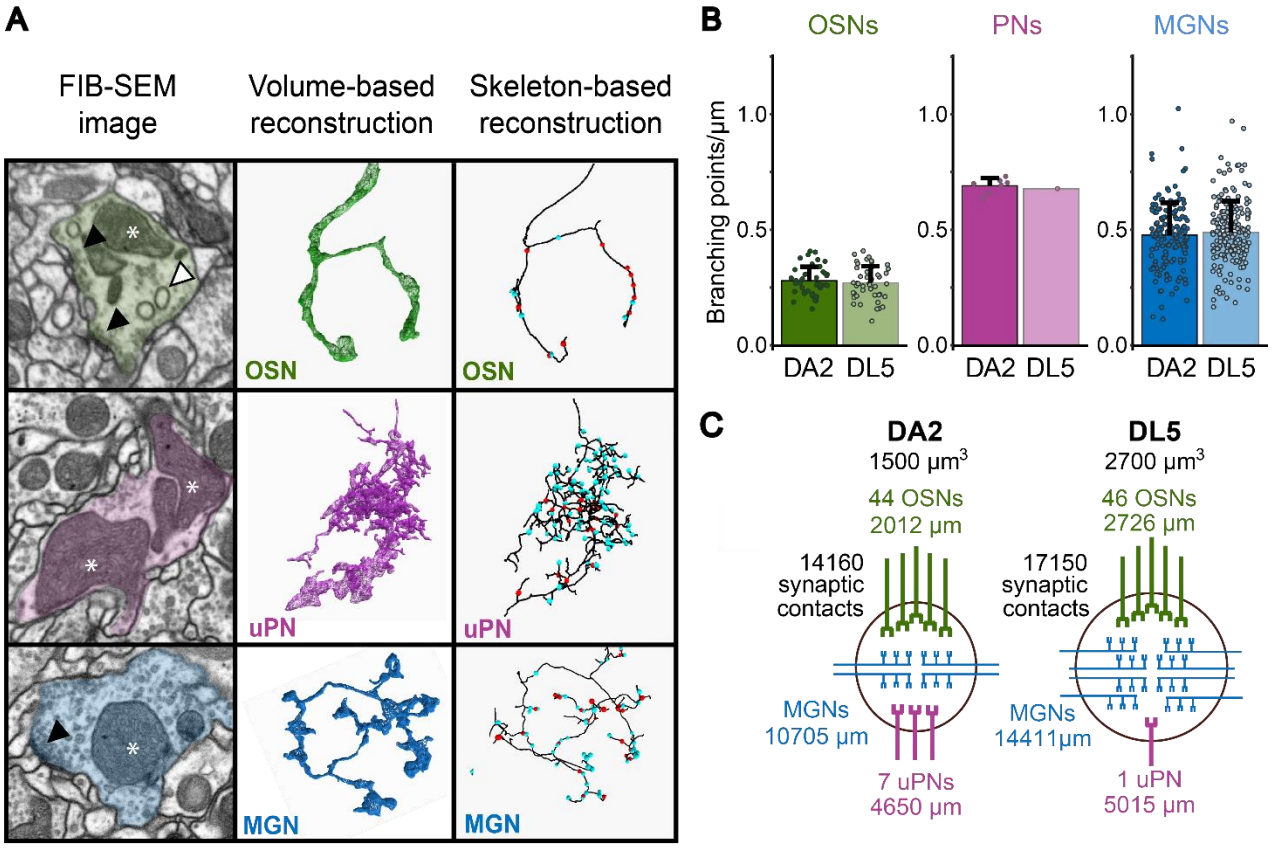
A
FIB-SEM image
Volume-based reconstruction
Skeleton-based reconstruction
OSN
OSN
uPN
uPN
MGN
MGN
B
OSNs
PNs
MGNs
Branching points/µm
1.0
0.5
0.0
DA2
DL5
C
DA2
1500 µm3
44 OSNs
2012 µm
14160 synaptic contacts
MGNs 10705 µm
7 uPNs 4650 µm
DL5
2700 µm3
46 OSNs
2726 µm
17150 synaptic contacts
MGNs 14411µm
1 uPN 5015 µm

**Figure 2**

| Row | Values | Unit | OSNs | | uPNs | | MGNs | | all neurons | |
|---|---|---|---|---|---|---|---|---|---|---|
| | | | DA2 | DL5 | DA2 | DL5 | DA2 | DL5 | DA2 | DL5 |
| 1 | Total neuronal length | µm | 2012 | 2727 | 4652 | 5015 | 10705 | 14411 | 17370 | 22153 |
| 2 | Total synaptic counts | input | 868 | 1083 | 3887 | 3955 | 7229 | 9018 | 11984 | 14056 |
| 3 | | output | 6671 | 6828 | 1624 | 3108 | 5659 | 6749 | 13954 | 16685 |
| 4 | | T-bars | 1063 | 1213 | 322 | 602 | 1263 | 1572 | 2648 | 3387 |
| 5 | Total innervation density (sum of length of all neuronal fibers/glomerular volume) | µm/µm$^3$ | 1.26 | 1.05 | 2.91 | 1.93 | 6.69 | 5.54 | 10.86 | 8.52 |
| 6 | Total glomerular synaptic density (total synaptic counts/glomerular volume) | inputs/µm$^3$ | 0.54 | 0.42 | 2.43 | 1.52 | 4.52 | 3.47 | 7.49 | 5.41 |
| 7 | | outputs/µm$^3$ | 4.17 | 2.63 | 1.02 | 1.20 | 3.54 | 2.60 | 8.72 | 6.42 |
| 8 | | T-bars/µm$^3$ | 0.66 | 0.47 | 0.20 | 0.23 | 0.79 | 0.60 | 1.66 | 1.30 |
| 9 | Neuronal synaptic density (synaptic counts/neuronal length) | inputs/µm | 0.42 | 0.39 | 0.83 | 0.79 | 0.62 | 0.59 | 0.59 | 0.56 |
| 10 | | outputs/µm | 3.37 | 2.62 | 0.33 | 0.62 | 0.52 | 0.51 | 1.06 | 0.87 |
| 11 | | T-bars/µm | 0.53 | 0.46 | 0.07 | 0.12 | 0.12 | 0.12 | 0.19 | 0.18 |
| 12 | Synaptic ratio | T-bars/inputs | 1.31 | 1.27 | 0.08 | 0.15 | 0.23 | 0.24 | 0.43 | 0.42 |
| 13 | | outputs/inputs | 8.29 | 7.29 | 0.40 | 0.79 | 1.04 | 1.11 | 2.40 | 2.17 |
| 14 | Polyadicity | outputs/T-bars | 6.35 | 5.70 | 4.95 | 5.16 | 3.22 | 2.64 | 3.88 | 3.17 |

**Table 1**

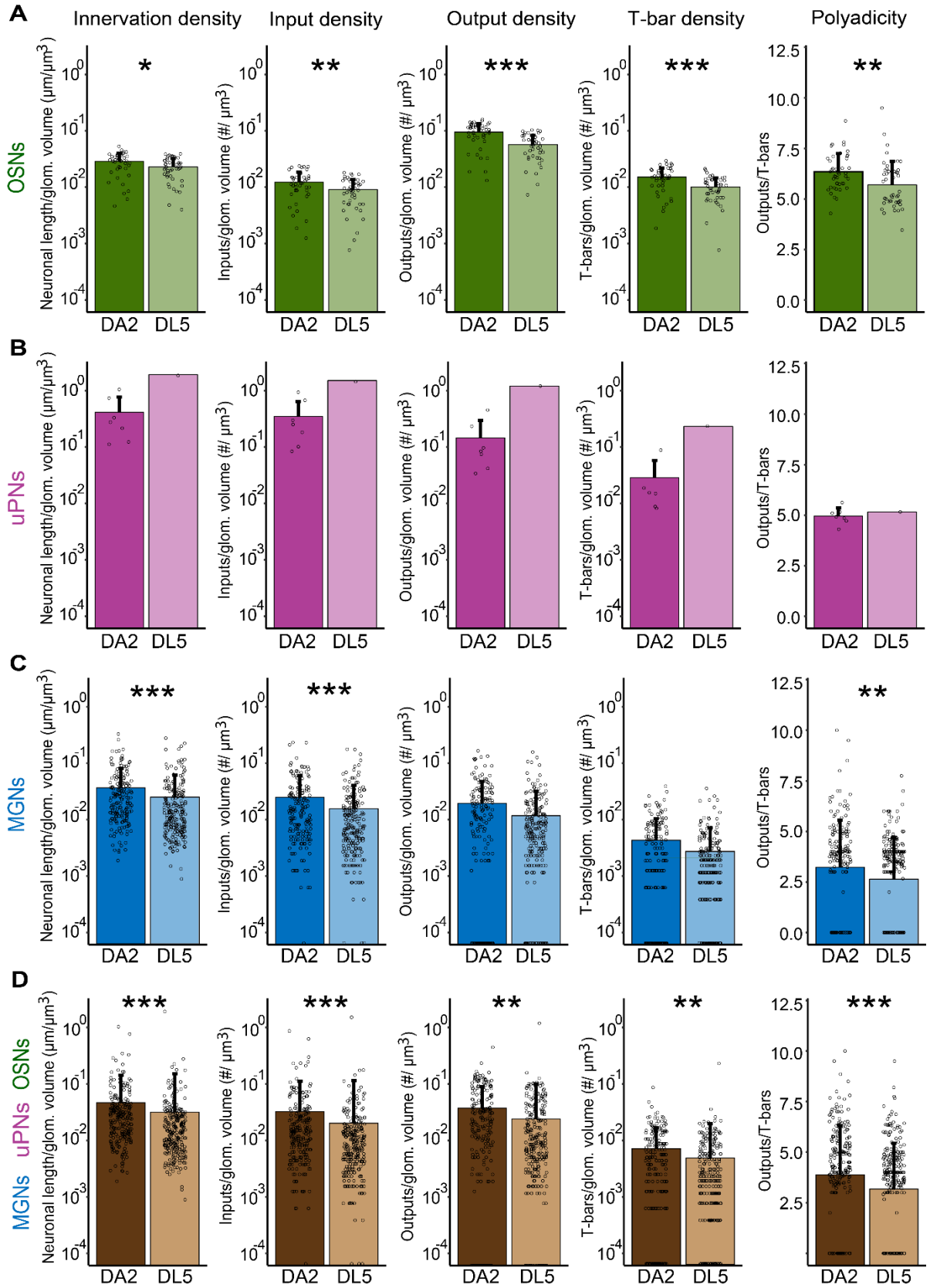
A
Innervation density
Input density
Output density
T-bar density
Polyadicity
OSNs
Neuronal length/glom. volume (µm/µm3)
Inputs/glom. volume (#/ µm3)
Outputs/glom. volume (#/ µm3)
T-bars/glom. volume (#/ µm3)
Outputs/T-bars
*
**
***
***
**
DA2
DL5
B
uPNs
C
MGNs
D
MGNs uPNs OSNs

**Figure 3**

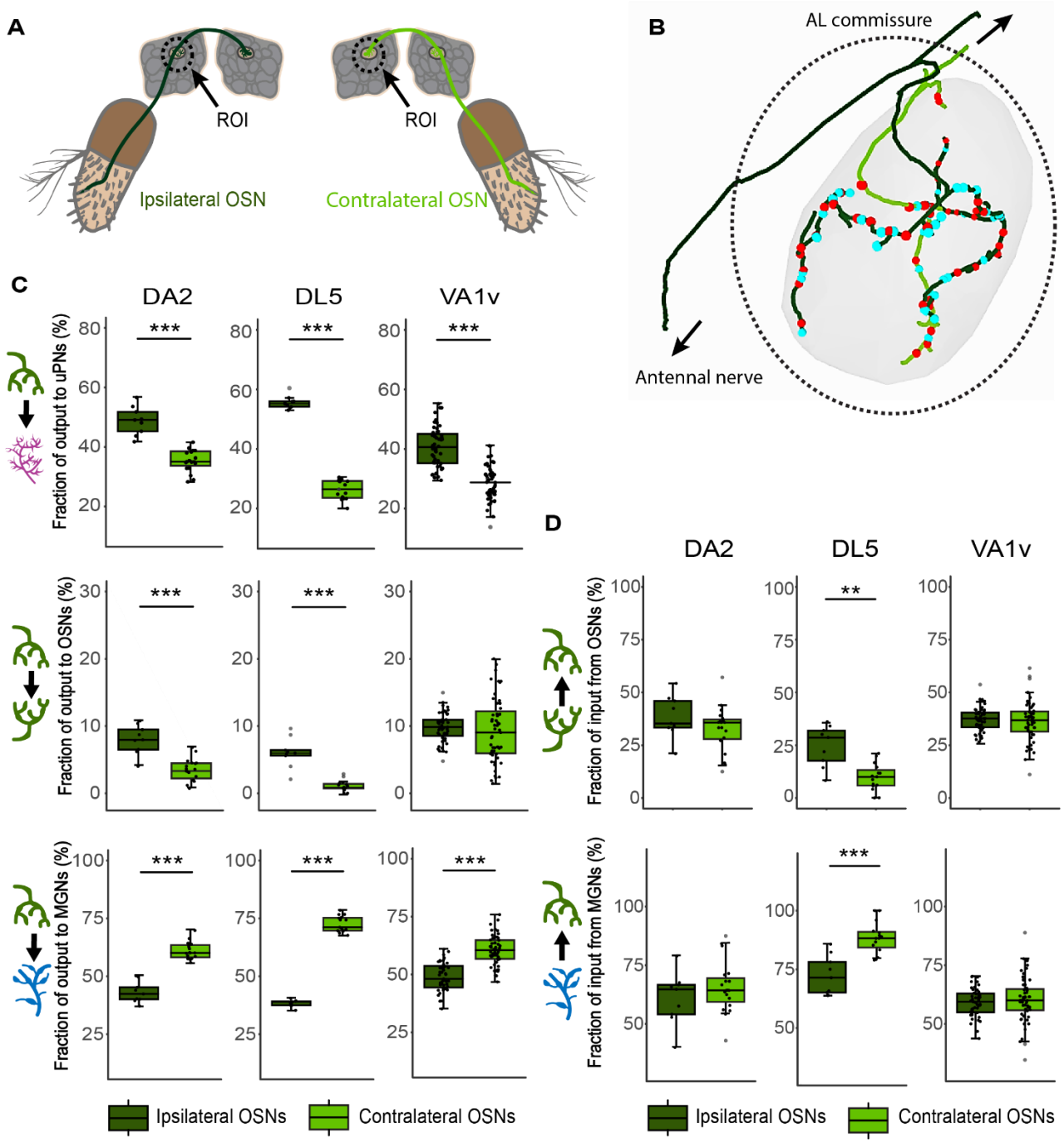
A
ROI
ROI
Ipsilateral OSN
Contralateral OSN
B
AL commissure
Antennal nerve
C
DA2
DL5
VA1v
Fraction of output to uPNs (%)
Fraction of output to OSNs (%)
Fraction of output to MGNs (%)
D
Fraction of input from OSNs (%)
Fraction of input from MGNs (%)
Ipsilateral OSNs
Contralateral OSNs

**Figure 4**

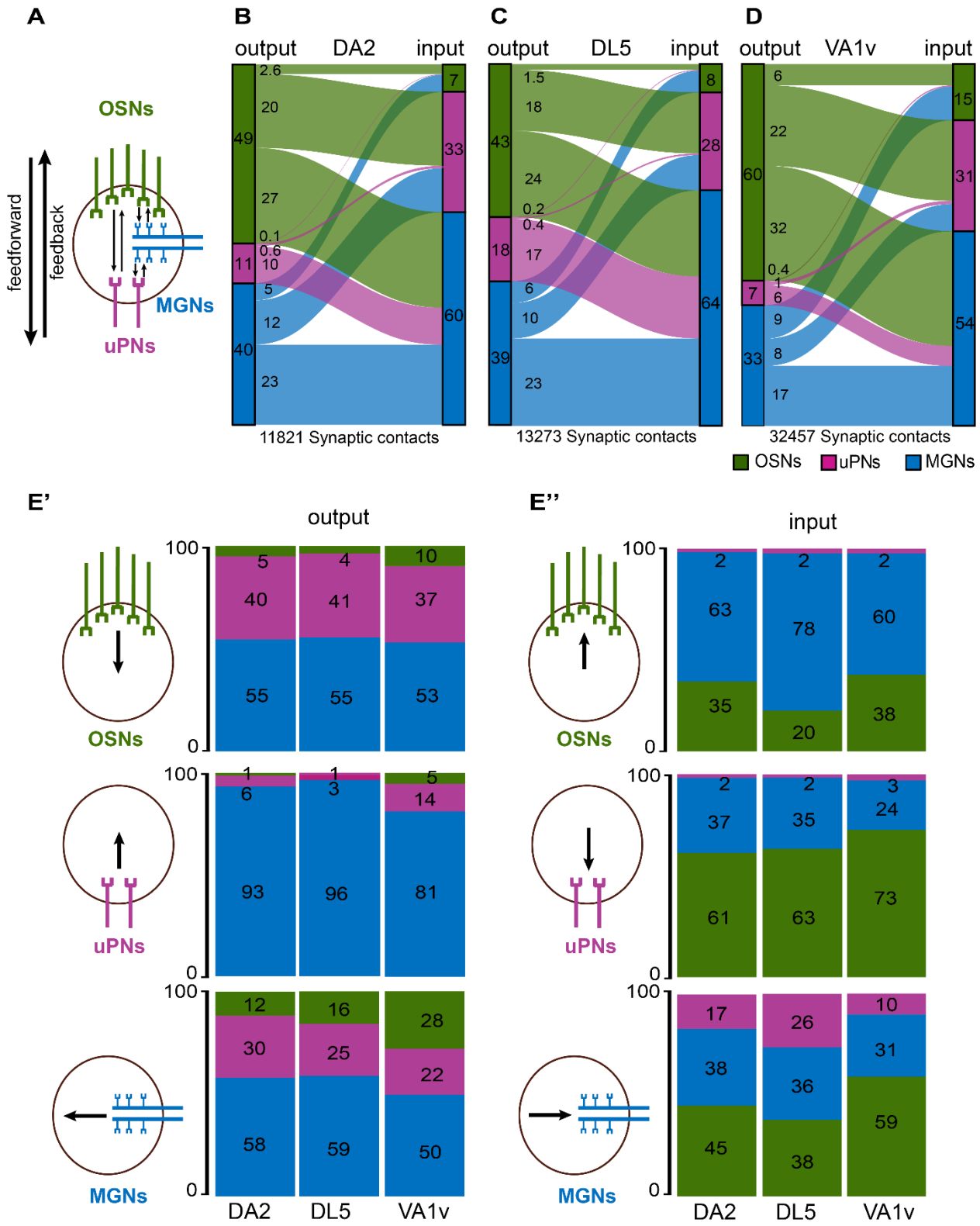
A
OSNs
feedforward
feedback
MGNs
uPNs
B
output
DA2
input
11821 Synaptic contacts
C
output
DL5
input
13273 Synaptic contacts
D
output
VA1v
input
32457 Synaptic contacts
OSNs
uPNs
MGNs
E'
output
E''
input
DA2
DL5
VA1v

**Figure 5**

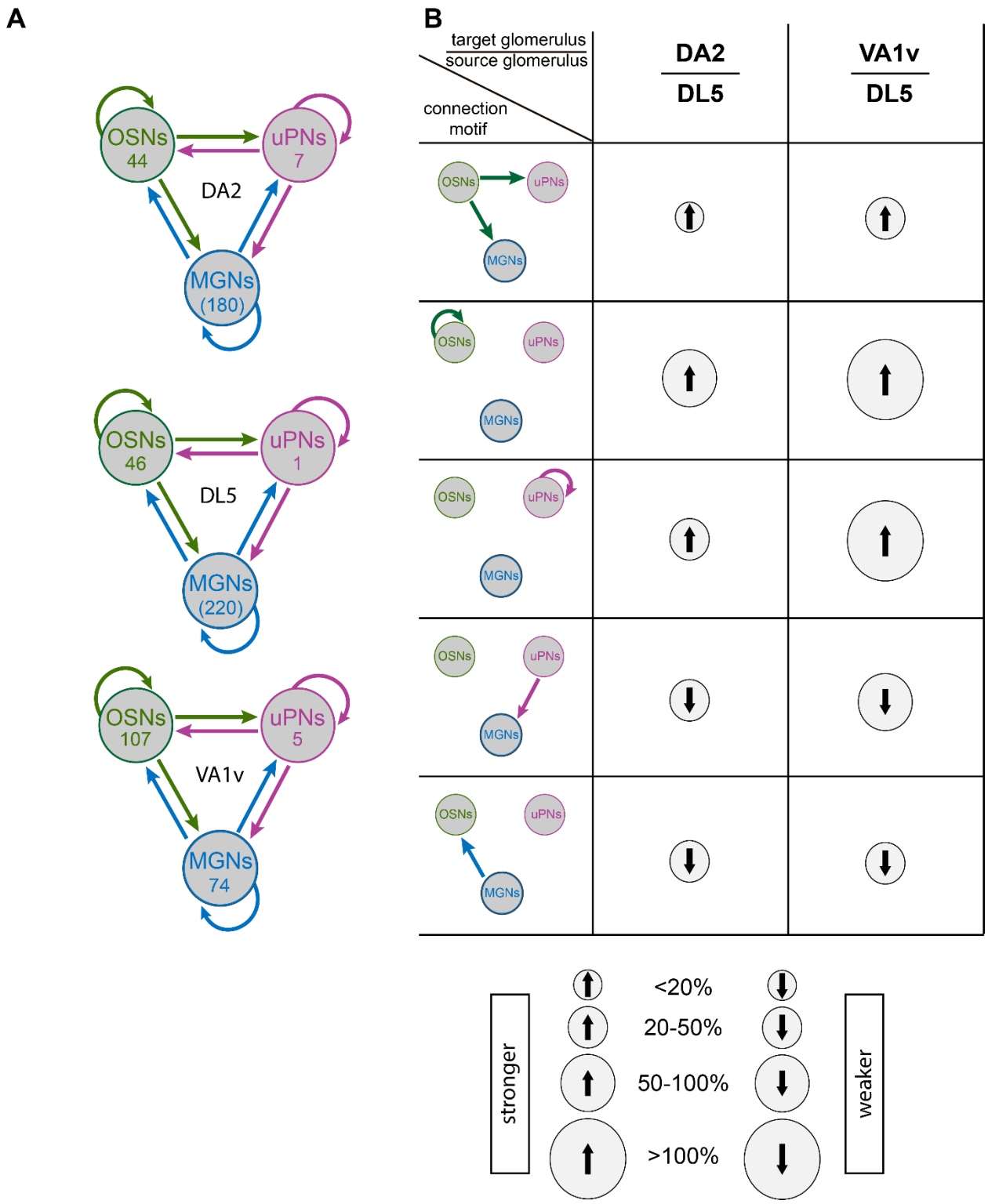
A
OSNs
44
uPNs
7
DA2
MGNs
(180)
OSNs
46
uPNs
1
DL5
MGNs
(220)
OSNs
107
uPNs
5
VA1v
MGNs
74
B
target glomerulus
source glomerulus
connection motif
DA2
DL5
VA1v
DL5
OSNs
uPNs
MGNs
<20%
20-50%
50-100%
>100%
stronger
weaker

**Figure 6**

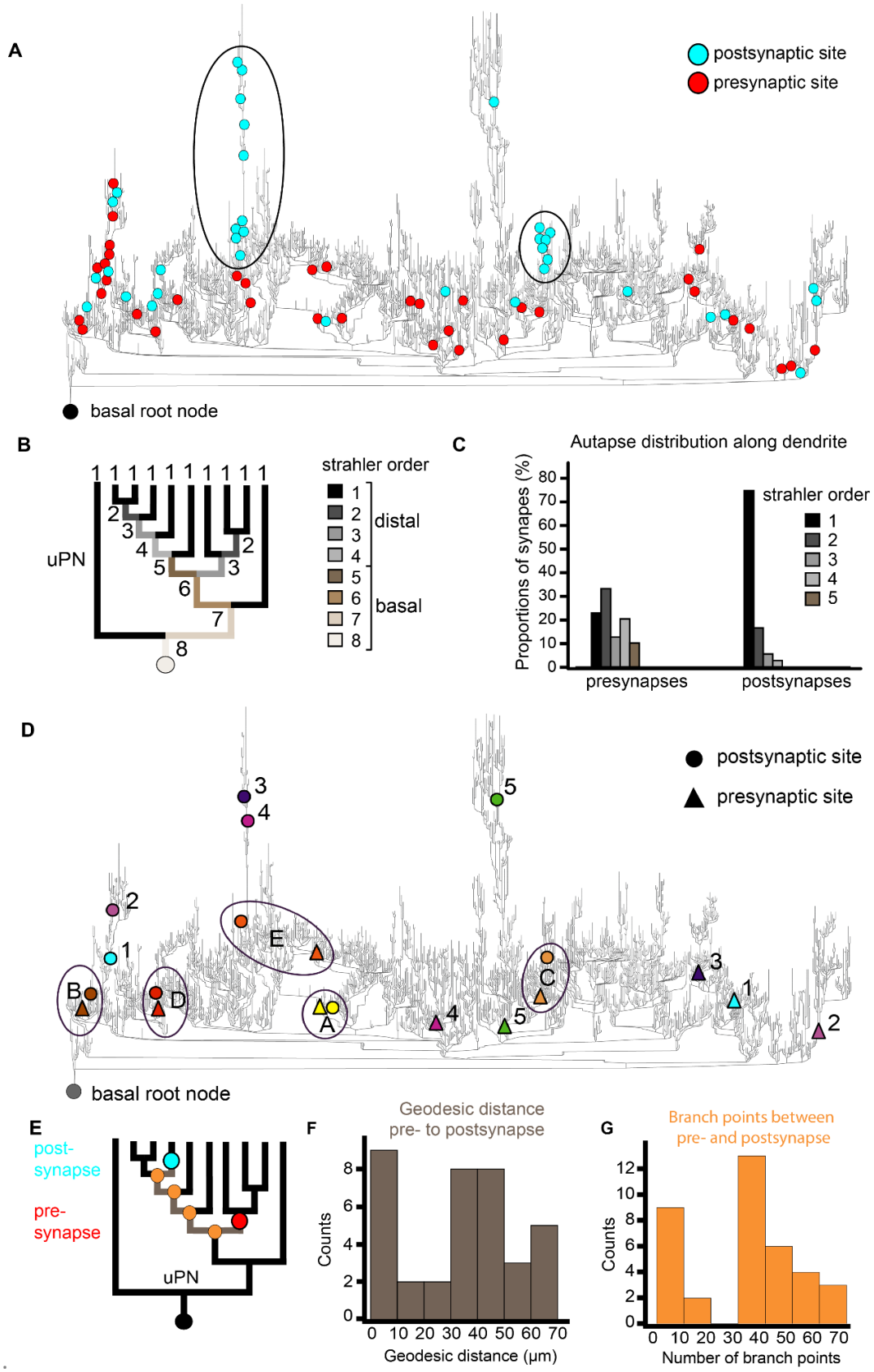
A
postsynaptic site
presynaptic site
basal root node
B
uPN
strahler order
distal
basal
C
Autapse distribution along dendrite
Proportions of synapses (%)
strahler order
presynapses
postsynapses
D
postsynaptic site
presynaptic site
basal root node
E
post-synapse
pre-synapse
uPN
F
Geodesic distance pre- to postsynapse
Counts
Geodesic distance (µm)
G
Branch points between pre- and postsynapse
Counts
Number of branch points

**Figure 7**

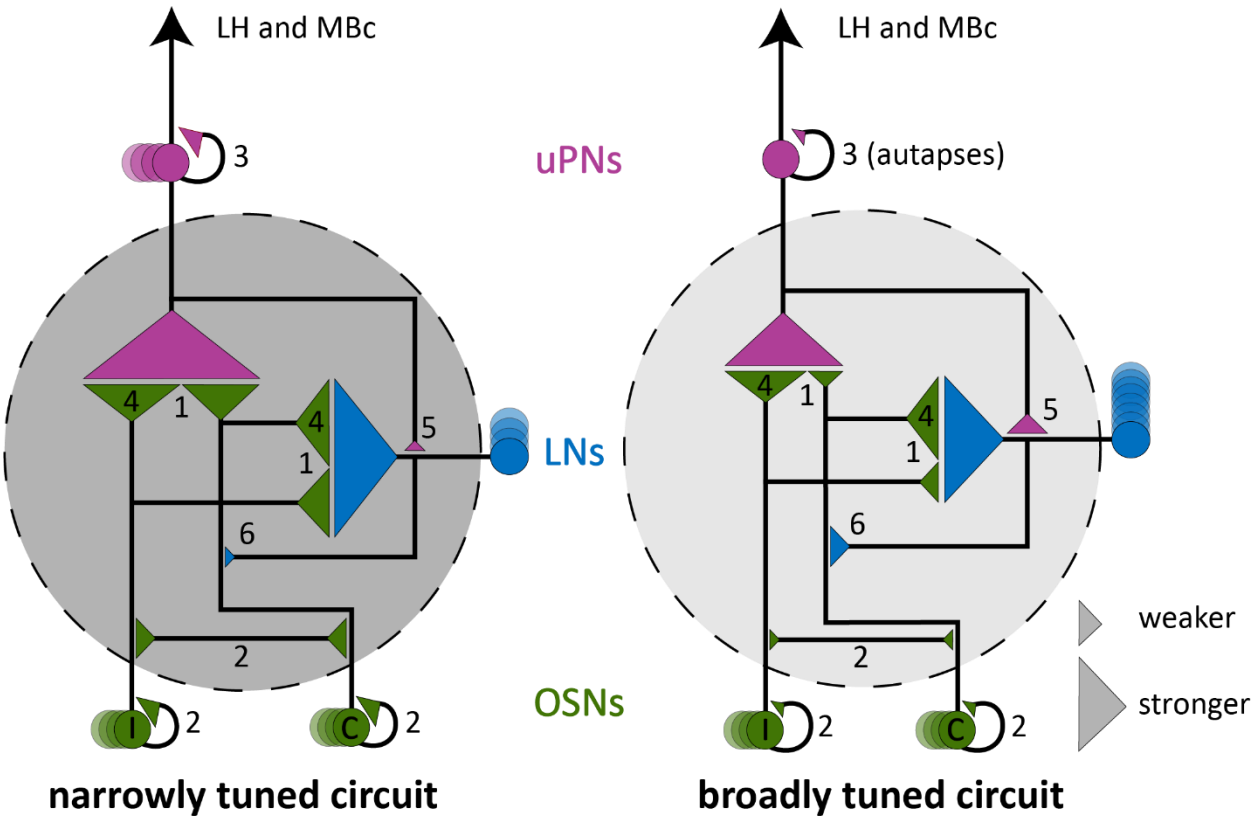
LH and MBc
3
uPNs
4
1
4
1
5
LNs
6
2
I
2
C
2
OSNs
narrowly tuned circuit
LH and MBc
3 (autapses)
4
1
4
1
5
6
2
I
2
C
2
weaker
stronger
broadly tuned circuit

**Figure 8**

## SUPPLEMENTARY FIGURES

**Figure 1 -- Video 1: FIB-SEM dataset of a DA2 glomerulus featuring a uPN reconstruction** (see extra file). The video shows a full FIB-SEM scan of a DA2 glomerulus at pixel resolution 4x4x20 nm, with the neuron trace of a single uniglomerular projection neuron (uPN#2) highlighted in yellow.

**Figure 2 – figure supplement 1: Neuronal volume and polyadicity**

**A**: Ratio between neuronal fiber volume and length in glomerulus DA2. Data represent mean + standard deviation (error bars) (OSNs n=30; uPNs n =5; MGNs n = 15). **B-D**: Frequency of T-bars associated with a number of postsynaptic contacts (Polyadicity) in OSNs (**B**), uPNs (**C**) and MGNs (**D**) in DA2 (dark shade) and DL5 (light shade)

**Supplementary Table S1: Relative differences of innervation and synaptic composition between glomeruli DA2 and DL5**

The table lists the relative differences between DA2 and DL5 (see Methods for calculations). Values that are at least 20% greater in DA2 than in DL5 are highlighted in dark shades and values that are at least 20% less in DA2 than in DL5 are highlighted in light shades.

**Figure 3 – figure supplement 1: Synaptic density along neuronal fibers in DA2 and DL5**

Counts of synaptic inputs, synaptic outputs and T-bars normalized to 1 µm of neuronal length along OSN, uPN or MGN fibers and collectively sampled for all neurons within the glomeruli DA2 (dark colors) and DL5 (light colors). DA2: OSNs (green) n= 44; uPNs (magenta) n= 7; MGNs (blue) n=180; all neurons n=231. DL5: OSNs n=46; uPN n=1; MGNs n=221; all neurons n=268. Data represent mean + standard deviation (error bars). Data points represent single values. Means are compared using either Student's T-test (in OSNs) or Wilcoxon two-sample test (in MGNs and all neurons). The uPNs of the DA2 are not compared to the single uPN of the DL5. Significance value: $p>0.05$ (not significant, no star), $p\leq0.05$ (*), $p\leq0.01$ (**), $p\leq0.001$ (***). Values are listed in Table 1, row 9-11.

**Figure 4 – figure supplement 1: Properties of ipsi- and contralateral OSNs.**

**A:** Boxplots depicting the total neuronal-fiber length and synaptic density (measured as the number of inputs, outputs, T-bars per unit of neuronal fiber length) for ipsilateral (dark green) and contralateral OSN terminals (light green). Dots represent single values. Means were compared using Student's T-test. Significance value: $p\leq0.05$ (*), $p\leq0.01$ (**), $p\leq0.001$ (***).

**Supplementary Table S2**: **Synaptic connectivity and relative differences between DA2, DL5 and VA1v**

Synapse counts and synaptic strength of each connection type in the DA2, DL5 and VA1v glomerulus. Three pairwise comparisons are shown: DA2 vs. DL5 (top table), VA1v vs. DL5 (middle table), and VA1v vs. DA2 (bottom table). The relative synaptic strength (rel syn strength) of each

connection type (listed on the left) and the relative differences (rel differences) (listed on the right) are color coded.

**Supplementary Table S3: Connectivity of single neurons in DA2**

**Supplementary Table S4: Connectivity of single neurons in DL5**

**Figure 7 – figure supplement 1: Distribution of synapses and autapses along the DL5 uPN dendrite in DL5**

**A**: 3D-reconstruction of the dendritic tree of the single uPN in glomerulus DL5, shown as a skeleton trace with artificial thickness scaled according to Strahler order. Autapses are indicated as cyan dots. The entry site of the uPN main dendrite into the glomerulus (the point closest to the soma) is defined as the basal root node. **B**: Number of autaptic presynaptic (magenta) and postsynaptic (cyan) sites plotted against their geodesic distance from the basal root node (indicated by a black circle in A). **C**: Proportional distribution of all presynaptic and postsynaptic sies (excluding autaptic connections) across Strahler orders in the DL5 uPN dendritic tree(see legend inset). Note the high proportion of postsynaptic sites located on the most distal dendritic branches.

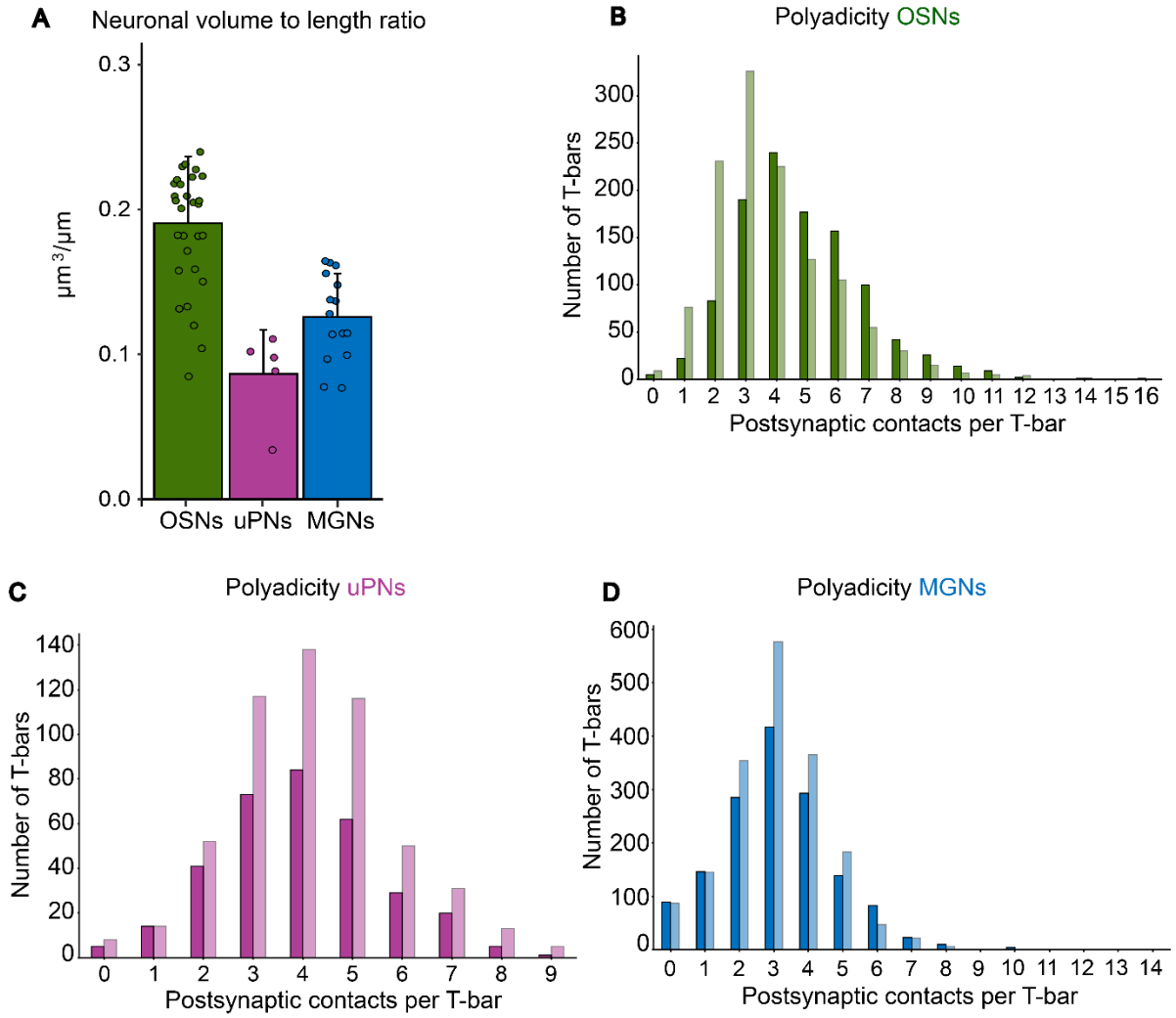


**Figure 2 – figure supplement**

| Row | Values | Unit | OSNs | uPNs | MGNs | all neurons |
|---|---|---|---|---|---|---|
| | | | Relative differences between DA2 and DL5 | | | |
| 1 | Total neuronal length | µm | -26 | -7 | -26 | -22 |
| 2 | Total synaptic counts | input | -20 | -2 | -20 | -15 |
| 3 | | output | -2 | -48 | -16 | -16 |
| 4 | | T-bars | -12 | -47 | -20 | -22 |
| 5 | Total innervation density (sum of length of all neuronal fibers/glomerular volume) | µm/µm$^3$ | 20 | 51 | 21 | 27 |
| 6 | Total glomerular synaptic density (total synaptic counts/glomerular volume) | inputs/µm$^3$ | 30 | 60 | 30 | 39 |
| 7 | | outputs/µm$^3$ | 59 | -15 | 36 | 36 |
| 8 | | T-bars/µm$^3$ | 42 | -13 | 31 | 27 |
| 9 | Neuronal synaptic density (synaptic counts/neuronal length) | inputs/µm | 8 | 5 | 5 | 6 |
| 10 | | outputs/µm | 29 | -47 | 2 | 21 |
| 11 | | T-bars/µm | 16 | -45 | -5 | 7 |
| 12 | Synaptic ratio | T-bars/inputs | 3 | -47 | -6 | 2 |
| 13 | | outputs/inputs | 14 | -50 | -6 | 11 |
| 14 | Polyadicity | outputs/T-bars | 11 | -4 | 22 | 22 |

**Supplementary Table S1**

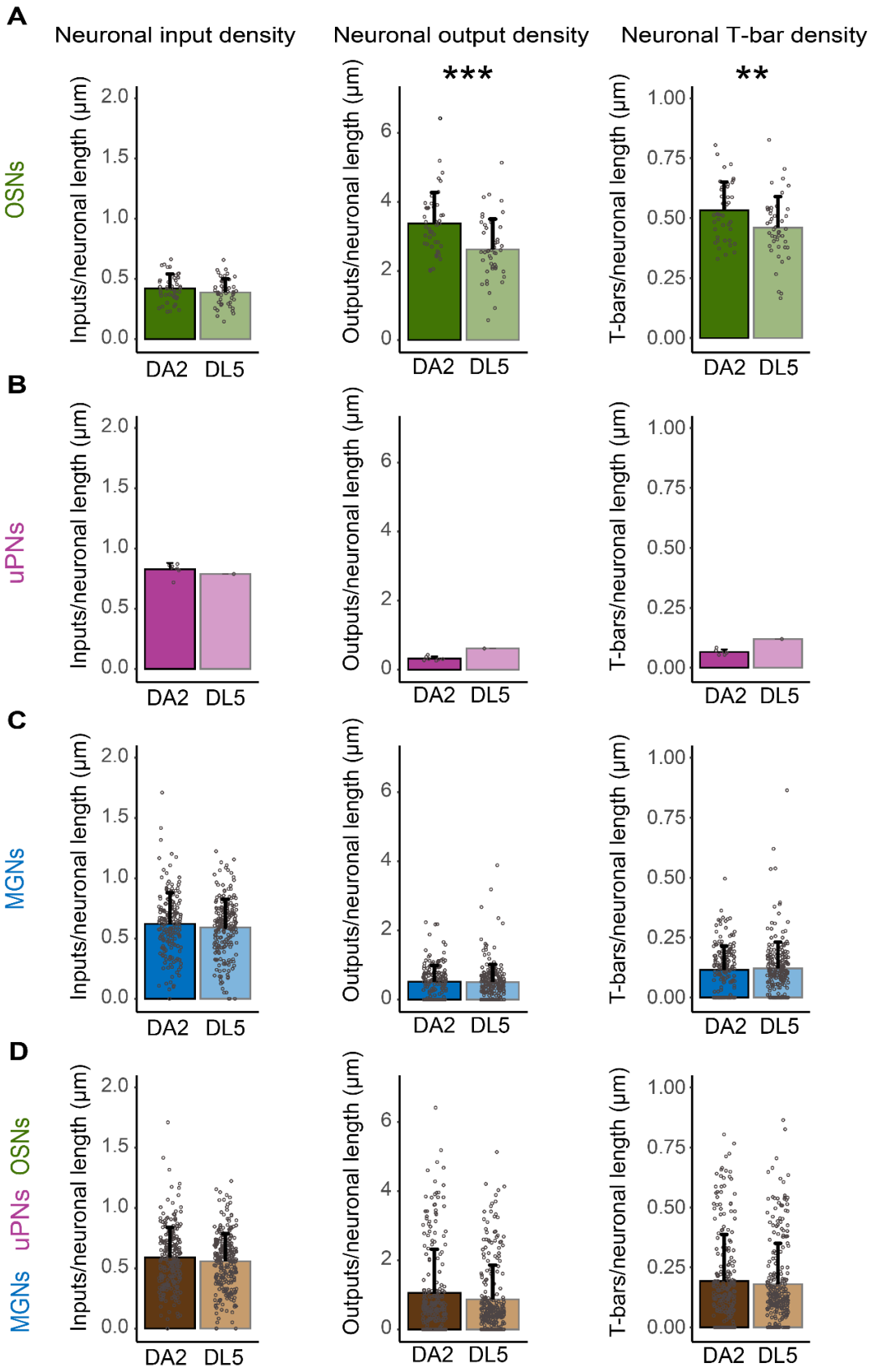


**Figure 3 – figure supplement 1**

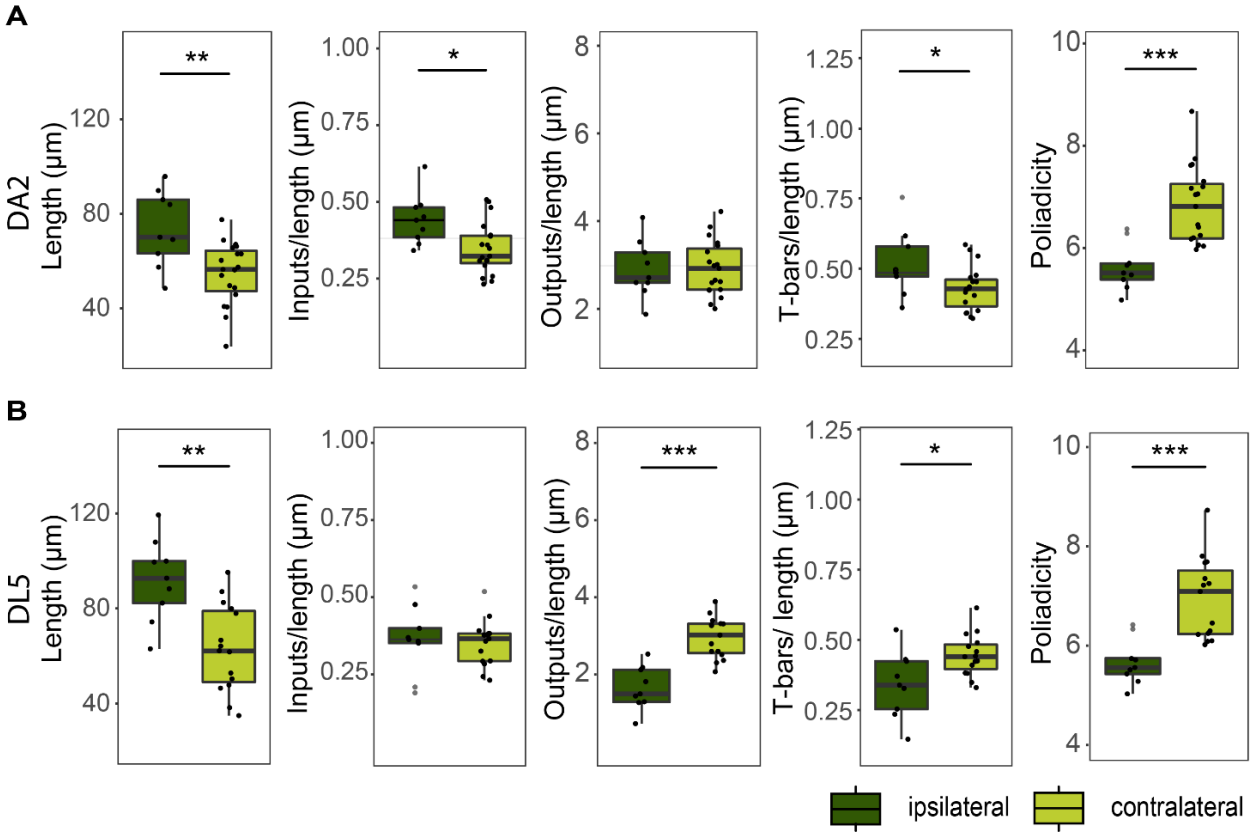


**Figure 4 – figure supplement 1**

| neuron class | connection motif | DA2 | rel syn strength (%) | rel out classes (%) | rel in classes (%) | DL5 | rel syn strength (%) | rel out classes (%) | rel in classes (%) | rel difference (%) | rel out difference (%) | rel in difference (%) |
|---|---|---|---|---|---|---|---|---|---|---|---|---|
| OSNs | OSNs>uPNs | 2365 | 19.99 | 49.48 | 7.37 | 2354 | 17.76 | 43.44 | 7.89 | 12.52 | 13.93 | -6.63 |
| | OSNs>MGNs | 3186 | 26.92 | | | 3201 | 24.15 | | | 11.47 | | |
| | OSNs>OSNs | 305 | 2.58 | | | 202 | 1.52 | | | 69.11 | | |
| uPNs | uPNs>OSNs | 16 | 0.14 | 10.92 | 32.62 | 26 | 0.20 | 17.50 | 28.07 | -31.08 | -37.63 | 16.18 |
| | uPNs>MGNs | 1205 | 10.18 | | | 2240 | 16.90 | | | -39.75 | | |
| | uPNs>uPNs | 71 | 0.60 | | | 54 | 0.41 | | | 47.26 | | |
| MGNs | MGNs>OSNs | 551 | 4.66 | 39.60 | 60.01 | 818 | 6.17 | 39.06 | 64.03 | -24.56 | 1.38 | -6.28 |
| | MGNs>uPNs | 1424 | 12.03 | | | 1313 | 9.91 | | | 21.47 | | |
| | MGNs>MGNs | 2711 | 22.91 | | | 3046 | 22.98 | | | -0.32 | | |
| | SUM | 11833 | 100 | 100 | 100 | 13254 | 100 | 100 | 100 | | | |

**Supplementary Table S2**

| neuron class | connection motif | VA1v | rel syn strength (%) | rel out classes (%) | rel in classes (%) | DL5 | rel syn strength (%) | rel out classes (%) | rel in classes (%) | rel difference (%) | rel out difference (%) | rel in difference (%) |
|---|---|---|---|---|---|---|---|---|---|---|---|---|
| OSNs | OSNs>uPNs | 7226 | 22.26 | 59.84 | 15.51 | 2354 | 17.76 | 43.44 | 7.89 | 25.35 | 37.76 | 96.53 |
| | OSNs>MGNs | 10295 | 31.72 | | | 3201 | 24.15 | | | 31.33 | | |
| | OSNs>OSNs | 1901 | 5.86 | | | 202 | 1.52 | | | 284.30 | | |
| uPNs | uPNs>OSNs | 117 | 0.36 | 6.83 | 30.67 | 26 | 0.20 | 17.50 | 28.07 | 83.76 | -60.96 | 9.26 |
| | uPNs>MGNs | 1801 | 5.55 | | | 2240 | 16.90 | | | -67.17 | | |
| | uPNs>uPNs | 300 | 0.92 | | | 54 | 0.41 | | | 126.86 | | |
| MGNs | MGNs>OSNs | 3016 | 9.29 | 33.33 | 53.82 | 818 | 6.17 | 39.06 | 64.03 | 50.56 | -14.68 | -15.96 |
| | MGNs>uPNs | 2430 | 7.49 | | | 1313 | 9.91 | | | -24.42 | | |
| | MGNs>MGNs | 5371 | 16.55 | | | 3046 | 22.98 | | | -27.99 | | |
| | SUM | 32457 | 100 | 100 | 100 | 13254 | 100 | 100 | 100 | | | |

**Supplementary Table S3**

| neuron class | connection motif | VA1v | rel syn strength (%) | rel out classes (%) | rel in classes (%) | DA2 | rel syn strength (%) | rel out classes (%) | rel in classes (%) | rel difference (%) | rel out difference (%) | rel in difference (%) |
|---|---|---|---|---|---|---|---|---|---|---|---|---|
| **OSNs** | **OSNs>uPNs** | 7226 | 22.26 | 59.84 | 15.51 | 2365 | 19.99 | 49.48 | 7.37 | 11.40 | 20.92 | 110.48 |
| | **OSNs>MGNs** | 10295 | 31,.2 | | | 3186 | 26.92 | | | 17.82 | | |
| | **OSNs>OSNs** | 1901 | 5.86 | | | 305 | 2.58 | | | 127.25 | | |
| **uPNs** | **uPNs>OSNs** | 117 | 0.36 | 6.83 | 30.67 | 16 | 0.14 | 10.92 | 32.62 | 166.60 | -37.41 | -5.96 |
| | **uPNs>MGNs** | 1801 | 5.55 | | | 1205 | 10.18 | | | -45.51 | | |
| | **uPNs>uPNs** | 300 | 0.92 | | | 71 | 0.60 | | | 54.06 | | |
| **MGNs** | **MGNs>OSNs** | 3016 | 9.29 | 33.33 | 53.82 | 551 | 4.66 | 39.60 | 60.01 | 99.57 | -15.84 | -10.33 |
| | **MGNs>uPNs** | 2430 | 7.49 | | | 1424 | 12.03 | | | -37.78 | | |
| | **MGNs>MGNs** | 5371 | 16.55 | | | 2711 | 22.91 | | | -27.76 | | |
| | **SUM** | 32457 | 100 | 100 | 100 | 11833 | 100 | 100 | 100 | | | |

| color code | rel syn strength (%) | <5 | 5-10 | 10-15 | 15-20 | >20 |
|---|---|---|---|---|---|---|
| | rel difference (%) | <10 | 10-20 | 20-50 | 50-100 | >100 |

**Supplementary Table S4**

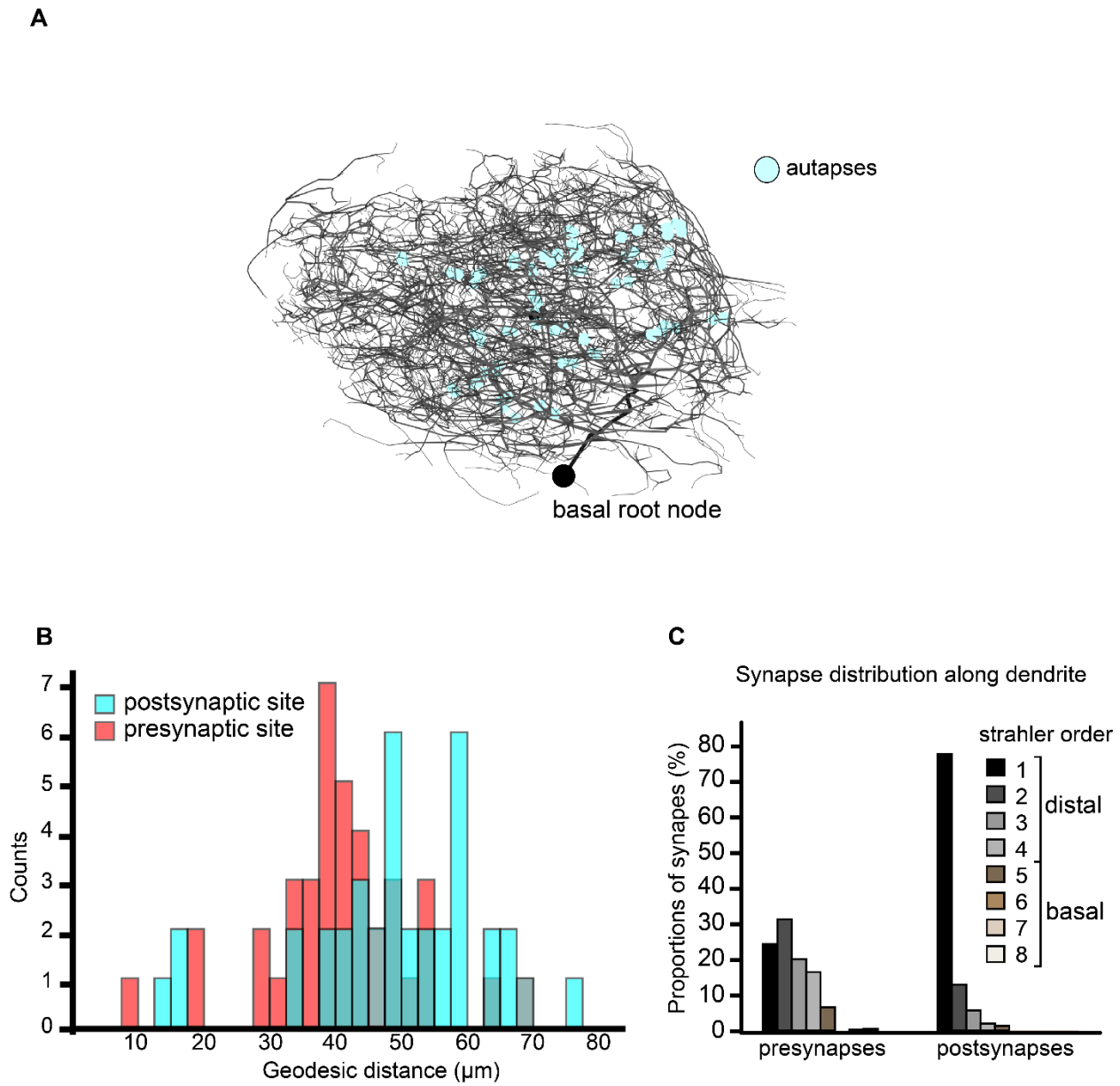


**Figure 7 – figure supplement 1**

Horne, J. A., Langille, C., McLin, S., Wiederman, M., Lu, Z., Xu, C. S., Plaza, S. M., Scheffer, L. K., Hess, H. F., & Meinertzhagen, I. A. (2018). A resource for the *Drosophila* antennal lobe provided by the connectome of glomerulus VA1v. *eLife*, *7*, e37550. https://doi.org/10.7554/eLife.37550